Distributed light sources for photocatalytic water treatment

Johannes Kuipers

Thesis committee

Promotor
Prof. Dr H.H.M. Rijnaarts
Professor of Environmental Technology
Wageningen University

Co-promotors
Dr H. Bruning
Assistant Professor at the Sub-Department of Environmental Technology
Wageningen University
Dr D.R. Yntema
Scientific Project Manager
Wetsus, Centre of Excellence for Sustainable Water Technology

Other members
Prof. Dr J.T. Zuilhof, Wageningen University
Prof. Dr G. Mul, University of Twente
Prof. Dr J.P. Malley, University of New Hampshire
Prof. Dr G.J Witkamp, Delft University of Technology

Distributed light sources for photocatalytic water treatment

Johannes Kuipers

Thesis
submitted in fulfilment of the requirements for the degree of doctor
at Wageningen University
by the authority of the Rector Magnificus,
Prof. Dr M.J. Kropff,
in the presence of the
Thesis Committee appointed by the Academic Board
to be defended in public
on Friday 10 October 2014
at 13.30 at the Post Plaza in Leeuwarden

Contents

Chapter 1

General introduction: Photocatalysis, light sources and inductive coupling

1.1   Introduction

A major challenge in the 21st century is to provide water with sufficient quality and quantity for human kind in a sustainable way [171, 201]. Currently, more than one third of the world's population does not have access to safe drinking water and almost half of the population has insufficient sanitation [171, 201]. One third of the total amount of renewable freshwater is already used for agriculture, industry and domestic use [172]. The demand for freshwater is expected to increase further due to the rising world population and the expected decline of freshwater supply due to the impacts of climate change and the drying out of non-renewable freshwater sources [83, 144]. In order to safeguard human health, fresh water sources need protection. This involves wastewater treatment for safe return to the natural aquatic system and reuse of the wastewater. Other water treatment technologies include freshwater production from seawater and brackish water in arid areas. The challenge for many water treatment technologies is the energy demand. For example, the removal of micropollutants and other manmade chemicals, and desalination of seawater are very energy demanding processes. New approaches and technologies are needed to decrease the energy demands and meet the freshwater demands of an increasing world population [132].

Examples of energy demanding water treatment technologies are advanced oxidation processes using ultraviolet light, such as UV/H_2O_2 advanced oxidation and UV/TiO_2 photocatalytic oxidation. These are promising technologies for the removal of micropollutants. One challenge for photoreactors in general and photocatalytic reactors specifically is the distribution of the light inside the reactor. In this thesis we evaluate the potential of distributing a multitude of small scale ultraviolet light emitting diodes (UV-LEDs) throughout the reactor in order to improve the distribution of light. Powering the UV-LEDs wirelessly with resonant inductive coupling (RIC) gives the UV-LEDs the ability to move around freely inside the reactor. A system with a multitude of wirelessly powered UV-LEDs distributed in the reactor is expected to have a better distribution of UV light in the reactor compared to a system with a small number of conventional fixed

UV lamps. A better distribution of UV light in the reactor is expected to result in a lower energy demand of the water treatment.

1.2 Photocatalysis

From the 1930s on, it has been known that solids can promote reactions when irradiated with light without being consumed [68]. Nowadays, these solids are known as photocatalysts. From the 1950s on, there have been reports about titanium dioxide (TiO_2) suspended in a solution and irradiated with ultraviolet light "auto-oxidizing" various organic solvents such as alcohols and hydro-carbons, although originally these reports failed to attract much attention. During the oil-crisis of the 1970s, however, the report of Fujishima and Honda, reporting a photoelectrochemical cell converting solar energy into chemical energy by photocatalytic reactions [65], did attract much attention and resulted in substantial research efforts in the field of photocatalysis. One of the results was the idea that photocatalysis could also be used for water purification. Since the 1980s, an extensive list has been composed of organic compounds, inorganic compounds, microorganisms, viruses and other compounds that can be oxidized, reduced, transformed or killed by photocatalysis [37, 33, 34, 35, 36, 14, 82].

1.2.1 Principle and applications

Chen [32] defined photocatalysis as "a substance associated with photons to activate a chemical reaction and/or to accelerate the rate at which a chemical reaction approaches equilibrium, without being consumed in the process". So the concept photocatalysis implies the catalysis of a chemical reaction by a catalyst and light. Normal catalysis can only increase the reaction rate of spontaneous reactions by reducing the activation energy for reactions that yield free energy (have negative Gibbs free energy difference). Photocatalysis differs on this point by providing energy input in form of photons. It can therefore also start reactions that need energy input, i.e. for which the Gibbs free energy of the reaction is positive. Often photocatalysis produces a highly energized intermediate compound that

subsequently reacts with the reactant. Examples are the splitting of water in hydrogen gas as occurs in the photoelectrochemical cells [65] and photocatalytic oxidation of alcohol in deaerated systems to produce hydrogen and aldehyde. Photocatalysis is different to other advanced oxidation technologies such as UV/H_2O_2 as the photocatalyst is not only able to oxidize but also to reduce dissolved components. Photocatalysis can be divided in heterogeneous photocatalysis and homogeneous photocatalysis. In homogeneous photocatalysis, the photocatalyst is a dissolved organic dye or a polyoxometalate [136, 108] such as $W_{10}O_{32}^{-4}$, $PW_{12}O_{40}^{-3}$ and $SiW_{12}O_{40}^{-4}$. In heterogeneous photocatalysis, the photocatalyst is a solid metal oxide such as TiO_2 and ZnO. In this thesis, the focus will be on heterogeneous photocatalysis, and when not specified we will refer with "photocatalysis" to "heterogeneous photocatalysis".

Photocatalysis is based on the electric properties of the catalyst. Most materials fall in the category of electrical conductors or electrical insulators. A few materials, however, fall into an intermediate category known as electrical semiconductors. Photocatalysts are n-type semiconductors i.e. they have the property that electrons in the valence band can be excited to the conduction band by absorbing energy of a photon or another source. Figure 1.1 shows a schematic drawing of a photocatalyst. The photon with an energy level ($h\nu$) that exceeds the band gap energy of the photocatalyst (E_{BG}) is absorbed by the photocatalyst and excites an electron. The resulting electron (e^-)-hole (h^+) pair can recombine (as indicated by the dashed arrow (Figure 1.1)) or can start redox reactions with adsorbed species on the surface of the photocatalyst. In photocatalysis, the participation of the electron-hole pair in redox reactions is the preferred route of the electron-hole pair. In Figure 1.1, as an example, the electron reduces molecular oxygen to a superoxide radical and the hole oxidizes a hydroxyl ion to a hydroxyl radical. A huge variety of redox reactions can occur at the surface of the photocatalyst depending on which species are present at the surface and the redox potential of the generated electron-hole pair.

The redox potential of an electron-hole pair depends on the band structure of the semiconductor. For application of photocatalysis for water treatment involving oxygen based radicals, the redox potential of the photo-
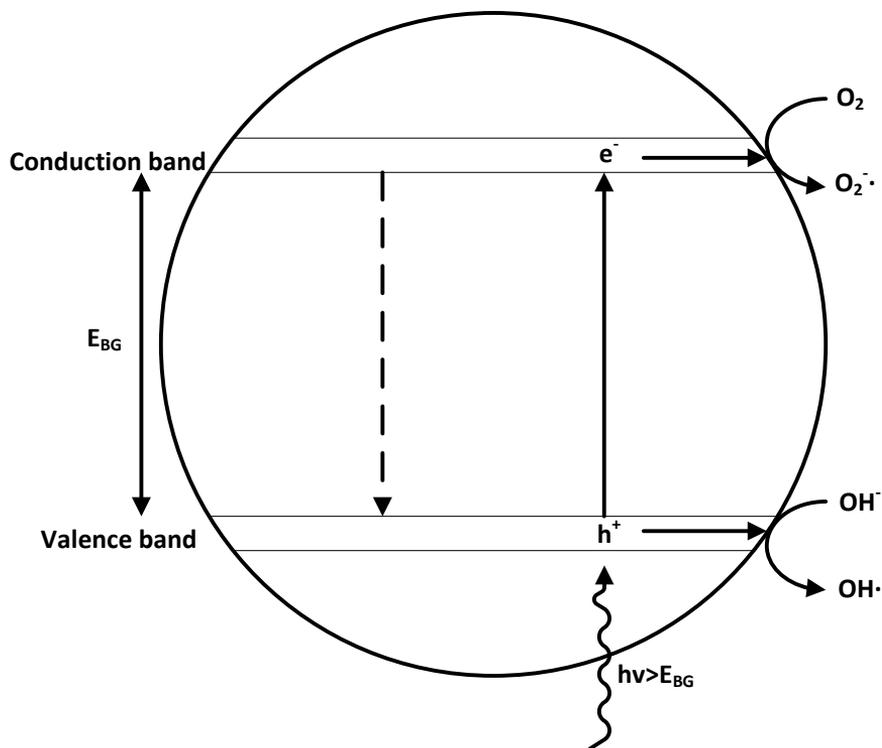
Figure 1.1: Schematic representation of the excitation of an electron from the valence band to the conduction band in the photocatalyst particle and the recombination (dotted line) or the redox reactions on the surface of the particle.

generated hole in the valence band needs to be sufficiently positive to generate hydroxyl radicals from absorbed water molecules and the redox potential of the photo-generated electron in the conduction band needs to be sufficiently negative to generate superoxide radicals from the absorbed

molecular oxygen. Figure 1.2 gives band positions for a variety of semiconductors and the relevant redox potentials.
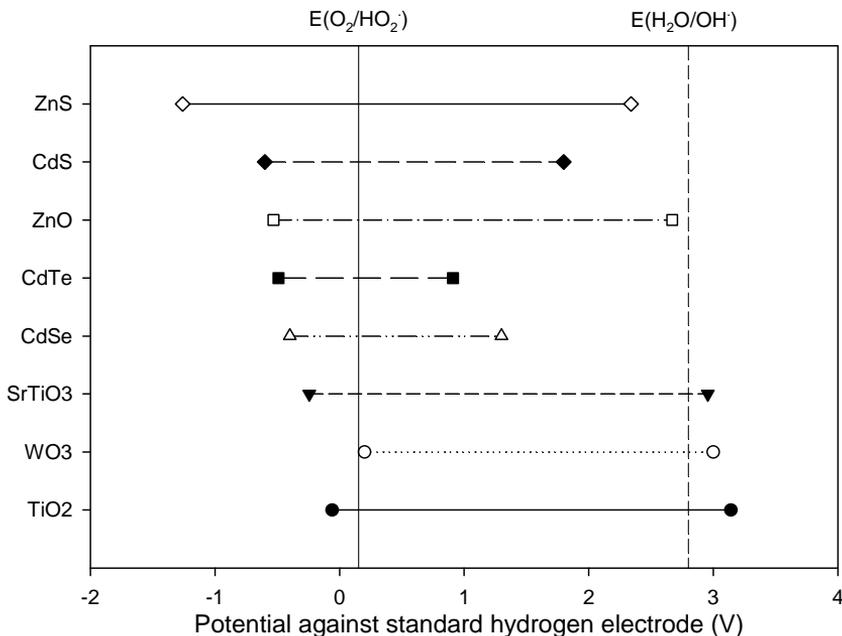
Figure 1.2: Band positions of common n-type semiconductors used in photocatalysis, and the redox potential of $H_2O/OH\bullet$ and $O_2/HO2\bullet$ redox couples (data from [130].

For a long time, titanium dioxide (TiO_2) is considered to be the most suitable photocatalyst for water treatment and the widely available TiO_2 P25 from Degussa is the research standard [181]. TiO_2 P25 is well defined, with 70% anatase and 30% rutile crystal structure, non-porous structure, BET surface area of 50 m^2/g and average particle size of 30 nm. The band gap energy of TiO_2 is 3.2 eV for the anatase crystal structure and 3.0 eV

for the rutile crystal structure, this corresponds to a photon wavelength of 385 nm or lower to achieve electron excitation.

A range of reactions can take place on the surface of the particle, the most important reactions considering oxidation in water treatment are the following [40]:

Photoexitation:
$$TiO_2 + hv \rightarrow e^- + h^+ \tag{1.1}$$

Electron-hole recombination:

$$e^- + h^+ \rightarrow \text{heat} \tag{1.2}$$
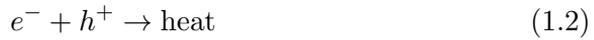
Reduction of oxygen:
$$O_2 + e^- \rightarrow O_2^{\bullet-} \tag{1.3}$$

Oxidation of hydroxyl ion:

$$OH^- + h^+ \rightarrow OH^{\bullet} \tag{1.4}$$

Oxidation by a hydroxyl radical:

$$\text{R-H} + OH^{\bullet} \rightarrow R^{\bullet} + H_2O \tag{1.5}$$

Direct oxidation by a hole:

$$R + h^+ \rightarrow R^{+\bullet} \tag{1.6}$$

Protonation of superoxide:

$$O_2^{\bullet-} + H^+ \leftrightarrow HOO^{\bullet} \tag{1.7}$$

Co-scavenging of electron:

$$HOO^{\bullet} + e^- \rightarrow HOO^- \tag{1.8}$$

Formation of hydrogen peroxide:

$$HOO^- + H^+ \leftrightarrow H_2O_2 \tag{1.9}$$

Additional radical reactions like propagation and termination reactions can take place in the solution. The excited electron (e^-) will recombine with the hole (h^+) in nanoseconds without the presence of oxygen (O_2) or other electron scavengers indicating the importance of electron scavengers. The strong hydroxyl radical ($OH^\bullet$) is considered to be the main oxidizing compound but the role of the weaker superoxide radical ($O_2^{\bullet-}$), hydroperoxyl radical ($HOO^\bullet$) and hydrogen peroxide (H_2O_2) are thought to be complementary to the hydroxyl radical oxidation process [181]. Secondary radical formation increases the complexity of the reaction mechanisms. Generally it can be stated that almost all organic compounds can be totally mineralized by photocatalytic oxidation to carbon dioxide, water and their corresponding mineral acids.

Even though TiO_2 is considered as one of the most photocatalytically active materials, the quantum yield (moles organic compound oxidized over moles photons absorbed) is rather low, $<5\%$. The quantum yield cannot easily be improved as it is a fundamental property of the material. Doping with silver and other metals are applied to reach higher quantum yields but until present no material has been developed that can replace TiO_2 P25 [181].

Photocatalytic oxidation can be used for oxidation and reduction of a wide variety of organic and inorganic compounds [14], micro-organisms and viruses [15]. Application of photocatalytic oxidation is limited to small to medium size [185, 134, 159]. Examples of applications are the treatment of industrial wastewaters [103], post-treatment of municipal wastewater [26, 13, 39, 81, 120] and production of drinking water [8, 9].

1.2.2   State of the art photocatalytic reactors

Photocatalytic reactors with good mass transfer, photon transfer and the ability for up-scaling need to be developed in order to further improve photocatalytic processes [185]. Mass transfer can be defined as the contact between the reactant and the photocatalyst inside a photocatalytic reactor. Photon transfer can be defined as the efficient irradiation of the photocatalyst with light [134]. Different types of photocatalytic reactors

can be distinguished by how the photocatalytst is present in the reactor: i) reactors with the photocatalyst particles suspended in the liquid and ii) reactors with the photocatalyst immobilized on a fixed surface inside the reactor, and by how the photocatalyst is irradiated with a) the lamps submerged in the reactor, b) the lamps placed outside the reactor and c) with waveguides (optical fibers) distributing the light from the lamps outside of the reactor. The different types of photocatalytic reactors each have their own advantages and disadvantages. The photocatalytic reactors with the photocatalyst particles suspended in the liquid generally have good mass transfer but poor photon transfer and need a post treatment step to remove the photocatalyst from the liquid. The photocatalytic reactors with the photocatalyst immobilized on a fixed surface inside the reactor generally have poor mass transfer but good photon transfer and do not need a post treatment step. Important parameters are the total amount of surface area per reaction liquid volume that determines the mass transfer rate and the irradiated amount of surface area per reaction liquid volume that determines the photon transfer rate. Very often, only values are reported for the total amount of surface area per reaction liquid volume, making it difficult to compare different reactor configurations. In Table 1.1 an overview is given of reported values of total surface area per reaction liquid volume (after Van Gerven et al. [185]).

Suspended photocatalyst reactors

In photocatalytic reactors with suspended photocatalyst, the photocatalyst is distributed throughout the reaction liquid as a fine powder. In case of TiO_2 P25, the nanoscale size particles will form agglomerates of micron size [63], depending on ionic strength, pH and cation valence of the water. These suspensions result in a high total amount of surface area and a small distance between the surface of the catalyst and the bulk of the solution and leads generally to good mass transfer. Good photon transfer, however, is more difficult to achieve as the light penetration into the suspension is shallow. Autin et al. [8] reported a penetration depth of 9 mm, only irradiating a thin film closely surrounding the light source. In conventional

Table 1.1: Photocatalytic surface area per reaction liquid volume of different reactor configurations.

Reactor type	Reference	Surface area photocatalyst per reaction volume (m^2/m^3)
Slurry reactor	[134]	2631
	[7]	8500-170000
Annular reactor	[134]	27
	[160]	69
	[134]	133
	[112]	170
	[85]	340
	[134]	2667
Optical fiber reactor	[195]	46
	[202]	53
	[46]	112
	[150]	210
	[160]	1087
	[79]	1920
	[134]	2000
Monolith reactor	[166]	943
	[113]	1333
Spinning disk reactor	[55]	50-130
Microreactor	[10]	7300
	[69]	12000
	[123]	14000
	[179]	250000

annular reactors, the irradiation of a low amount of the total surface area is the case. The irradiated surface area can be increased by using multiple lamps or light guides and by increasing the mixing as in multiple annular and vortex reactors. Thin film reactors such as fountain reactors and falling thin film reactors try to adopt the good mass transfer of photocatalyst

suspensions and irradiate a large surface area per unit volume.

Immobilized photocatalyst reactors

In photocatalytic reactors with immobilized photocatalyst, the photocatalyst is coated on a support material. A range of materials can be coated with photocatalysts such as glass beads, glass disks, cloths, meshes, glass walls, porous materials and ceramic monoliths. The challenge is to increase the mass transfer between the immobilized photocatalyst and bulk of the solution while retaining a good photon transfer. Examples of photocatalytic reactors employing immobilized photocatalysts are packed bed reactors, fluidized bed reactors, spinning disk reactors, optical fiber/hollow tube reactors, internally illuminated monolith reactors and microreactors. In the following paragraphs, descriptions are given of some of these photocatalytic reactors.

Annular photocatalytic reactor

In an annular photocatalytic reactor (Figure 1.3) the lamp is placed in a cylindrical reactor and the reaction liquid flows along the lamp. The photocatalyst can be present in different forms inside the reactor, 1) as suspension, 2) immobilized on glass beads to create a packed or fluidized bed of coated glass beads or 3) immobilized on the wall of the reactor.

The mass transfer rate is high with suspended photocatalyst. Dijkstra et al. [53] showed that immobilized photocatalyst can also reach high mass transfer when applied in a packed or fluidized bed reactor [54, 51, 52]. The photocatalyst immobilized on the reactor wall will result in the lowest mass transfer rate of the three. In an empty reactor the light intensity decays inversely with the distance from the lamp. In the suspension the light intensity decay is increased by the strong adsorption. Photocatalyst particles close to the lamp receive a high light intensity and this drops off very quickly with increasing distance from the lamp. This results in a bad photon transfer. Solutions such as multiple annular and vortex reactors have been developed to increase the performance by increased mixing
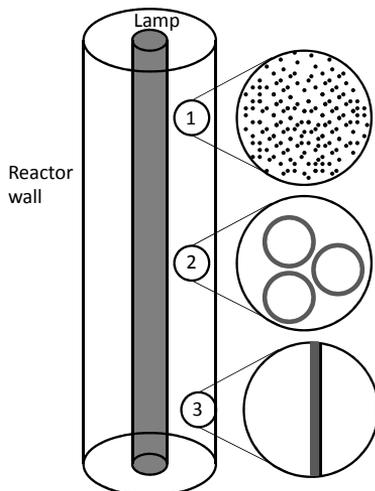
Figure 1.3: Annular photocatalytic reactor with 1) suspended photocatalyst, 2) immobilized photocatalyst on glass beads and 3) immobilized photocatalyst on the reactor wall.

and flowing the suspension in thin films across the lamp. The packed or fluidized glass beads show similar problems in photon transfer [134]. The photocatalyst coated on the glass wall surrounding the lamps results in good irradiation of the photocatalyst but a low surface per reaction liquid volume.

Thin film reactors

In thin film reactors, the photocatalyst is in suspension and irradiated as a thin film. An efficient design is a falling-film photoreactor with the suspension descending down a slope of the reactor wall and irradiated by a lamp mounted in the middle. A high surface per reaction liquid volume is irradiated when only the thin film is taken into account. When the effluent is mixed in a reservoir and recirculated, this high irradiated surface area per reaction liquid volume is lost. A high surface area results in a large footprint

for this technology. Another design example is a fountain reactor in which a thin film is created by creating a fountain as can be seen in Figure 1.4. The fountain is irradiated from the top and results in similar implications as is the case with the falling film photoreactor. High irradiated surface per reaction liquid volume are reported but these exclude the reaction liquid in the reservoir which is not irradiated.
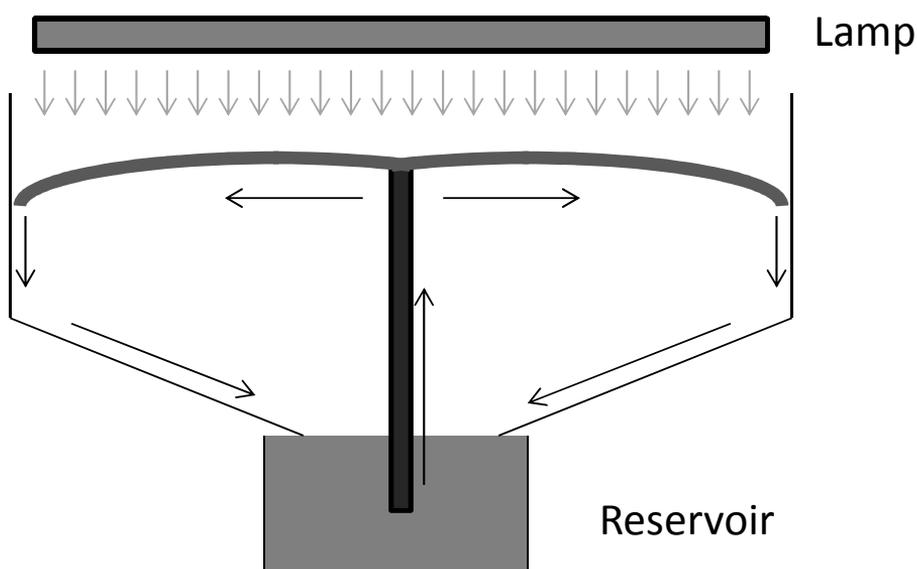
Figure 1.4: Schematic drawing of a fountain reactor.

Spinning disk reactor

A spinning disk reactor consists of a disk placed horizontally or vertically. The vertically placed disk is coated with a photocatalyst and spins around in a reservoir filled with the reaction liquid as can be seen in Figure 1.5. Half of a disk is submerged in the reaction liquid and a thin film is formed on the other half of the disk, which is irradiated by the lamp. The irradiated

surface per reaction liquid volume present on the disk is very high. When, however, the volume of the reservoir is taken into account this number is much lower. Dionysiou et al. [55] showed a non-uniform illumination of the spinning disk reactor with two UV lamps. Up-scaling of such a system can be done by increasing the diameter of the disks, using multiple disks or using a rotating drum.
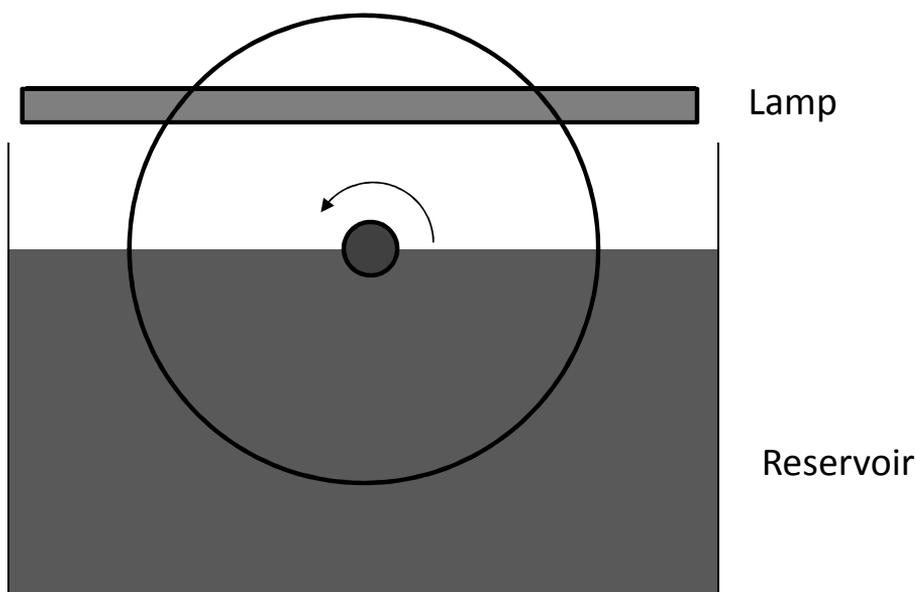
Figure 1.5: Schematic drawing of a vertical spinning disk reactor.

Optical fiber reactor with coated optical fibers

In optical fiber reactors, the optical fibers are used to distribute the light and as a support for the immobilized photocatalyst. Light propagates along the length of the optical fiber by reflection where the fiber has cladding as can be seen in Figure 1.6. Inside the reaction volume the fiber cladding is

stripped and the fiber is coated with TiO_2. The light that would otherwise be reflected by the fiber cladding is now refracted and can be adsorbed by the catalyst coating. The catalyst surface per reactor volume is relatively high but the light intensity along the length of the fiber decays exponentially resulting in non-uniform distribution of the light over the length of the optical fiber. Research groups work on solving the problem of this exponential decay. Other issues are the distance between the activated photocatalyst and the water and the large amount of reactor volume the fibers take up [185].
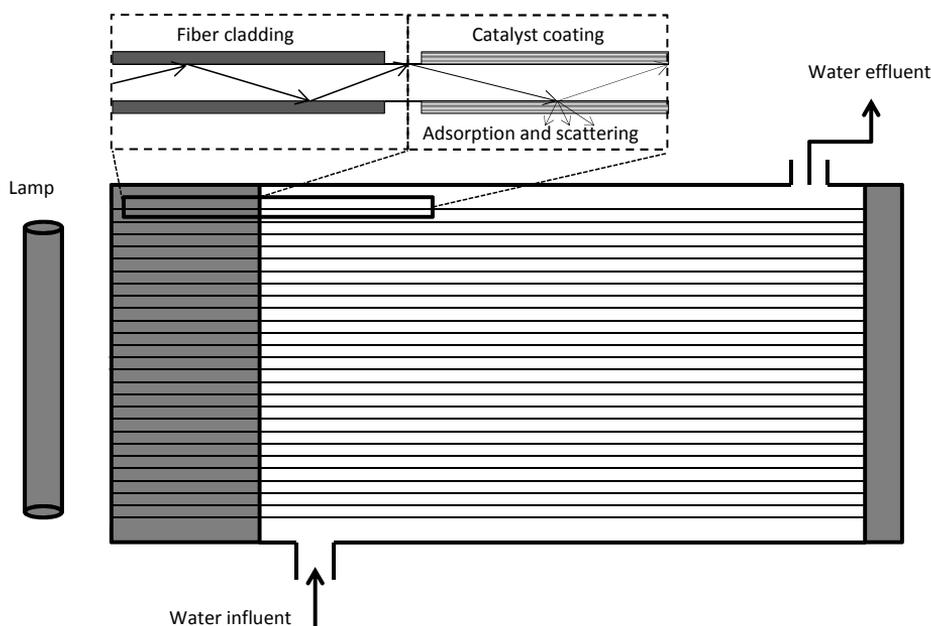
Figure 1.6: Optical fiber reactor with the light source on the left irradiating into the optical fiber and the optical fibers distributing the light over coated catalyst.

Ceramic monolith coated with photocatalyst and irradiated with optical fibers

Promising developments are porous monolith structures coated with photocatalyst that can be irradiated from the inside by optical fibers which emit light sideways. Lin and Valsaraj [113] reported high surface areas with efficient irradiation.

Microreactor

Microreactors are a rather new development and show high total amount of surface per reaction volume but with very low flow rates [10, 69, 6]. Microreactors consist of channels, micron size in diameter, that are coated with photocatalyst. The microreactors have advantages of high surface per reaction liquid volume and the possibility of good process control. The disadvantage is that a microreactor cannot be up-scaled.

1.3   Light sources

The source of UV light is an important factor in photocatalytic systems as it determines for a large part the design and application of the technology. Solar light and mercury discharge lamps are commonly used light sources in research and application of TiO_2 photocatalysis. Around 3-5% of solar light is ultraviolet in the suitable wavelength. In mercury gas discharge lamps, the light originates from an excited electron in the mercury atom falling back to its ground state energy level and emitting radiation. Two types are mostly used for photocatalysis: low pressure and medium pressure lamps. Low pressure mercury discharge lamps produce ultraviolet light with around 15% of the radiant flux at a wavelength of 180 nm and 85% of the radiant flux at a wavelength of 254 nm, with an energetic efficiency of around 32% and typical radiant power of 45 W. Medium pressure mercury discharge lamps produce ultraviolet light from 180 to 400 nm, have a generally lower energetic efficient of around 12%, but with typical radiant power of 750 W. Recently, solid state lighting in the UV range has become

reality in the form of ultraviolet light emitting diodes (UV-LEDs).

1.3.1 Light emitting diodes

Light emitting diodes (LEDs) are a type of solid state lighting that is fundamentally different from the traditional light sources such as incandescent, halogen, fluorescent, neon and mercury discharge lamps. In 1907, Round discovered the light emitting diode effect when he passed a current through a variety of substances and noticed some of them gave off light. In 1962, the first visible LEDs, which emitted red light, were reported using a Gallium Arsenide semiconductor [80, 72]. LEDs emitting yellow and green light were soon developed after the red LED. The energetic efficiency was increased in the following decades as can be seen in Figure 1.7. Gallium Nitride, a new LED material, was discovered in the 1970s by Pankove et al. [147], which emits blue light. The first commercial blue LEDs took until 1991 when Nakamura developed a successful procedure to grow GaN crystals [137, 138]. After blue LEDs became reality it was possible to make white LEDs by combining the red, green and blue LED in one device and later on by using blue or UV-LEDs irradiating a fluorescent layer. Due to the improvements in energetic efficiency, political pressure, marketing and other advantages of LEDs over the last years, LEDs are expected to take over as the main light source in visible lighting [139].

Principle

In LEDs, light is produced by electroluminescence from a semiconductor. Typical semiconductor materials used for LEDs are gallium arsenide (GaAs), gallium arsenide phosphide (GaAsP) and gallium nitride (GaN). A way to produce a LED is to deposit an n-type layer of the semiconductor on a substrate, followed by an active layer and finally, a p-type layer of the semiconductor. A n-type material is doped in such a way that extra, free electrons are present in the valence band of the material. A p-type material is treated in a way that electrons are depleted, or holes are present in the valence band. When the two materials are placed in contact, electrons
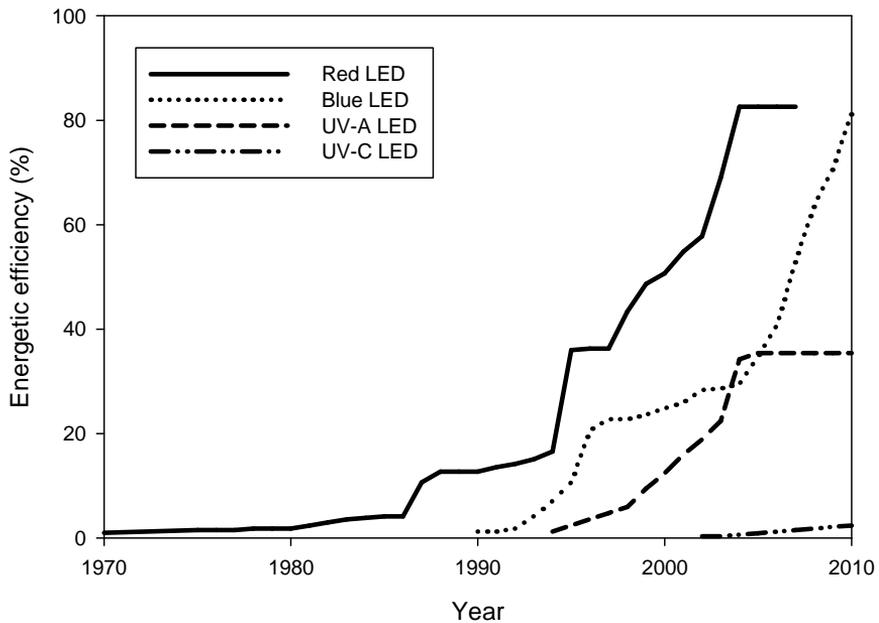
Figure 1.7: Energetic efficiencies of different LEDs over the years

easily flow trough the junction from n to p but not in the other direction, creating a diode as can be seen in Figure 1.8. When an electron flows from the n-type layer to the p-type layer, the electron drops in energy level and the excess energy is released as a photon with energy level equal to the band gap. The band gap energy is determined by the material of the LED. For example, GaAs emits infrared light and GaAsP emits red, orange or yellow depending on the ratio of phosphide in the material.
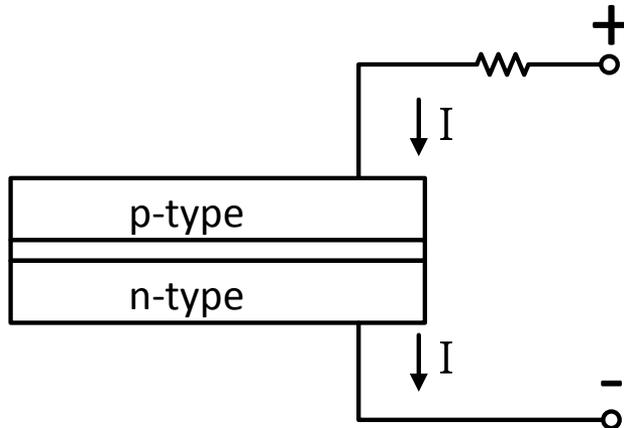
Figure 1.8: A schematic drawing of a light emitting diode with a p and n-type material with current (I) flowing from the p-type to the n-type material.

Ultraviolet light emitting diodes

Technology has advanced such that UV irradiation with semiconducting elements is possible now. Ultraviolet light emitting diodes (UV-LEDs) are developed from GaN compounds with mixtures of indium or aluminum. The mixtures allow for emissions ranging from the UV-A region (400 to 320 nm) all the way into the UV-C region (280 to 210 nm). The higher the ratio of indium or aluminum in the GaN material, the lower will be the emitted wavelength of the light. The UV-A LEDs have reached energetic efficiencies of 35% in 2010, comparable to energetic efficiency of low pressure mercury discharge lamps. The challenge in the development of UV-C LEDs is the difficulties growing GaN crystals with high Al or In content needed for emitting UV-C light. Other problems are the internal reflection and

absorption of the UV light in the GaN. Similar kinds of problems existed for visible and near-UV LEDs and have been solved indicating a good chance for a solution for high efficiency UV-C LEDs [174]. It is expected that the technological development of UV-LEDs will continue and that energetic efficiency will be increased in the future.

1.3.2   Mercury lamps versus solid state light sources

Mercury gas discharge lamps are well integrated in the market, with reliable and documented performance, and remain a good UV source. They have some disadvantages though, under which one of the most pressing ones the use of mercury. The use of mercury is severely restricted due to its high toxicity to humans and to the environment. Another disadvantage is the requirement of a high voltage ignition pulse and relatively high operating voltages, which makes application less versatile. LEDs can be made out of non-toxic materials and require low voltage for operation. Another difference between mercury discharge lamps and LEDs is the size, LEDs are much smaller than mercury discharge lamps and makes the LEDs less fragile.

1.3.3   Power and light intensity

The radiant power of a LED increases almost linearly with the forward current. This results in the ability to accurately control the emitted radiant power with the forward current. This is a useful characteristic for water treatment as the amount of radiant power can be controlled for the amount of pollution and is not a fixed value as it often is with low pressure mercury lamps or a uncontrolled varying value as with solar light. The intensity of mercury discharge lamps are generally much less tunable. The intensity of a high power UV-LED, for instance the 2.3 W radiant power UVA LED from Nichia 0.425 by 0.425 cm, in power emitted per surface area is 12.7 W/cm^2. This is more than a factor 500 higher than the intensity of a low pressure mercury lamp with radiant power of 45 Watt, diameter of 3.8 cm and length of 160 cm resulting in intensity of 0.02 W/cm^2. Compared to

the UV-LED and the low pressure mercury lamp the UV radiation from the sun is low, 0.003 W/cm^2. Current UV-LEDs have the characteristics of small size and a high radiant power output resulting in high light intensity. With these new UV-LEDs more intensified reactors can be constructed.

1.3.4 Radiation pattern

A LED radiates light in the direction perpendicular to the emitting surface. The emission angle describes the angle at which the intensity of the radiation has dropped to 50% of the intensity perpendicular to the LED. The emission angle of a LED can be adjusted by using small lenses integrated in the packaging of the LED, providing the opportunity to alter the light pattern and can be useful for designing photoreactors with homogeneous distribution of light.

1.3.5 Costs

LEDs are expensive in terms of capital costs compared to mercury discharge lamps per amount of emitted light unit. In the past, progress in LED performance has been fast and is described by a logarithmic "law" known as the "Haitz's law" which predicts that every 10 years the light generated by a LED increases by a factor 20 and the costs per amount of emitted light unit decreases by a factor 10. The long operational life results in lower maintenance and life-cycle costs compared to mercury discharge lamps. UV-LEDs have some distinctive characteristics making them completely different compared to a mercury lamp and this allows for many different designs of a photocatalytic reactor. The characteristics that LEDs are robust against shocks, small in size, need low power and are energy efficient makes them useful as light sources in this thesis as small, distributed and freely moving light sources.

1.4   Inductive coupling

Electromagnetic induction was discovered independently by Michael Faraday and Joseph Henry around 1831 [61]. Electromagnetic induction is defined as the electromotive force induced by a changing magnetic field. An application is the generation of electricity by moving a permanent magnet across a conducting wire. Electromagnetic induction was one of the discoveries that led to the development of technologies that would electrify the world. Induction can be used to transfer electric energy. The main application of this is found in the transformer to step-up or step-down the voltage of alternating current. A transformer consists of two electromagnetic inductors, the primary or transmitting inductor and secondary or receiving inductor, mostly as copper wire coils wound around a core with a high magnetic permeability. When a current, I_t, flows through an inductor, a magnetic field, B_t, is induced, depending on the magnetic permeability, μ, of the inducor's core and the number of turns, N_t, as stated by a derivative of Amperes Law:

$$B_t = \mu N_t I_t \tag{1.10}$$

This changing magnetic field can in turn induce an electromotive force, emf_r, in a receiving inductor, with number of turns, N_r, and area of the inductor, A, as stated by a derivative of Maxwell-Faraday equation:

$$emf_r = -AN_r \frac{dB_t}{dt} \tag{1.11}$$

Combining Equation 1.10 and 1.11, and using mutual inductance, $M = N_t N_r A\mu/l$ it follows:

$$emf_r = -M \frac{dI_t}{dt} \tag{1.12}$$

The electromotive force emf_r will result in a current I_r in the receiving inductor and an electromotive force emf_t in the transmitting inductor:

$$emf_t = -M \frac{dI_r}{dt} \tag{1.13}$$

A core with a high magnetic permeability ensures that all of the magnetic field is coupled from transmitting L_t to the receiving inductor L_r. In that case the mutual inductance is maximal and equal to:

$$M = \sqrt{L_t L_r} \tag{1.14}$$

With the self-induction of the inductor given by:

$$L = \frac{\mu N^2 A}{l} \tag{1.15}$$

Without a core with a high magnetic permeability, the mutual inductance will be lower. The ratio of mutual inductance and maximum mutual inductance is used as a figure of merit, the coupling factor:

$$k = \frac{M}{\sqrt{L_t L_r}} \tag{1.16}$$

The coupling factor ranges between perfect coupling with k = 1, and no coupling with k = 0. Generally, a good coupling factor is between two inductors with small distance and equal diameter (see Figure 1.9a). The coupling factor decreases with increasing distance (Figure 1.9b) and difference in diameter (Figure 1.9c) between the transmitting and receiving inductor.

1.5 Resonant inductive coupling

Loosely coupled inductors can reach high energetic efficiency when the inductors resonate at the same frequency [94, 102]. A medical team did one of the first investigations to power biomedical implants with resonant inductive coupling in the 1960s [170, 168, 169]. Application and research into powering biomedical devices with resonant inductive coupling still continues. More scientific and popular attention for resonant inductive coupling came after a publication of Kurs et al. [102] in which they reported wirelessly powering a 60 watt light bulb over 2 meter distance with resonant inductive coupling. Since then, scientific and popular interest in resonant inductive coupling has increased.
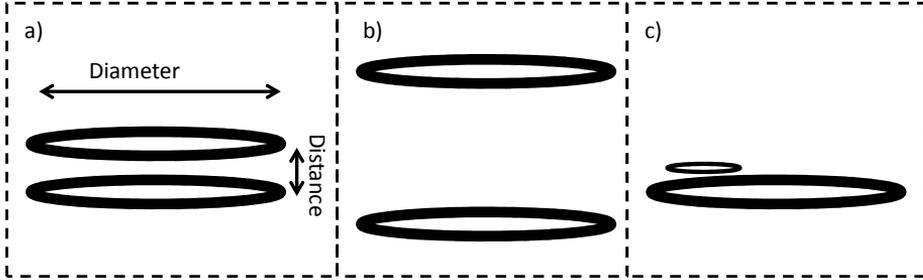
Figure 1.9: Schematic drawing of (a) inductors tightly coupled, (b) loosely coupled inductors with increased distance between the inductors and (c) loosely coupled inductors with difference in diameter.

1.5.1   Principle

Figure 1.10 shows a lumped element model of two inductors. When V_p is an alternating voltage with angular frequency ω, Kirchhoff's Law yields the following equations:

$$V_t = I_t R_t + j\omega L_t I_t - j\omega M I_r \qquad (1.17)$$

$$0 = I_r(R_r + R_L) + j\omega L_r I_r - j\omega M I_t \qquad (1.18)$$

Inductive coupling is energetic efficient with a high mutual inductance and when R_L is optimized. When the mutual inductance decreases also the efficiency decreases. The efficiency is high when the current in the receiving inductor, I_r is attained with a low current in the transmitting inductor, I_t. With a low mutual inductance still a high efficiency can be reached by eliminating jωL by adding a capacitor (C) in series and operating at the resonance frequency. With the capacitors in series the equations become:

$$V_t = I_t R_t + j\omega L_t I_t + \frac{I_t}{j\omega C_t} - j\omega M I_r \qquad (1.19)$$

$$0 = I_r(R_r + R_L) + j\omega L_r I_r + \frac{I_r}{j\omega C_r} - j\omega M I_t \qquad (1.20)$$
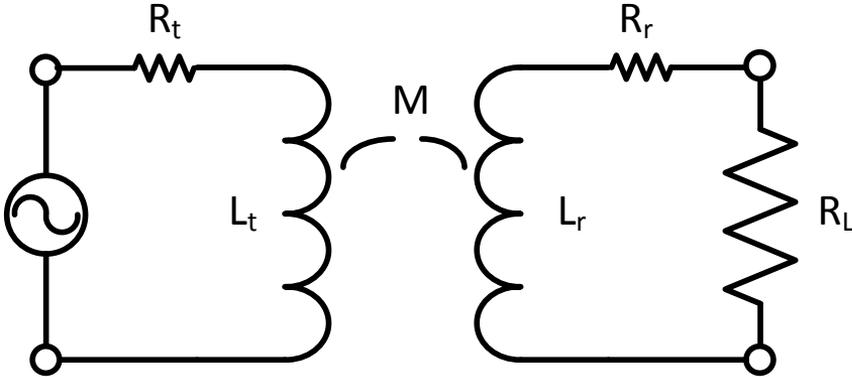
Figure 1.10: Lumped element model of two inductively coupled inductors.

When both circuits are tuned to have the same resonance frequency $\omega = 1/\sqrt{L_t C_t} = 1/\sqrt{L_r C_r}$ the Kirchhoff equations reduce to:

$$V_t = I_t R_t - j\omega M I_r \tag{1.21}$$

$$0 = I_r (R_r + R_L) - j\omega M I_t \tag{1.22}$$

The reduced impedance of both circuits results in that the current in the receiving inductor is reached with a lower current in the transmitting inductor and thereby reducing the energy losses.

The energy transfer efficiency can be described, derived from Equation 1.21 and 1.22, using dimensionless figures of merit, the coupling factor between the two inductors and the quality factors of the two inductors. The losses in the capacitor are generally so small that they can be ignored. The quality factor describes the selectivity and power dissipation of a resonating circuit. The quality factorn (Q) is defined as:

$$Q = \frac{\omega_0}{\Delta\omega} \tag{1.23}$$

With ω_0, the resonance frequency and $\Delta\omega$ the width of the resonance curve at which the power is half of the maximum power. The width of the resonance curve is equal to the resistance over the self- inductance, $\Delta\omega$=R/L, expressing Q as:

$$Q = \frac{\omega L}{R} \qquad (1.24)$$

The equation describing the energy transfer efficiency for an optimized load and using the figures of merit is described by:

$$\eta_{opt} = \frac{k^2 Q_t Q_r}{(1 + \sqrt{1 + k^2 Q_t Q_r})^2} \qquad (1.25)$$

The coupling factor declines strongly when the distance between the two resonators is increased. In order to achieve high energetic transfer efficiency, the sum of the quality factors of both resonators has to be high as can be seen in Figure 1.11. From Equation 1.24 can be seen that when the inductance (L) and resistance (R) of the resonator remains constant, the angular frequency (ω) can be increased to increase the quality factor. Unfortunately, the resistance increases as well with the frequency resulting often in a broad peak of quality factor in the kilohertz to megahertz region.

1.5.2 Applications

Resonant inductive coupling is applied to charge batteries in electric toothbrushes and electric shavers since the 1960s [165], but basically all electronic devices can be powered by resonant inductive coupling. Research is conducted on powering biomedical implants and equipment, mechatronic systems, electronic vehicles, household electronics, robots, sensors and many others. Reasons to use RIC can be the advantage of lack of cords and connectors i.e. the system needs to be wireless. An example of a RIC powered medical device is a wirelessly powered endoscopes [28, 27, 107, 157, 186] with three dimensional receiving inductors able to receive energy independent on the orientation of the device, wireless powering and transmitting of information from sensors and cameras and a propelled and steerable
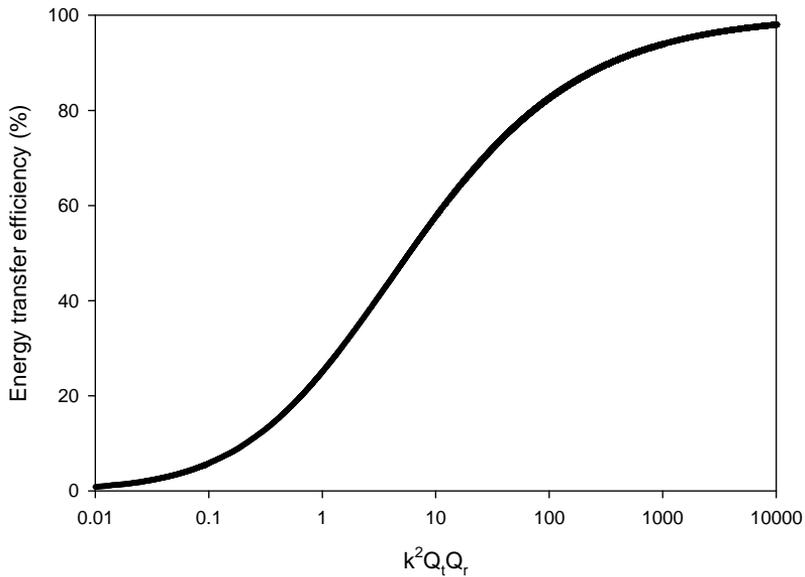
Figure 1.11: Energy transfer efficiency as function of $k^2Q_tQ_r$

endoscope. Other examples are research done into powering electrical vehicles while driving, charging of electrical busses and other electrical vehicles [117, 189, 191]. As can be concluded from the examples described above, many different electrical devices are able to be powered wirelessly with resonant inductive coupling.

1.5.3 State of the art

Research on resonant inductive coupling focusses on the increase of energy transfer efficiency [102, 38, 73, 91, 115]. Increase of energy transfer efficiency is generally achieved by using components with very high quality

factors. Challenging is the development of mass produced inductors with high Q factors and increasing Q factors of small scale inductors [41, 205]. The advantages of using components with high Q factors are stated as being higher energy transfer efficient over larger distances and low radiation losses in other obstacles. The highly tuned resonators are also the main disadvantage as a small shift in resonant frequency of one of the resonators results in a strong reduction of energy transfer efficiency. Other research is done on using multiple transmitting and receiving inductors [29, 1], applying magnetic field receivers to increase the distance [2] and automated impedance matching where the load is automatically matched with the impedance of the system [11].

1.6   Aims of this thesis

The aim of this thesis is to develop and investigate a new photocatalytic reactor with RIC powered UV-LEDs to increase the light distribution in photocatalytic reactors. The first part of the thesis deals with the energy transfer efficiency of RIC in water. The second part deals with the increase of light distribution in photocatalytic reactors. Three main objectives can be identified that are investigated: i) Powering a multitude of small scale light sources distributed in water with resonant inductive coupling, ii) increase of the light distribution in photocatalytic reactors with small scale distributed light sources and iii) identification of limiting factors of photocatalytic oxidation. The application of RIC is to distributed energy to small scale electronic devices in water in an efficient, reliable, flexible and cost effective method. Because the light distribution is often a limiting parameter in photocatalytic oxidation it was chosen as a case for to investigate the use of RIC.

1.7   Thesis outline

The aim of this thesis is to develop a new photocatalytic reactor with ultraviolet light emitting diodes that are powered with resonance inductive

coupling. The potential of resonant inductive coupling to power multiple small scale electronic devices submerged in water is investigated in Chapter 2.

The influence of saline water on the energy transfer efficiency of RIC is discussed in Chapter 3.

Chapter 4 shows the ability to use resonant inductive coupling to power porous electrodes for capacitive deionization.

The use of ultraviolet light emitting diodes as immersed light sources for photocatalytic oxidation is investigated in Chapter 5.

Chapter 6 introduces a novel photocatalytic reactor with resonant inductive coupling to power ultraviolet light emitting diodes in a TiO_2 suspension.

Removal of pharmaceuticals from municipal wastewater effluent from a membrane bioreactor is investigated in Chapter 7.

In Chapter 8 the general conclusion and future perspectives are given for the technologies investigated in this thesis.

Chapter 2

Near field resonant inductive coupling to power electronic devices dispersed in water

Abstract

The purpose of this research was to investigate inductive coupling as a way to wirelessly power electronic devices dispersed in water. The most important parameters determining this efficiency are: 1) The coupling factor between transmitting and receiving inductors, 2) the quality factors of the transmitting and receiving inductors, 3) the number of receiving inductors and 4) the matching of the receiving inductor with the load. Experimentally we show that 1 transmitting inductor can wirelessly power 18 or more receiving inductors dispersed in water with an efficiency higher than 75%. Compared to vacuum or air, water as the core material of the transmitting inductor has a negative influence on the quality factor by increasing the turn to core parasitic capacitance and lowering the self resonance frequency of the transmitting inductor. The results demonstrate a promising way to wirelessly power electronic devices, e.g. UV-LEDs, ultrasound transducers, electrodes and sensors, and that inductive coupling can be used in new, innovative designs for water treatment and related process technologies.

2.1 Introduction

Power transfer via inductive coupling has been a topic of great interest for the last decade. Inductive coupling is regarded to be an attractive approach to power autonomous electronic devices, e.g. laptops, cell phones, robots, mechatronic systems [48], biomedical devices [94], electronic vehicles [189] etc. It has been reported by Kurs et al. [102] that 60 Watts can be transferred over 2 meters with an efficiency of 40%.

Inductive coupling can also be an attractive technology to power electronic devices used in water treatment. An inductive link has certain advantages over electric conducting wires, since a fixed physical connection to the electronic device is not required, and an inductive link does not wear, tear, corrode or break, and will avoid an electric short circuit of the wires into the water. With the recent development in Light Emitting Diode (LED) technology it will be possible to have small ultraviolet light sources with a high power to size ratio [178]. Currently the appropriate use for UVC-LEDs are point of use and low flow applications [18]. In recent years large improvements have been made in the development of more efficient LEDs, e.g. the research laboratory of Nichia developed a blue LED with a wall plug efficiency of 81.3% [139]. The current wall plug efficiencies of UVC-LEDs are much lower, around 2% [84] but it is expected that UVC-LEDs will become more efficient and will have a longer lifetime [167] than low pressure mercury lamps which are currently widely used in water treatment technologies. Typical low pressure mercury lamps have a wall plug efficiency of 33 to 37%, depending on the power of the lamps, and a lifetime of 12000 hours [152]. When these UV-LEDs can be integrated with wireless power transfer via inductive coupling, an extensive variety of reactor designs for UV irradiation can be imagined, even to the point of having autonomous free moving UV-LEDs as in a fluidized bed. Hayashi et al. [75] showed that LEDs dispersed in a reactor resulted in a higher photocatalytic degradation rate compared to the LEDs that were fixed to the wall of the reactor. The LEDs in the experiment of Hayashi et al. [75] were powered with the piezoelectric effect by ultrasonic waves.

Other electronic devices used in water treatment and related process

technologies that can be powered with inductive coupling are electrodes, ultrasound transducers and sensors. Inductive coupling makes it possible to have mobile sensors for water treatment systems similar to the endoscopic capsules which are investigated by Carta et al. [28] who showed that an endoscopic capsule can be powered by inductive coupling, be self-propelled and steerable [27]. Using a 3D inductor to receive power, independent of the orientation of the receiving inductors inside the transmitting inductor and wireless data transmission, creates the possibility for sensors with many potential applications [157]. The possibility of having a wireless sensor network inside reactors can greatly improve the process monitoring and control of chemical reactors.

With inductive coupling, power is transferred between a transmitting or primary inductor and a receiving or secondary inductor via magnetic fields. When the magnetic fields are strongly coupled, energy can be exchanged very efficiently as occurs in standard transformers. Transformers use iron cores to couple almost all of the magnetic field induced by the transmitting inductor into the receiving inductor. The inductors become more loosely coupled i) in absence of an iron core to couple the magnetic fields ii) increasing difference in reciprocal size and iii) increasing distance between the inductors. To increase the energy transfer efficiency, the otherwise lost energy of the non-coupled magnetic field is attempted to be stored in a resonant circuit. Two inductors with the same resonance frequency can exchange energy efficiently even when their magnetic fields are loosely coupled [186].

We propose a water treatment system with a large transmitting inductor, a solenoid, wound around a non magnetic, non conducting tube which contains the water that has to be treated and multiple receiving inductors inside as can be seen in Figure 2.1. The transmitting inductor transfers energy to the small receiving inductors which power the electronic devices. The diameters of the receiving inductors are 20 to 30 times smaller than the diameter of the transmitting inductor. Because of the small receiving inductors a loosely coupling between transmitting and receiving inductor is expected. The receiving inductors have ferrite cores which will result in an increased coupling compared to receiving inductors with air or vacuum

cores. The aim of this study is to investigate the inductor to inductor en-
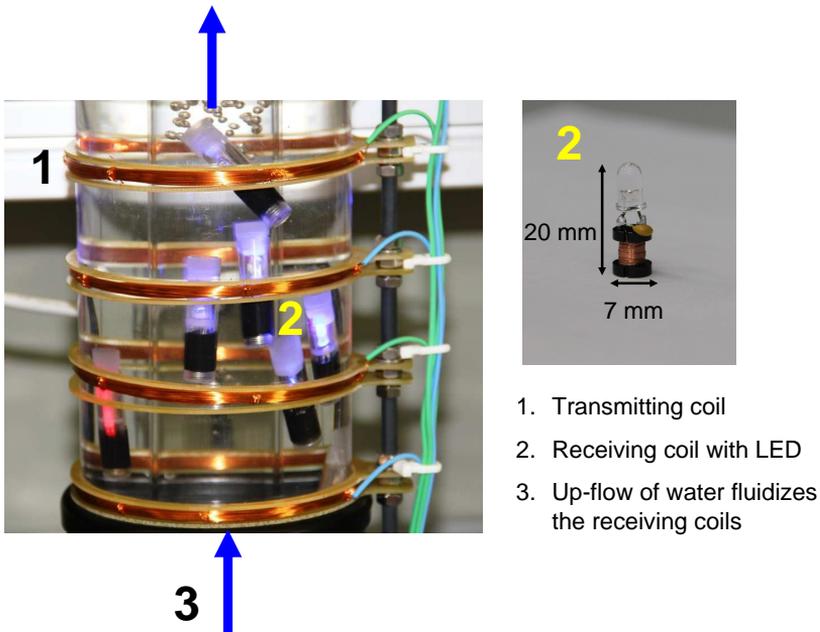
Figure 2.1: Demonstration of proposed water treatment system with dispersed LEDs powered wirelessly with inductive coupling.

ergy transfer efficiency of a large transmitting inductor inductively coupled to multiple smaller receiving inductors dispersed in water. The following was investigated: i) the coupling between the transmitting inductor and multiple receiving inductors dispersed in water, ii) the influence of water with a low conductivity (100 mS/m) on the quality factors of the inductors and iii) the energy transfer efficiency between the transmitting and receiving inductors. The experimental results will be verified by theoretical calculations.

2.2   Theoretical section

This section describes the lumped element model used for calculation of the energy transfer efficiency with inductive coupling between one transmitting and multiple receiving inductors. When the diameters of the receiving inductors are 25 times smaller than the transmitting inductor it is expected that the inductors are loosely coupled. Inductive coupling is most efficient when the frequency of alternating current applied to the transmitting inductor is the resonance frequency of both the transmitting and receiving inductors. The inductors can be part of a resonance tank by connecting a capacitor in series to obtain an RLC circuit. In Figure 2.2 a schematic representation of the lumped element model is shown which represents one transmitting RLC circuit RLC_t and n receiving RLC circuits RLC_r. At the resonance frequency $\omega = 1/\sqrt{L_t C_t} = 1/\sqrt{L_r C_r}$, the reactance of the inductor and capacitor cancel out. Work is done by the load R_L of each receiving RLC circuit. The energy transfer efficiency between transmitting and receiving inductors, which is the power received at the load of the receiving circuits P_r over the power applied to the transmitting circuit P_t, can be derived from the circuit scheme of Figure 2.2:

$$\eta = \frac{P_r}{P_t} = \frac{nk^2 Q_t Q_r}{1 + \frac{R_L}{R_r} + nk^2 Q_t Q_r} \times \frac{R_L}{R_r + R_L} \tag{2.1}$$

with n the number of receiving inductors, k the coupling between the transmitting and one receiving inductor, Q_t and Q_r the quality factor of respectively the transmitting and receiving inductor, R_L the resistance of the load and R_r the series resistance of the receiving inductor. We assume that the receiving inductors are all coupled with the same coupling factor k to the transmitting inductor and there is no coupling between the receiving inductors. Maximizing the efficiency is done by matching the properties of the receiving inductor to the load:

$$R_L = R_r \times \sqrt{1 + nk^2 Q_t Q_r} \tag{2.2}$$
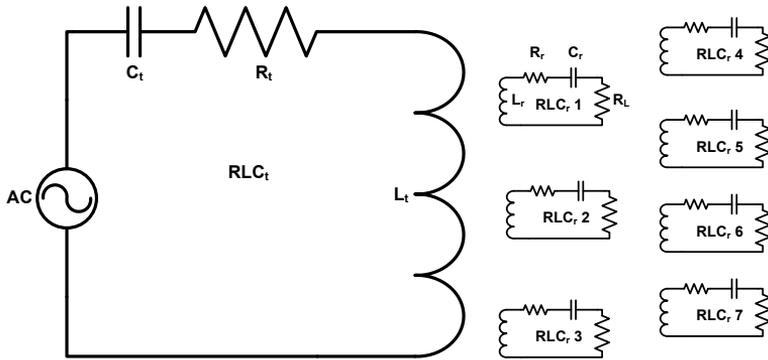
Figure 2.2: Schematic model of 1 transmitting RLC (RLC_t) circuit and $n = 7$ receiving RLC (RLC_r) circuits.

When Equation 2.2 is substituted in Equation 2.1 the equation for optimal efficiency follows:

$$\eta_{opt} = \frac{nk^2 Q_t Q_r}{(1 + \sqrt{1 + nk^2 Q_t Q_r})^2} \tag{2.3}$$

From Equation 2.3 it is clear that the quality factors Q_t and Q_r, which describes the ratio of energy storage to energy loss of a inductor, the coupling factor k which is the ratio of shared magnetic field to the total magnetic field between transmitting and receiving inductors as well as the number n of receiving inductors are the important parameters for the energy transfer

efficiency. Equation 2.1 and 2.3 are consistent with the equations reported by Ko et al. [94] for the case of $n = 1$. The fact that the efficiency increases with the number of receiving inductors is already suggested qualitatively by Puers et al. [157] which call the lost energy a power reserve that can be used by adding more receiving inductors.

2.3   Material and Methods

2.3.1   Transmitting and receiving inductors

The transmitting inductor consisted of a solenoid inductored around a tube made from the polymer polyvinyl chloride (PVC). The height of the PVC tube was 0.34 m, the outer diameter was 0.2 m and the inside diameter was 0.19 m. The PVC tube was closed at the bottom so it could contain water. In the experiments 9.6 liter of water was used to fill the PVC tube. Starting at 0.09 m from the bottom of the tube enameled copper wire of 1 mm in diameter was wound tightly around the PVC tube and after each 10 turns a tap was made. The transmitting inductor had a total of 140 turns, a height of 0.16 m and diameter of 0.2 m. The inductance of the transmitting inductor was 3.2 mH measured at 10 kHz. Ceramic multilayer capacitors were connected in series to select the preferred resonance frequency.

The receiving inductors were ferrite cored radio frequency inductors from Fastron with diameter of 7 mm and a height of 10 mm. The inductance of the receiving inductors was 1 mH measured at 10 kHz. The capacitor and load of the receiving inductors were placed outside the transmitting inductor's magnetic field with insulated copper wires in order to measure the voltage across these components without the interference of this magnetic field. To each receiving inductor a ceramic multilayer capacitor was connected in series to attain the preferred resonance frequency and a metal-film resistor was connected in series which simulated the load.

2.3.2 Electrical measurements

De-ionized water was used to fill the PVC tube of the transmitting inductor and sodium chloride was used to increase the conductivity of the water. The conductivity was measured with a WTW 340i conductivity meter. The inductance, mutual inductance, resistance and quality factors of the inductors were measured with a HP 4194a impedance analyzer. Mutual inductance was measured at 10 kHz. The receiving inductors were dispersed in the water of the transmitting inductor and the transmitting and receiving inductors were axially aligned. The inductance of the transmitting and receiving inductors connected in series were measured with the windings complementing each other and opposing each other without altering the physical setting or positions of the inductors. With the windings complementing each other the inductance consists of: $L_c = L_t + L_r + 2M$, with the windings opposing each other the inductance consists of : $L_o = L_t + L_r - 2M$. The mutual inductance follows from: $M = (L_c - L_o)/4$, the coupling factor follows from: $k = M/\sqrt{L_t L_r}$. No mutual inductance was measured between the receiving inductors when they were placed 1 cm apart. The cumulative coupling factor with multiple receiving inductors was measured with the same method as described above. A number of receiving inductors were connected in series, always ensuring that the windings of the receiving inductors were complementing each other. In this way the receiving inductors could be taken as one receiving inductor and the cumulative mutual inductance between the transmitting and receiving inductors was measured.

The energy transfer efficiency from one transmitting to multiple receiving inductors was measured as follows. The first step was to measure the resistance of the transmitting inductor. The transmitting inductor was filled with water with a conductivity of 100 mS/m. The receiving RLC circuits with a resonance frequency of 50 kHz were placed in the water inside the transmitting inductor. Now the series resistance of the transmitting inductor was measured with the HP 4194a impedance analyzer at the resonance frequency of the receiving RLC circuits. Next step was to measure the current in the transmitting RLC circuit. The transmitting inductor was tuned to the same resonance frequency as the receiving RLC circuits

by connecting a capacitor in series. A function generator was connected
to the transmitting RLC circuit and the signal was adjusted to the res-
onance frequency. The root mean square voltage over the capacitor was
measured with a digital storage oscilloscope IDS8064 from Isotech, the cur-
rent in the transmitting RLC circuit was than calculated from this voltage:
$I = V \times C_t \times \omega$, now the power applied to the transmitting circuit was calcu-
lated with the series resistance of the transmitting inductor: $P_t = I^2 \times R_t$.
The last step was to measure the voltage received at the loads of the re-
ceiving RLC circuits. The root mean square voltages over the loads were
measured and the power was calculated as follows: $P_t = V^2/R_L$. The en-
ergy transfer efficiency between transmitting and receiving inductors is the
power received at the load of the receiving circuit over the power applied
to the transmitting circuit.

2.4   Results and discussion

2.4.1   Influence of water with a conductivity of 100 mS/m on quality factors of transmitting and receiving inductors

The quality factor of the transmitting inductor in air compared to the trans-
mitting inductor filled with water can be seen in Figure 2.3. The quality
factor of the water filled inductor starts to deviate from that of the air core
inductor at around 40 kHz. This deviation is due to the lower self resonance
frequency of the transmitting inductor. The self resonance frequency of the
transmitting inductor in air is 1.16 MHz. When the transmitting inductor
was filled with water with a conductivity of 100 mS/m the self resonance
frequency dropped to 0.257 MHz. The self resonance frequency depends
on the length of copper wire of the inductor and the velocity of the elec-
tromagnetic wave travelling through and alongside the copper wire. The
permeability and permittivity of the medium surrounding the copper wire
changes the velocity of the electromagnetic wave and by this the self reso-
nance frequency of the inductor [128]. Compared to air, water has a higher
permittivity than air with a relative permittivity of $\epsilon_r = 80.1$ at $20\,°C$. The
water increases the overall permittivity of the medium surrounding the cop-

per wire of the transmitting inductor which causes the lower self resonance frequency. An additional increase of inter winding capacitance is caused by conductive water short circuiting the electric field lines of the transmitting inductor [107]. Because of the lower self resonance frequency the reactive and resistive part of the impedance start to deviate at a lower frequency which causes a lower optimal frequency of the quality factor as can be seen in Figure 2.3. The quality factors of the receiving inductors were both in
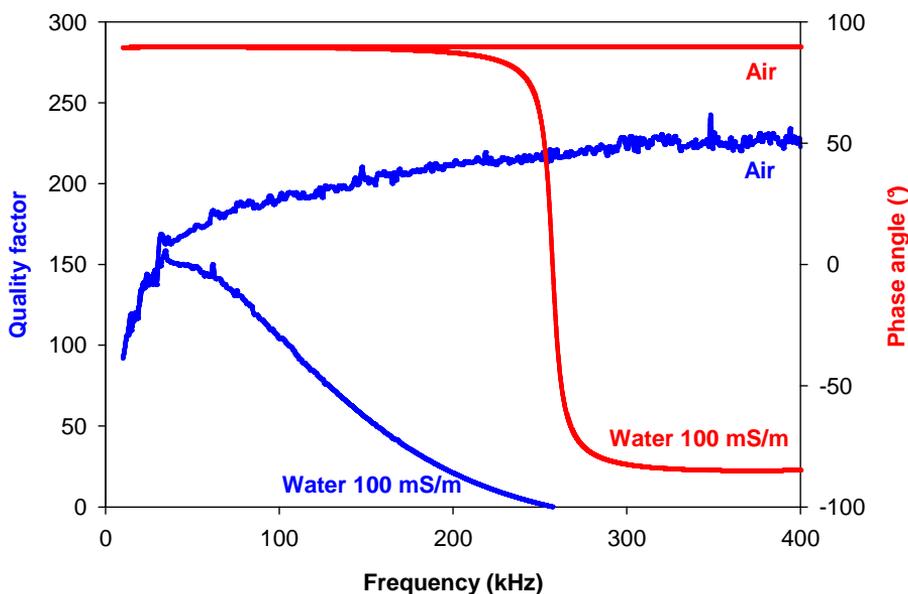
Figure 2.3: Quality factor and phase angle of transmitting inductor in air and filled with water with 100 mS/m conductivity.

air and water 90 at 50 kHz. The quality factor of the ferrite cored receiving inductors were not changed when the inductors were submerged in water as compared to air. The ferrite core of the receiving inductors most likely cause this independence of medium surrounding the inductor because of

the very high permeability of the ferrite compared to air and water.

To increase the quality factors, Litz wire can be used for the transmitting and receiving inductors. Especially at frequencies lower than 500 kHz the resistance of Litz wire is much lower than compared to single strand copper wire [182]. In future experiments and design it is a promising way to further increase the efficiency.

In the following experiments the quality factor of the transmitting inductor was determined to be 150 at 50 kHz.

2.4.2   Mutual inductance and resulting coupling factor between one transmitting and multiple receiving inductors

The cumulative coupling factor of multiple receiving inductors coupled to one transmitting inductor can be seen in Figure 2.4. The cumulative coupling factor increases with the square root of the number of receiving inductors times the coupling factor of one receiving inductor. When a number of n receiving inductors are equally coupled to one transmitting inductor the cumulative coupling will be $k = n \times M/\sqrt{L_t \times n \times L_r} = \sqrt{n} \times M/\sqrt{L_t \times L_r}$. The last point in Figure 2.4 shows 39 receiving inductors each coupled $k = 0.017$ to the transmitting inductor, resulting in a cumulative coupling factor of $k = 0.107$. The measured results start to deviate from the square root line above 15 receiving inductors due to the positions of the inductors. The receiving inductors were placed closer to the centre of the transmitting inductor resulting in small differences in coupling. When the transmitting inductor was filled with water this did not result in a difference in coupling compared to air. This is due to the equal electromagnetic permeability of water and air. The coupling factor is influenced mainly by the sizes and reciprocal positions of the inductors.
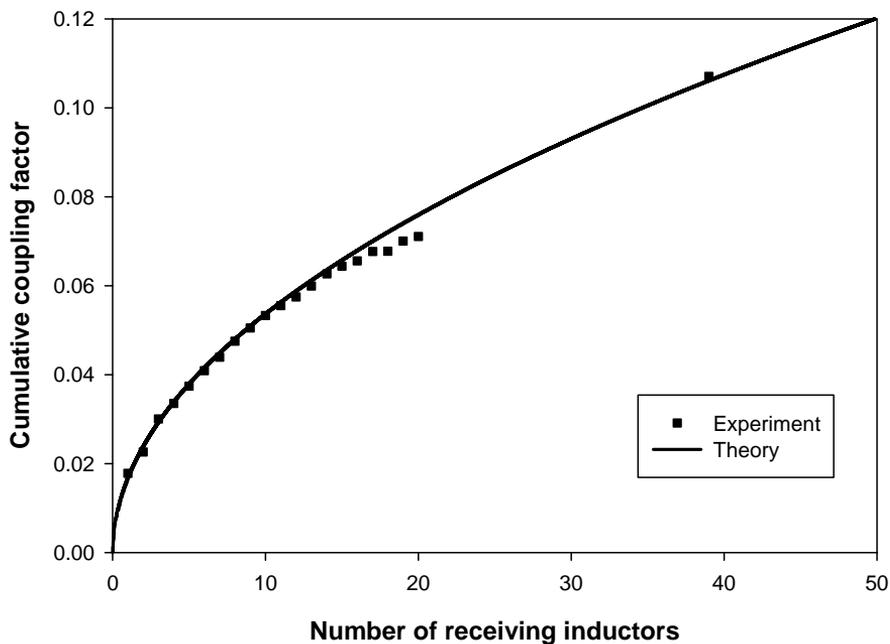
Figure 2.4: Cumulative coupling factor measured between one transmitting and multiple receiving inductors.

2.4.3 Energy transfer efficiency between one transmitting and one receiving inductor with differences in load

The experimental and theoretical results of the energy transfer efficiency between one transmitting and one receiving inductor can be seen in Figure 2.5. The theoretical results were calculated with Equation 2.1 and fit the experimental results well. The optimal resistance of the load was calculated to be 1.8Ω. With the 12Ω resistance the highest energy transfer efficiency of 17.3% was measured. With an increase of resistance to 27Ω the energy transfer efficiency drops to lower than 9%.
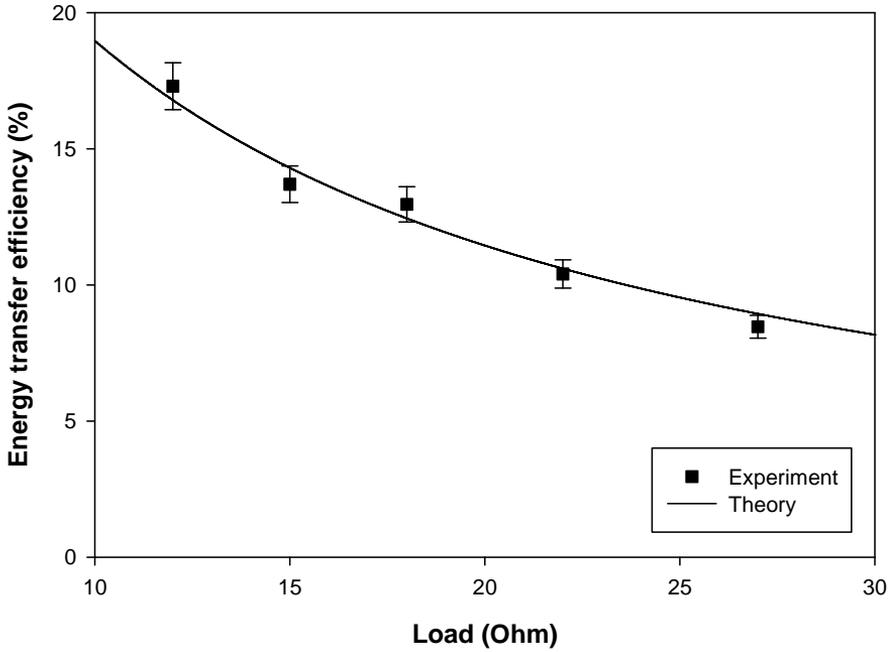
Figure 2.5: Energy transfer efficiency measured and calculated (Equation 2.1) between one transmitting inductor coupled to one receiving inductor with differences in load.

2.4.4 Energy transfer efficiency between one transmitting and multiple receiving inductors

The energy transfer efficiency between one transmitting and multiple receiving inductors can be seen in Figure 2.6. The theoretical results were calculated with Equation 2.1 and fit the experimental results well. With 18 receiving inductors dispersed in water with a conductivity of $100mS/m$

an energy transfer efficiency of 75% was achieved. For the design to power
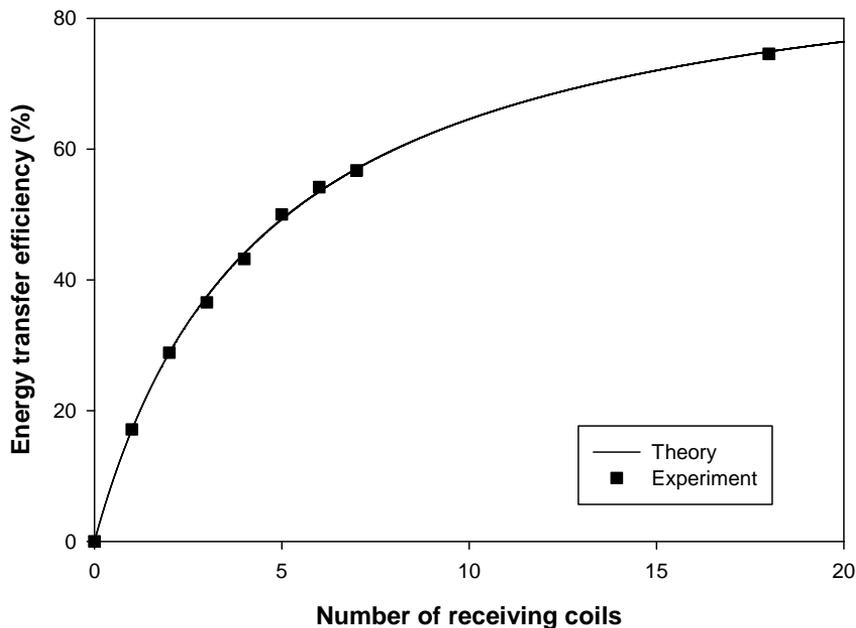
Figure 2.6: Energy transfer efficiency measured and calculated (Equation 2.1) between one transmitting inductor coupled to multiple receiving inductors.

a certain load by inductive coupling it is important to match the receiving inductor to the load of the electronic devices as can be seen in Equation 2.2 in order to attain high energy transfer efficiencies. Typical values of commercial available ferrite core inductors are between 10 μH and 33 mH. With a reasonable assumption of a quality factor of $Q_r = 90$ at 50 kHz, the resulting series resistances of these inductors vary between 0.035Ω and

115Ω. With a coupling of $k = 0.017$, a number of $n = 50$ receiving inductors
and quality factor of $Q_t = 150$ for the transmitting inductor the possible
optimal resistance of the load is calculated to be between 0.4 and 1500Ω.
Theoretically 50 loads, submerged in water, with a resistance between 0.4
and 1500Ω can be powered by inductive coupling with an energy transfer
efficiency of 86%.

With an increase of the number of receiving inductors, the range of
resistance of the load which can still be powered with a reasonable high
efficiency becomes broader as can be seen in Figure 2.7. In this example
the series resistance of the receiving inductor is $R_r = 115\Omega$ and the number
of receiving inductors $n = 1$, 10, 20 and 50. The coupling and quality
factors are the same as used in the previous example. As can be seen in
this example the resistance of the load can vary between 500 and 5000
Ω and the energy transfer efficiency is still above 80%. This shows that
inductive coupling is a robust way to power electronic devices.

Energy transfer efficiency between transmitting and receiving inductors
is an important part of the overall energy efficiency but is not the only factor
in the system. The efficiency of the oscillator to power the transmitting
inductor and, when necessary, the efficiency of a rectifier in the receiving
circuit are also important factors for the overall energy efficiency.

2.5   Conclusions

The results obtained in this study show that autonomous electronic de-
vices dispersed in water can be powered wirelessly by inductive coupling.
One receiving inductor can be powered with an energy transfer efficiency
from transmitting inductor to receiving inductor of 17%. With an increase
in the number of receiving inductors also the energy transfer efficiency
increases. With 18 receiving inductors the energy transfer efficiency is in-
creased to 75%. The results show the possibilities to use inductive coupling
in water treatment and other related process technologies but further work
will be needed to make inductive coupling useful for practical applications.
For possible practical applications we look into powering Ultraviolet Light
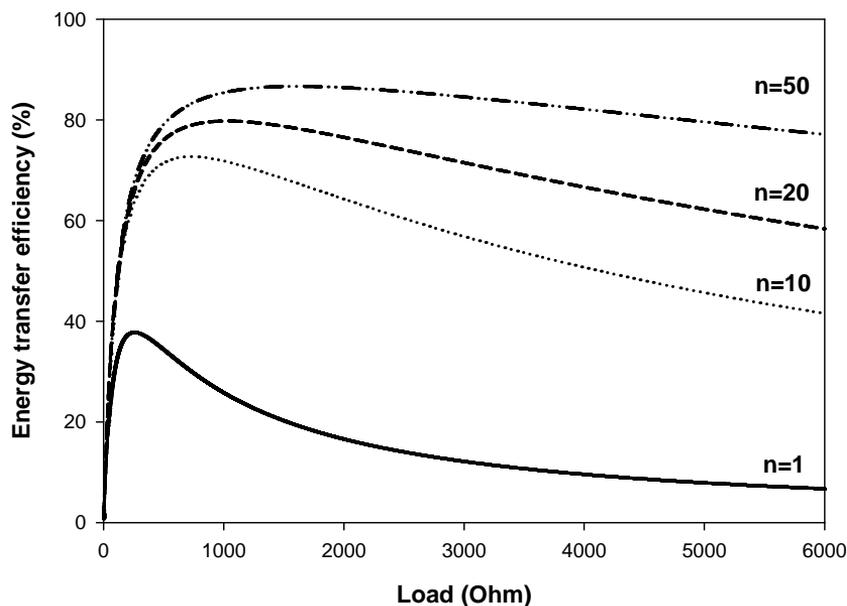
Figure 2.7: Energy transfer efficiency as function of the resistance of the receiving circuit's load, with n = 1, 10, 20 and 50 receiving inductors.

Emitting Diodes (UV-LEDs) for water disinfection [203], advanced oxidation processes with hydrogen peroxide and photocatalysis with titanium dioxide [188]. The advantage of UV-LEDs, aside the elimination of mercury, is that together with inductive coupling it will be possible to design irradiation reactors with a better spatial distribution of ultraviolet light resulting in more efficient photochemical reactors. Inductive coupling can likely be used in electrochemical reactors, where innovative solutions are necessary to distribute electrical current equally over porous, 3 dimensional packed or fluidized electrode surfaces [190]. In sonochemical reactors mul-

tiple ultrasound transducers are used to attain different acoustic patterns which have to be spatially uniform [67]. To be able to do this the position of the transducers have to be easily modified which can be made possible by using inductive coupling to power the transducers. Sensors and small robotic machines can be powered by inductive coupling and be applied in e.g. wireless sensor networks and for inspection and cleaning of different kind of equipment. A wide variety for applications can be imagined but further creative thinking and research is needed to identify and develop what would be suitable applications for this technology.

Acknowledgements

Chapter 3

Self-capacitance and resistive losses of saline water filled inductors

Abstract

Properties of water filled inductors are relevant for underwater wireless energy transfer. The influence of the relative permittivity and resistivity of the core material on the impedance of an inductor can be modeled with a lumped parameter circuit. The relative permittivity of the core material has influence on the turn-to-core capacitance of the inductor. The resistivity of the core material has a linear relation with the resistance of the turn-to-turn capacitance. With this model the influence of the conductivity on the quality factor of an inductor can be predicted. This is a helpful tool to find the optimal frequency at which the quality factor is maximum.

3.1   Introduction

The ability to power electronic devices wirelessly with resonant inductive coupling (RIC) provides advantages for a wide range of appliances [115], e.g. biomedical equipment [94], [157], mechatronic systems [48], electronic vehicles [189], [117], household electronics [102], charging batteries of portable devices [29], [164], sensors [116] and many others [135]. RIC can also be used to transfer electrical energy from a primary inductor outside water to one or multiple smaller secondary inductors underwater. This is an attractive approach to power electronic devices used in water treatment, e.g. ultraviolet light emitting diodes (UV-LEDs), UV lamps, electrochemical electrodes, sensors, etc. In Chapter 2 it was shown that one primary inductor wound around a cylindrical tube containing conductive water, powered 18 small secondary inductors which were submerged in water, with an efficiency of more than 75%.

The efficiency of power transferred from one inductor to the other is important for the understanding how the reactor is functioning and delineate which RIC applications are feasible. Table 3.1 shows that efficiencies between 80 to 90% are to be expected for near field RIC in air. The alternating current (AC) behaviour of the inductors influences the efficiency strongly. For a high efficiency the inductive reactance $\omega L (\Omega)$ of the inductor has to be high and the AC resistance $R (\Omega)$ low [191]. Both the inductive reactance as well as the AC resistance depend on frequency.

The inductive reactance is influenced by the self-capacitance of the inductor. All inductors have self-capacitance [128], sometimes called stray or parasitic capacitance. Self-capacitance of an inductor results from i) turn-to-core capacitance and ii) turn-to-turn capacitance [121]. Turn-to-core capacitance is influenced by the permittivity of the core material [206, 207]. Measurements and numerical simulations show that higher permittivity of the core of inductors results in a higher self-capacitance [206, 207, 125].

Turn-to-turn capacitance is due to short cutting of turns [121, 70]. When the conductivity of the core material increases the short cutting of the turns increases, resulting in a higher self-capacitance.

AC resistance does not equal DC resistance. With increasing frequency,

Table 3.1: Energy transfer efficiencies of resonance inductive coupling

Distance	Frequency	Power	Efficiency	Reference
mid field	9.9 MHz	60 W	40%	[102]
near field	240 kHz	9.75 W	80%	[29]
near field	190 kHz	265 W	90%	[48]
near field	14.9 kHz	4.8 kW	90%	[189]
near field	1 MHz	150 mW	10%	[107]
near field	1 MHz	-	90%	[114]
near field	10 kHz-1MHz	20 W	80%	[186]
near field	50 kHz	500 mW	75%	[97]

resistance increases because of skin effect [199], proximity effect [158] and eddy current losses in neighboring conductive objects [182]. The increase of resistance by skin effect and proximity effect can be calculated with existing equations [182], [161], [200]. More difficult is to calculate the eddy current losses in neighboring conductive objects, some analytical equations are given by [57], [92], [198].

In this article the frequency behaviour of inductors filled with water with different conductivities was studied, more specific the influence of the permittivity and conductivity of the water on the self-capacitance and AC losses of the inductor. The goal was to investigate single layer solenoids and show a general lumped circuit model which describes the losses and self-capacitance and their origin.

3.2   Theoretical section

The maximum efficiency η_{opt} with RIC can be calculated with Equation 2.3. With n the number of secondary inductors, k the coupling factor between the inductors and Q_p and Q_s the quality factors of the primary and secondary inductor. The coupling factor is the ratio of mutual inductance M (H) over the maximum value of mutual inductance $\sqrt{L_p L_s}$ that can exist between the primary inductor L_p (H) and secondary inductor L_s (H);

$k = M/\sqrt{L_p L_s}$. The coupling factor is a dimensionless quantity with a maximum value of 1.

The quality factor Q is a number of merit for inductors resulting from the ratio of inductive reactance ωL (Ω) over the AC resistance R (Ω), $Q = \omega L/R$. The quality factor is a dimensionless value with typical values between 1 and 1000 highly depend on the design of the inductor and the frequency. Inductors typically have a maximum value at a broad frequency range. The frequency dependence and the maximum quality factor depend on the dimensions and materials used in the inductor and the materials directly surrounding the inductor.

An inductor can be modeled with a basic lumped parameter circuit as seen in Figure 3.1. It consists of an inductance L (H), series AC resistance R_{AC} (Ω) and overall self-capacitance C_s (F) [122]. This basic model does
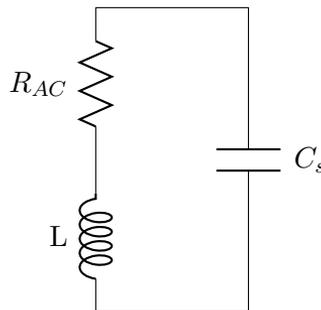
Figure 3.1: Basic lumped equivalent circuit of an inductor.

not fit the frequency behavior of inductors with water as core material. The adjusted lumped parameter circuit for inductors with water as core material can be seen in Figure 3.2. It consists of inductance L (H) with series resistance R_L (Ω) and two parallel capacitances with series resistances, C_1 (F), R_{C_1} (Ω) and C_2 (F) and R_{C_2} (Ω). L and R_L represent the inductive reactance and resistance. C_1 and R_{C_1} represent the turn-to-core capacitance; C_1 is a function of the permittivity of the core material, when the permittivity of the core is changed C_1 changes. C_2 and R_{C_2} represent the turn-to-turn capacitance; R_{C_2} is a function of the conductivity of the core

material, when the conductivity of the core material changes R_{C_2} changes.
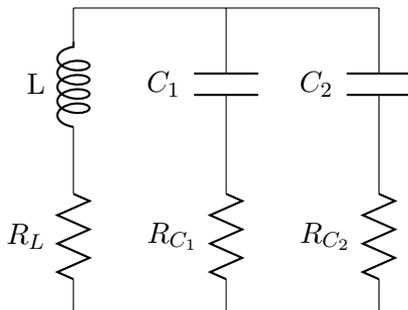
Figure 3.2: Lumped equivalent circuit of a water cored inductor, the inductance L (H) with series resistance R_L (Ω) and two parallel capacitances C_1 and C_2 (F) and two series resistances R_{C_1} and R_{C_2} (Ω).

3.3 Material and Methods

3.3.1 Inductors

The inductor used in the experiments was a single layer solenoid wound around a 1 liter laboratory beaker of borosilicate glass (VWR International LLC) (Figure 3.3). Experiments were conducted with the glass beaker (outer diameter was 0.09 m) and a volume of 1 liter of liquid resulting in a level of 0.18 m from the bottom of the beaker. Enameled (polyurethane) copper wire of 0.5 mm in diameter was wound tightly around the glass beaker, starting at 0.045 m from the bottom and directed upwards. The inductor had a total of 165 turns, a height of 0.09 m and diameter of 0.09 m. The inductance of the inductor was 1.80 mH measured at 10 kHz with water as core material. It was assumed that the magnetic field lines in the core of the inductor were enclosed by the liquid because no difference in self resonance frequency (SRF) was measured when the liquid level was at 0.18 m (1 liter) or at 0.16 m (900 ml). The SRF started to increase at liquid levels lower than 0.16 m.

Figure 3.3: Photograph of the inductor around a 1 liter glass beaker.

Air ($\epsilon_r = 1$), aceton ($\epsilon_r = 20.7$), ethanol 99.9% ($\epsilon_r = 32$), ethanol 70% ($\epsilon_r = 46$), glycerol ($\epsilon_r = 47$), ethanol 35% ($\epsilon_r = 63$) from VWR BDH prolabo and de-ionized water ($\epsilon_r = 80.1$) were used to vary the permittivity

of the core of the inductor. The conductivity of these liquids were all below
<1 μS/cm measured with a WTW 340i conductivity meter.

De-ionized water (MilliQ millipore) was used to fill the inductors and
99.5% analytical grade sodium chloride (VWR BDH Prolabo) was used to
increase the conductivity of the water. The conductivity was measured
with a WTW 340i conductivity meter.

3.3.2   Electrical measurements

The impedance of the inductor was measured with an HP 4194a impedance
analyzer, with 401 linear steps between 10 kHz to 1.2 MHz or 1.8 MHz,
depending on the SRF. The impedance of the inductor was measured with
water with different conductivities between deionized water <1 μS/cm and
water with conductivity of 3 mS/cm in 13 steps.

3.3.3   Fitting procedure

The results of the impedance analyzer were fitted to the equivalent circuit
seen in Figure 3.2. The value of L, R_L and C_1 were calculated from the
impedance of the inductors filled with de-ionized water. The inductance
L and resistance R_L were calculated from the real and imaginary part of
the impedance at 10 kHz, at this frequency it can be assumed that the
imaginary part of the impedance is entirely inductive. C_1 was calculated
from the SRF ω_{resd} of the inductor with de-ionized water $C_1 = 1/(\omega_{resd}^2 L)$
and R_{C_1} was determined by fitting. C_2 was calculated from the SRF ω_{resc}
of the inductor filled with conductive water, $C_2 = 1/(\omega_{resc}^2 L) - C_1$ Now five
parameters of the equivalent circuit were known and R_{C_2} was fitted for the
different conductivities.

3.4   Results and discussion

3.4.1   Self-capacitance with change in permittivity

The impedance of the inductor was measured with liquids with difference in permittivity and very low conductivities (<1 μS/cm). Because of the very low conductivity, R_{C_2} was very high, basically excluding C_2 from the model. The inductance and series resistance were fixed $L = 1.8$ mH and $R_L = 4.59$ Ω, for all the measurements with the various liquids at 10 kHz. R_{C_1} was calculated at 130 Ω. C_1 was fitted for the different permittivities and the results can be seen in Figure 3.4. The increase of the relative permittivity of the core material of the inductor increases the self-capacitance of the inductor. This shows that the turn-to-core self-capacitance of the inductor increases with increasing relative permittivity of the core material.

3.4.2   Self-capacitance of water filled inductor with change in conductivity

With deionized water as core material of the inductor, the SRF was measured at 820 kHz resulting in a turn-to-core capacitance C_1 of 21 pF. Increasing the conductivity of the water to values of 0.5 mS/cm and higher, the SRF shifted to 520 kHz (Figure 3.5). The turn-to-turn capacitance C_2 adds 31 pF in parallel resulting in a total self-capacitance of 52 pF.

The same experiment was done with a water/ethanol mixture of 65/35 %. The SRF was measured at 884 kHz resulting in a lower turn-to-core capacitance C_1 of 18 pF due to the lower permittivity of the water/ethanol mixture. When the conductivity of the water/ethanol mixture was increased the SRF shifted to 520 kHz for conductivities of 0.6 mS/cm and higher as can be seen in Figure 3.6. The turn-to-turn capacitance added 34 pF in parallel resulting in a total self-capacitance of 52 pF for the conductive water/ethanol mixture.

These results show the same self-capacitance for conductive core materials ≥ 0.5 mS/cm when the permittivity of the core material is different. The conductive core material results in turn-to-turn capacitance. From these results it was concluded that above a minimum value of conductivity,
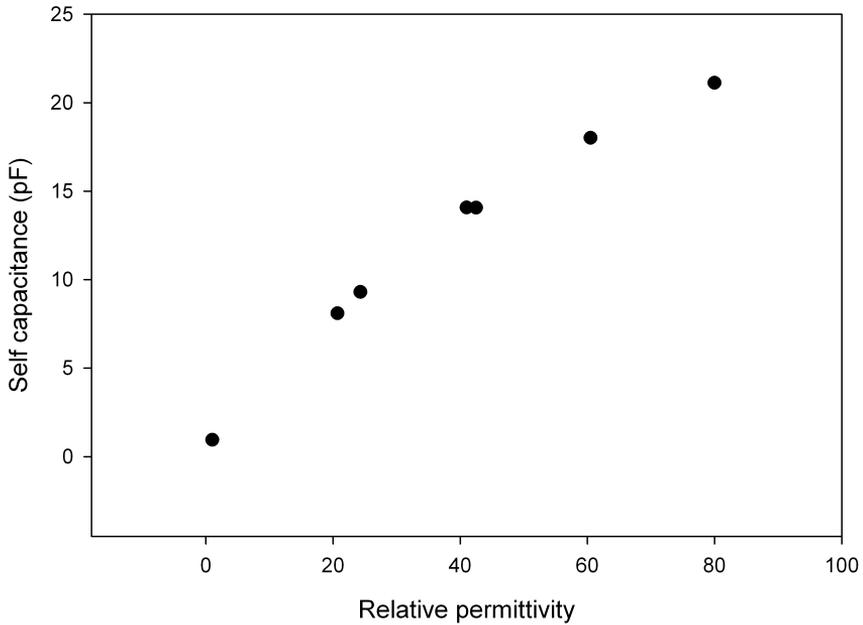
Figure 3.4: Self-capacitance of inductor filled with liquids with difference in relative permittivity.

the conductive core material shields the permittivity of the core material. At conductivities above a minimum value the permittivity has lost its effect on the self-capacitance.

Deionized water and water/ethanol mixture with conductivity $<1\ \mu$S/cm as core material show relative sharp peaks and high impedances in Figure 3.5 and 3.6. Also the most conductive water and water/ethanol mixture of 3 mS/cm as core material show sharp peaks and impedances in the same order of magnitude. The sharp peaks and high impedances imply low AC losses. The highest AC losses are around 50 μS/cm where the impedance

is lowest and peaks are softer.
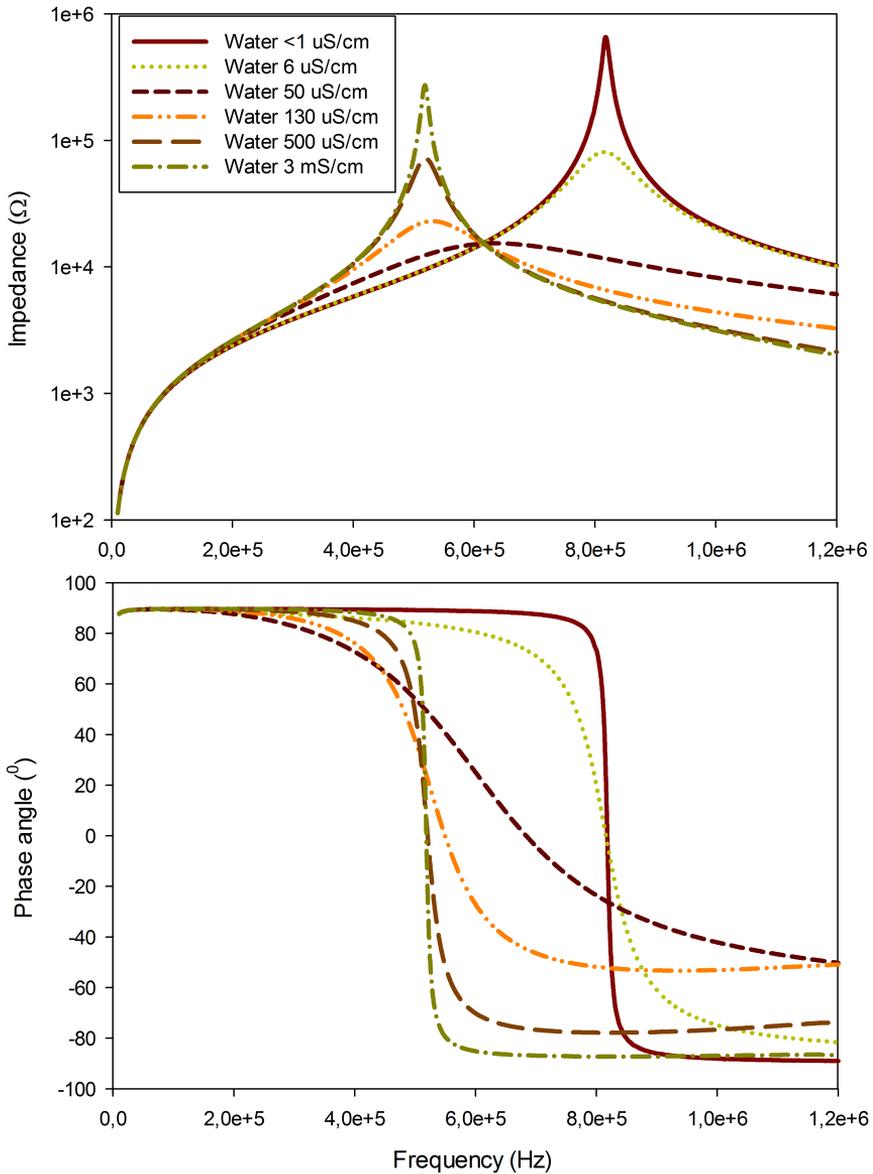
Figure 3.5: Impedance and phase angle as a function of frequency for inductor wound around the glass beaker, filled with water with different conductivities.
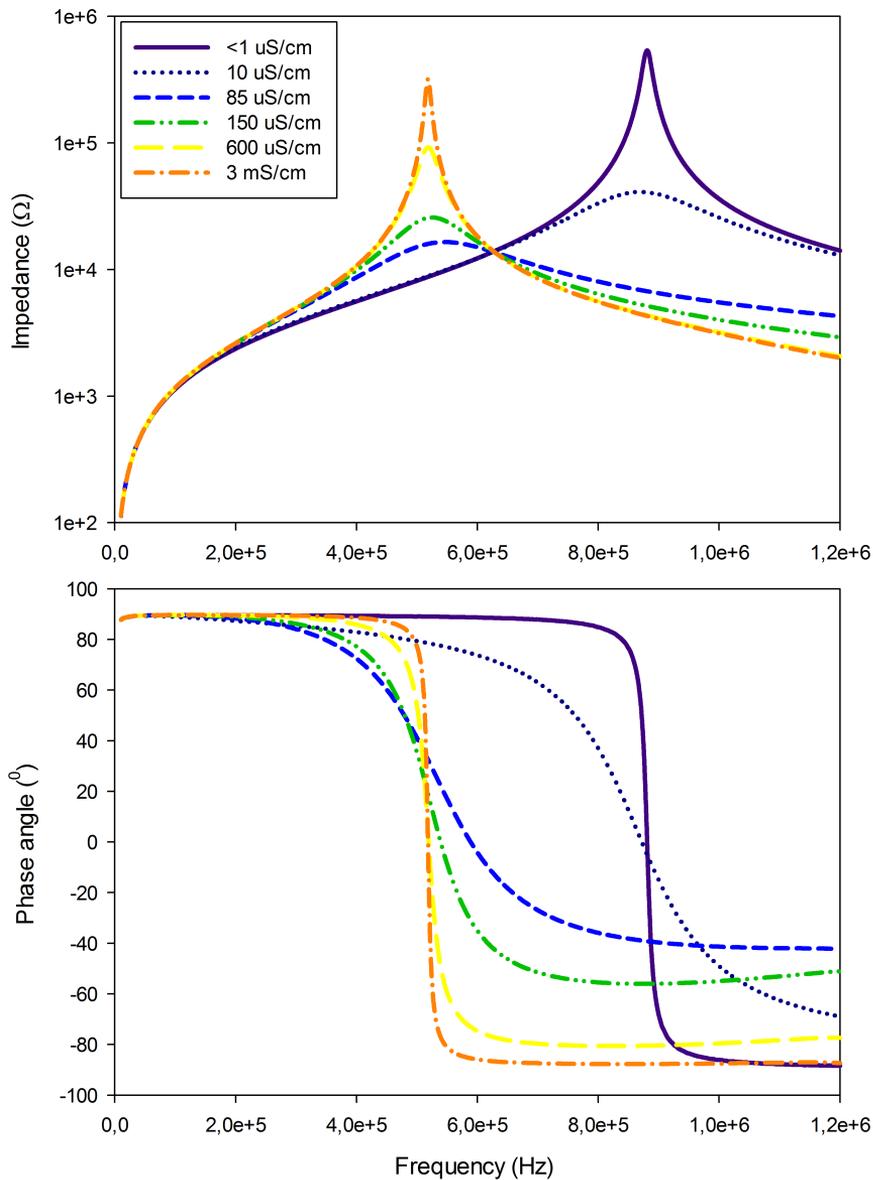
Figure 3.6: Impedance and phase angle as a function of frequency for inductor wound around the glass beaker, filled with water/ethanol mixture with different conductivities.

3.4.3   Lumped equivalent circuit for water filled inductor

The inductor around the glass beaker was modeled with the equivalent circuit of Figure 3.2. With water as core material the following parameters were calculated: L= 1.8 mH, R_L= 4.59 Ω, C_1= 21 pF, R_{C_1}= 130 Ω and C_2= 31 pF. The series resistance R_{C_2} of the second parallel capacitor C_2 was fitted to the impedance measurements of the inductor. The model fitted the measured values well. The fitted values of R_{C_2} can be seen in Figure 3.7. The values of R_{C_2} show a linear relation to the resistivity of the core material (in this case water). The coefficient of determination of the regression line is good $R^2 = 0.99$. This result shows that the regression line can be used to predict R_{C_2} for a given resistivity of the water.

3.4.4   Quality factor

The quality factor was calculated from the lumped circuit model with the predicted value of R_{C_2} and compared with the measured results. In Figure 3.8 the results of the measured and calculated quality factors can be seen. The quality factor of the inductor around the glass beaker filled with de-ionized water shows an optimum quality factor of 150 at 150 kHz. When the conductivity was increased, the quality factor decreased to 80 at 60 kHz, this can be explained by the addition of the second capacitance with a high initial series resistance. The resistance decreases with increasing conductivity resulting in an increase of quality factor to the value of 150 around 150 kHz. The results show that with a predicted value of R_{C_2} and the calculated parameters of the lumped circuit model a good prediction of the quality factor can be made. The frequency for the optimum quality factor is important for RIC. Since in a water-filled-inductor this optimum depends strongly on the conductivity of the water which must be taken into account for selecting the adequate operating frequency. The optimal frequencies depend on the dimensions of the inductor. The losses are due to resistive losses and the increase of self-capacitance of the inductors. Shielding of the inductor from the water makes the quality factor independent from the conductivity of the water. However, this results in a very low
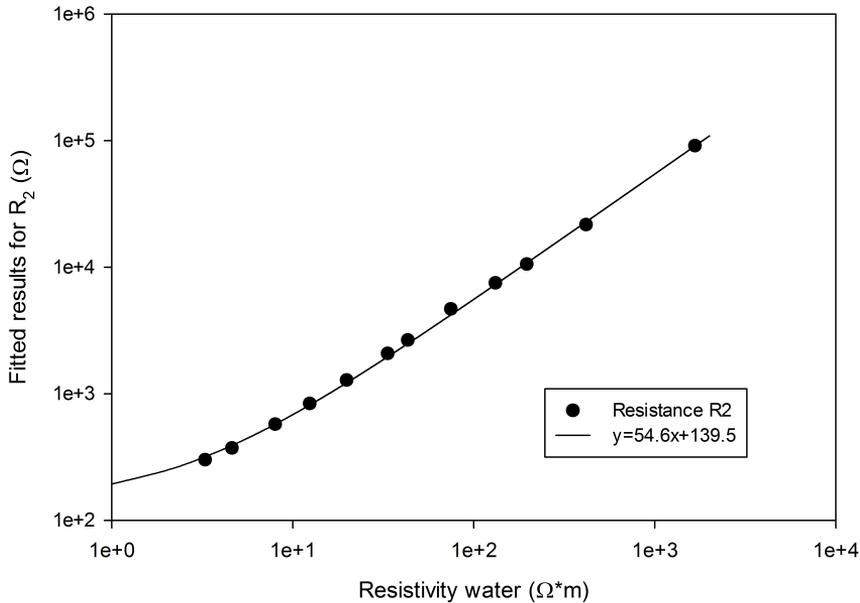
Figure 3.7: Fitted results of R_{C_2} (glass beaker inductor) as a function of resistivity water.

quality factor because of the losses in the conductive shielding.

The results show that the impedance measurements of an inductor can be used to measure the conductivity of an electrolyte and relative permittivity of non conductive materials. Additionally to the measurement of inductance and mutual inductance in non contact measurement techniques also the change in SRF of an inductor can be used as a non contact measurement technique and can be used for example to measure levels of non conducting dielectric liquids or conducting liquids.
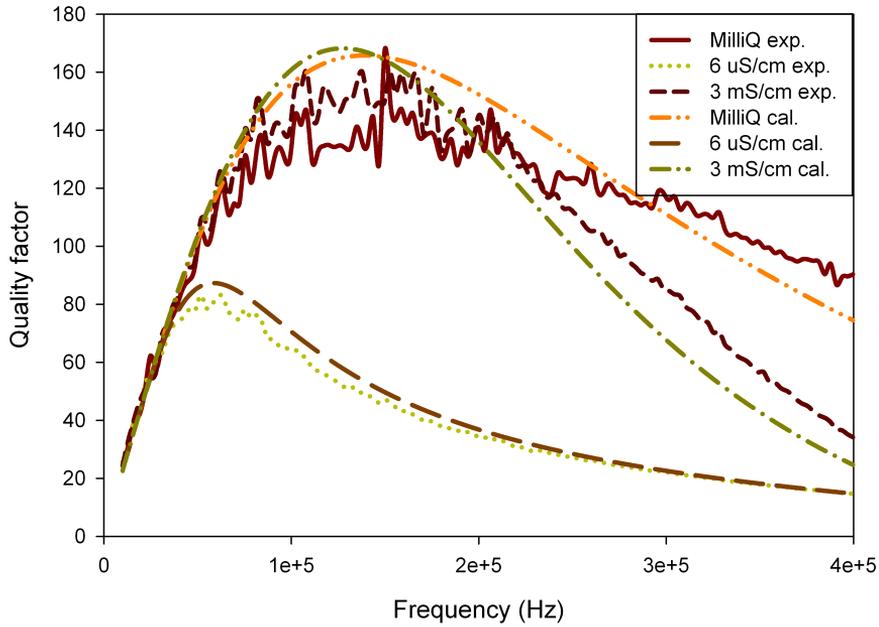
Figure 3.8: Quality factor as a function of frequency for the inductor wound around the glass beaker, measured and calculated with water with different conductivities.

3.5   Conclusions

For the losses and self-capacitance of an inductor the core material of the inductor plays a significant role. The permittivity of the core has influence on the turn-to-core capacitance of the inductor. When the core material is conductive this will lead to short cut of turns resulting in turn-to-turn capacitance also increasing the self-capacitance of the inductor. The changes caused by the core of an inductor can be modeled with the lumped parameter circuit shown in this article.

Acknowledgment

Chapter 4

Wireless desalination using inductively powered porous carbon electrodes

Abstract

Water desalination by capacitive deionization uses electrochemical cell pairs formed of porous carbon electrodes, which are brought in contact with the water that must be desalinated. Upon applying a cell voltage or current between the electrodes, ions are electrosorbed and water is produced of a reduced salinity. Such cells are directly connected to the electrical circuit via current collectors and wires. In this work we demonstrate for the first time wireless desalination by porous carbon electrode cells. Here, the cells are charged, at constant current, by wireless energy transfer via the mechanism of resonant inductive coupling (RIC) by the use of an external transmitting inductor that induces a magnetic field which is picked up by an energy receiving circuit which charges the electrodes one relative to the other. We present data for wireless power transfer, for charge transfer between one electrode and the other, and desalination degree, at various levels of the maximum cell voltage in cycles of a typical duration of a few minutes. In the present work, one wireless desalination cell is placed within the transmitting inductor, with the two porous electrodes placed parallel. A future design may use optimized spherical desalination capsules, placed in a packed bed or continuous fluidized bed water desalination reactor.

4.1 Introduction

Water is the most widespread substance to be found in the natural environment, playing an important role in both the environment and human life. Unfortunately, the majority of water i.e., 97.5% is saline water, which is not directly consumable. The remaining 2.5% fresh water is constituted by underground and surface waters. However, the greater portion of this fresh water i.e., 70% is present as solid water in glaciers, and 30% exists as fresh ground waters. Only a very small amount of 0.3% is stored in readily accessible lakes and rivers. Due to unequal fresh water distribution across the planet, as well as the anticipated population and economic growth, the stress on fresh water resources for agriculture, industry and households is rapidly increasing. Based on such developments, it has been estimated that by the year 2040 the world demand for freshwater will be greater than the amount available [42]. The most straightforward solution to increase the amount of fresh water is desalination of either of sea or brackish water.

Desalination is the general term to describe any process to separate salts from feed water, where the salts are preferably concentrated in a small volume of "brine" stream which is then discharged. For large scale production of fresh water the two commercially available technologies are Multi Stage Flash Distillation (MSF) [93] and Reverse Osmosis (RO) [64, 71, 60]. In recent times, novel approaches are being developed such as membrane-based desalination via ion concentration polarization in microporous media [119], systems based on batteries [148, 149], new types of membranes based on a single layer of graphene [44, 192] and desalination via capacitive deionization (CDI) [105, 210, 177, 74].

Capacitive Deionization (CDI) is a desalination technology in which an electric field is used to temporarily adsorb ionic species close to a charged surface [154]. This happens when two oppositely charged electrodes, are submerged into a solution containing ions. Upon applying a cell voltage difference between the two electrodes, an electric field is created in the solution, which causes ions to be transported towards the oppositely charged electrodes. Positive charged ions (the cations) are attracted to the negative charged electrode caused by the accumulation of electrons within the

porous carbon matrix. The exact opposite process occurs at the positive electrode, where the negative charged ions (anions) are attracted to the positive charged electrode caused by the depletion of electrons within the porous carbon matrix. Adsorption of ions is an interfacial process based on formation of an electric double layer and in order to have a maximum contact area between the electrode and the water, CDI employs high surface area porous electrode materials [193, 194, 162]. Various configurations of the CDI technology have been developed in order to improve the efficiency and design of deionization stacks. These include the application of, (i) either fixed porous carbon electrodes or movable carbon slurry combined with ion exchange membranes [86], (ii) chemically modified porous carbon materials [142, 204], (iii) different electrolyte flow patterns with respect to the porous carbon electrode position such as the flow-by configuration, where the electrolyte flows along the electrodes, or the flow-through configuration, where the water flows straight through the electrode [177, 17]. None of the developments mentioned above have focused on the way the electrons are transferred or pumped through a current collector into the carbon electrode. Typically this is achieved by a physical connection between an external power source and the current collectors or electrodes directly. The reversed process of CDI has recently been used to produce energy from the controlled mixing of river and sea water [19, 20].

In this work we demonstrate a different charging mechanism for CDI that has several potential advantages. We will combine CDI with "resonant inductive coupling" (RIC), as can be seen in Figure 4.1, which is a promising technology to power electronic devices wirelessly. In this technology electrical energy is transferred from a transmitting or primary inductor to a receiving or secondary inductor through the shared magnetic field. RIC has developed from charging batteries in toothbrushes [165] with low power and small distances between inductors, to the charging of batteries in electronic vehicles [189] with high power and larger distances between inductors. Many other applications [135] show advantages from being powered wirelessly by RIC, such as: biomedical equipment [94], mechatronic systems [48], household electronics [102], portable devices [29], and sensors [116].
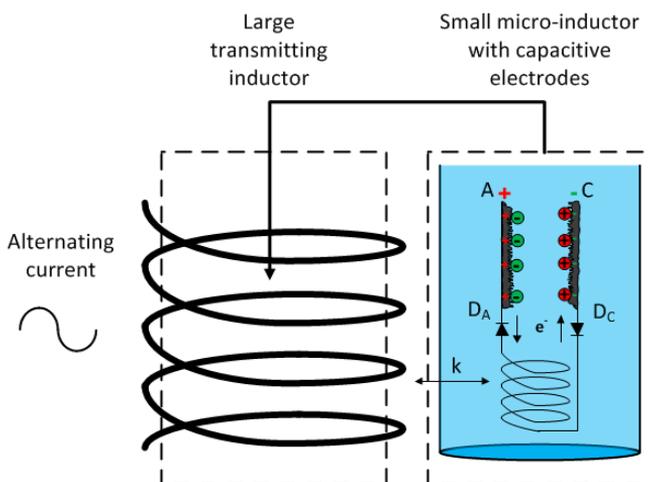
Figure 4.1: Schematic drawing of the experimental setup. A large transmitting inductor is wound around a beaker that contains water and a small inductor with capacitive electrodes. Alternating current of 45 kHz is applied to the large transmitting inductor. The small inductor is inductively coupled (k) to the transmitting inductor, inducing a voltage in the receiving inductor. The electrons (e^-) are forced by the diodes in one direction from the anode (A) to the cathode (C) by respectively the anode diode (D_A) and the cathode diode D_C. The charged porous carbon electrodes remove ions from the water by capacitive deionization.

For electronic devices used in water technology it can also be advantageous to be powered with RIC for reasons similar to the electric toothbrush, for instance safety against electric short-circuiting in water. Another advantage is the additional degree of freedom in the design of application of

these electronic devices in reactors. In water treatment technology, ions, chemicals and pathogenic microorganisms often have to be removed to a low concentration, and thus the rate of removal is slow [185]. Very often the kinetics of the processes are surface-related and thus, to attain a cost effective removal, the surface-per-volume ratio of a reactor has to be high. With the miniaturization of the electronic devices and increase of their number a very high surface area per reactor volume can be attained if these electronic devices are powered by RIC.

In Chapter 2 we showed that RIC can be used to power a multitude of small receiving inductors submerged and floating in water, with only one single transmitting inductor placed outside the water reservoir. With the increase of the number of small receiving inductors in the water vessel, the energy transfer efficiency increased with a factor scaling with the square root of the number of receiving inductors. In Chapter 3 we showed that the energy transfer efficiency was not retarded by the conductivity of water, but in fact the increase of conductivity of saline water (relative to deionized water) increased the energy transfer efficiency.

A combination of RIC with porous carbon electrodes coated with membranes allows the design of a desalination system that can operate as a packed bed or fluidized bed reactor, with multiple small devices each being charged by RIC. Each of those devices will be similar to the one single device that will be tested in the present study, and can be coated with ion exchange membranes which can be used to remove ionic species from water or other liquids. Related to the presented concept, systems powered with RIC may also include devices that are used to store energy, e.g. supercapacitors [155]. In summary, our work reports on the possibility of charging porous carbon electrodes with RIC, and demonstrate its application for water desalination using capacitive deionization. Note that in this study only the charging step is performed by RIC, while discharge is achieved by simple short-circuiting without energy recovery [50, 56]. However, a full desalination cycle consisting of an adsorption and desorption step can be achieved by implementing an extra controller which governs the moment that the electrical circuit opens (adsorption step) or closes (desorption step).

4.2 Experimental section

4.2.1 Transmitting and receiving circuit

To demonstrate validity of our wirelessly powered porous carbon electrodes approach, transmitting and receiving circuits were constructed. The AC source was a function generator, TG2000 from Thurlby Thandar Instruments, whose signal was amplified by a class AB amplifier from THEL type AccuSound 101. The transmitting inductor, (see Figure 4.2), was wound as a solenoid with a copper enameled wire, 0.4 mm in diameter, with 160 turns around a polyvinyl chloride (PVC) tube with a diameter of 0.075 m and a height of 0.065 m. The inductances, capacitances and resistances were measured with a HP 4194A impedance analyzer. The inductance of the transmitting inductor was 1.18 mH at 10 kHz and the quality factor QT was 65 at 45 kHz. Two parallel ceramic capacitors of 4.7 nF were connected in series with the inductor resulting in a resonance frequency of 45 kHz. A 1 Ω resistor was connected in series with the inductor and capacitor. The voltage over the circuit and over the 1 Ω resistor was measured with an oscilloscope from PicoScope 3000 series. From these two signals the difference in phase angle (Φ) between voltage over the circuit (V) and the voltage over the 1 Ω resistor (I) was calculated. Power was calculated with: $P_t = cos(\Phi)VI$.

The receiving circuit, (see Figure 4.3), consisted of a ferrite cored inductor from Fastron with a diameter of 0.007 m and a height of 0.01 m, the induction was 10 mH at 10 kHz with a quality factor of 90 at 45 kHz. A 1 nF ceramic capacitor and a bridge rectifier, B80C1500G from Vishay, were connected in series. Carbon slurry was prepared by adding 85 wt% of activated carbon, 5 wt% of carbon black and 10 wt% of polymeric binder (PVDF) (to N-methyl-2-pyrrolidone with a 30:1 NMP:PVDF weight ratio). Electrodes were prepared by painting platinum coated titanium plates which served as a current collector and support layer, with the carbon slurry, and drying in air. The average coating thickness after three applications of slurry was approximately 230 μm, and mass of a single carbon electrode was 0.041 g. The power received at the electrodes was calculated with: $P_r = I^2 R_L$. The
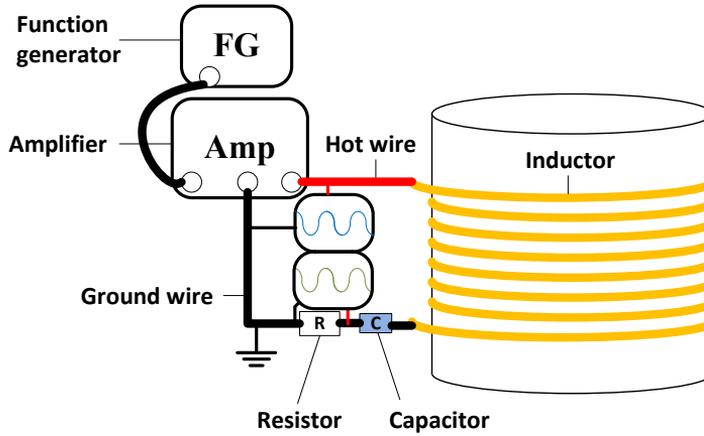
Figure 4.2: Scematic drawing of the transmitting circuit with the function generator and amplifier as the AC source, the inductor, capacitor, resistor and oscilliscope. The hot wire is the wire with non-zero potential.

energy transfer efficiency was calculated with the following equation:

$$\eta = \frac{I^2 R_L}{P_t} \tag{4.1}$$

where I stands for the current measured during salt removal step, R_L is the resistance of the load (rectifier plus electrodes) and P_t the power applied to the transmitting circuit.

4.2.2   Desalination experiments

Desalination experiments were performed using one receiving inductor and one pair of carbon electrodes, see Figure 4.3. The distance between the electrodes was equal to 1 mm. Electrical wires running from the electrodes were connected to a potentiostat which was only used to measure the cell voltage during salt removal step and the current during the salt release step;
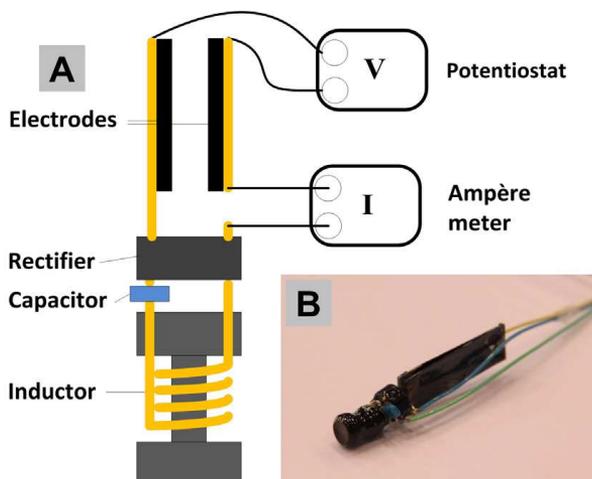
Figure 4.3: (A) Schematic drawing of the receiving circuit combined with two electrodes coated with porous carbon. (B) Photograph of the receiving circuit and two parallel carbon electrodes used for wireless water desalination.

it was not used to charge the cell or apply a voltage (Iviumstat, IVIUM Technologies, Eindhoven, The Netherlands). The current that is generated due to RIC between the electrodes during the salt removal step was measured with an Ampre meter (Fluke 8845A precision multimeter), connected in series between the rectifier and one of the electrodes. The experiments were based on sequentially adsorbing and releasing ions inside two saline water compartments, with equal initial salt concentrations, similar to that presented by Porada et al. [153]. The receiving circuit was placed inside the freshwater compartment of a total volume of V= 10 mL. At the start of an experiment, the alternating current to the transmitting circuit was switched on. The induced alternating current in the receiving inductor was then rectified into direct current. As a result a constant electrical current

flows in the receiving circuit, directed from one porous electrode to the other, thus driving the ion adsorption step. After reaching a defined maximum cell voltage difference, the receiving circuit was manually lifted from the freshwater compartment and inserted into the brine compartment, with the same total volume as the freshwater compartment. In the brine compartment, the previously adsorbed ions were released upon short-circuiting the cell (V_{cell}= 0 V) for t= 500s and the electrical current was measured. Experiments with various maximum cell voltages and number of desalinations cycles were performed. The concentration changes of the chloride ion, Cl^-, inside the freshwater and brine compartment were measured with ion exchange chromatography as function of time, to calculate the NaCl salt uptake by the pair of electrodes.

4.3   Results and discussion

In this section we show the results of ion adsorption by porous carbon electrodes powered by resonance inductive coupling, focusing on proof-of-principle and not on process optimization itself. At the end of this section we discuss several possible improvements that may further develop the presented concept.

Results of the generated current between the two electrodes and the build-up of cel voltage are presented in Figure 4.4. As a consequence of wireless energy transfer, a constant current (CC) of 75 mA/g flowed between the two porous carbon electrodes, see Figure 4.4. Note that this operational mode is different from the widely used constant voltage (CV) mode of operation in CDI, where a constant voltage is applied during the ion removal step. CC has been described recently, and can produce freshwater with a stable salt concentration in the effluent, unvarying in time [208]. The electrical constant current running between the two capacitive porous electrodes is compensated by the ionic flux of both positive and negative ions present in solution. The salt adsorption step lasts until the defined maximum cell voltage difference was reached, for instance in Figure 4.4 until V_{cell}=1.2 V. To regenerate the carbon electrodes, the device (pair of CDI

electrodes and ERC) was manually lifted from solution, and inserted into the brine compartment in which upon shortcutting the electrodes current flowed in the opposite direction (insert of Figure4.4), leading to ion release and an increase in salt concentration.
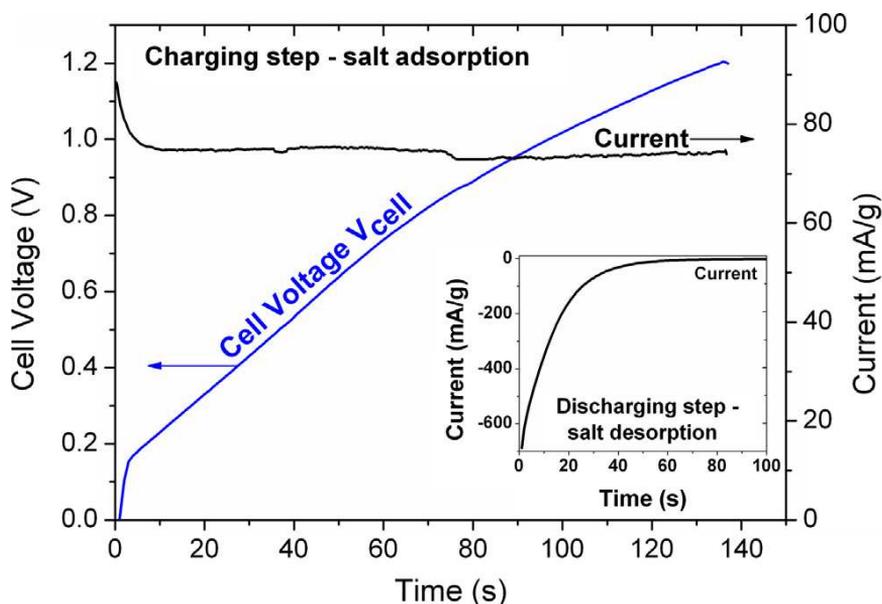
Figure 4.4: Experimental data for the cell voltage between the two porous electrodes of the wireless CDI design, V_{cell} (blue line), and current (black line) in one desalination cycle upon wireless energy transfer by resonant inductive coupling (RIC). Insert shows desorption step during which current flows in the opposite direction.

Figure 4.5 shows the salt adsorption calculated per gram of both electrodes combined and charge transfer per cycle as a function of the total number of desalination cycles, both for the adsorption and the desorption step. With an increasing number of cycles the salt adsorption per cycle

decreases, while the charge transfer remains constant. The decrease of salt adsorption is due to undesired effect of water adhering to the outside of the receiving circuit and the carbon electrodes. This adhering water, once the device is being transferred back from the brine to the freshwater compartment, slightly increases the concentration of salt inside the freshwater container, and so is a limiting factor for the achievable concentration difference between the two compartments that initially had equal salt concentration. The decrease of salt adsorption per cycle with increasing the total amount of cycles, can not be explained by a higher resistance of adsorption at lower salt concentrations in the freshwater compartment because than one would expect the time duration of each of the following cycles to decrease. However, this was not observed during the performed desalination experiments.

Next, in Figure 4.6 we show the salt adsorption and charge per cycle, measured during the adsorption and desorption step, and defined per gram of both electrodes, vs. the maximum cell voltage difference. For all the experimental conditions tested we observe that a higher maximum cell voltage (and therefore an elongated ion adsorption step) leads to higher salt removal and charge storage capacities per cycle. Secondly, for a maximum cell voltage above 1.0 V we observe a difference in charge transfer between the adsorption and desorption step. This is especially clear for the maximum cell voltage of 1.4 V where this difference is significant and may originate from undesired faradaic reactions e.g., porous carbon oxidation, water chemistry or carbon redox reactions [154, 17, 106, 209].

Figure 4.7 shows the power received at the load and the power transfer efficiency to the load as function of the power input in the transmitting circuit. The resistance of the load (R_L) consists of the resistance of the bridge rectifier (R_{BR}) and the resistance of the electrodes (R_E), $R_L = R_{BR} + R_E$. R_L was unknown and could not be accurately measured due to the nonlinear ohmic behavior of the bridge rectifier, R_E was 20 Ω in a 20 mM solution. With equation 1 and 4, both R_L and the power transfer efficiency η were calculated. With increasing power input, R_L decreased due to the nonlinear behavior of the bridge rectifier resulting in higher power transfer efficiency. The highest power transfer efficiency of 18.5% was calculated for 700 mW
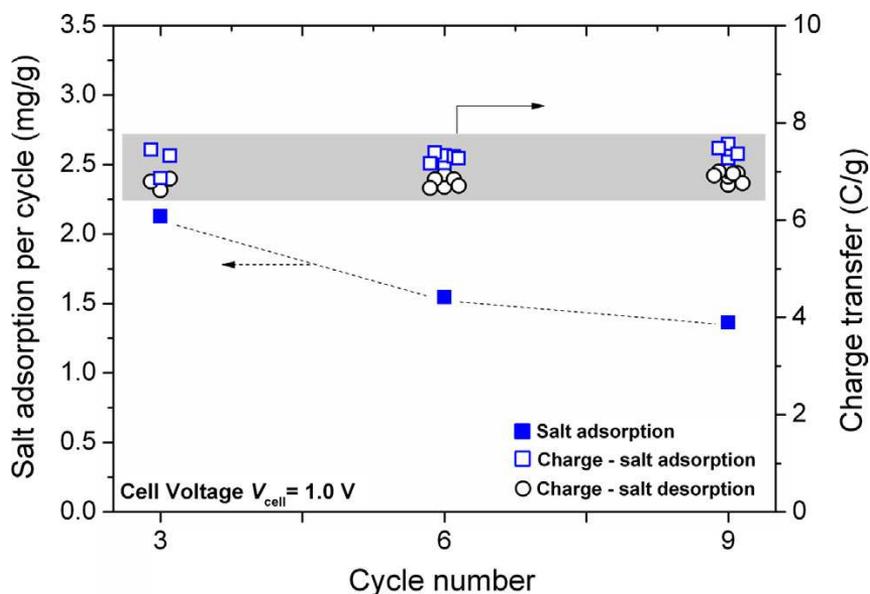
Figure 4.5: Experimental data of salt adsorption and charge transfer per cycle as function of total number of desalination cycles, $c_{salt}= 20$ mM, data given per mass of both electrodes. Each desalination cycle consist of ion adsorption and desorption step.

power input, with R_L of 1.96 kΩ. Because the resistance of the bridge rectifier during these experiments was a factor of 100 larger than the resistance of the electrodes, 99% of the input power was captured by the bridge rectifier and only 1% was utilized by the porous carbon electrodes. Increasing the percentage of the power received by the porous carbon electrodes can be done by: (i) decreasing the resistance of the bridge rectifier, (ii) increasing the power input or, (iii) by using a bridge rectifier with lower resistance at lower power. The minimum series resistance of the type of bridge rectifier used in this research is 1 Ω, theoretically resulting in < 5% of the power
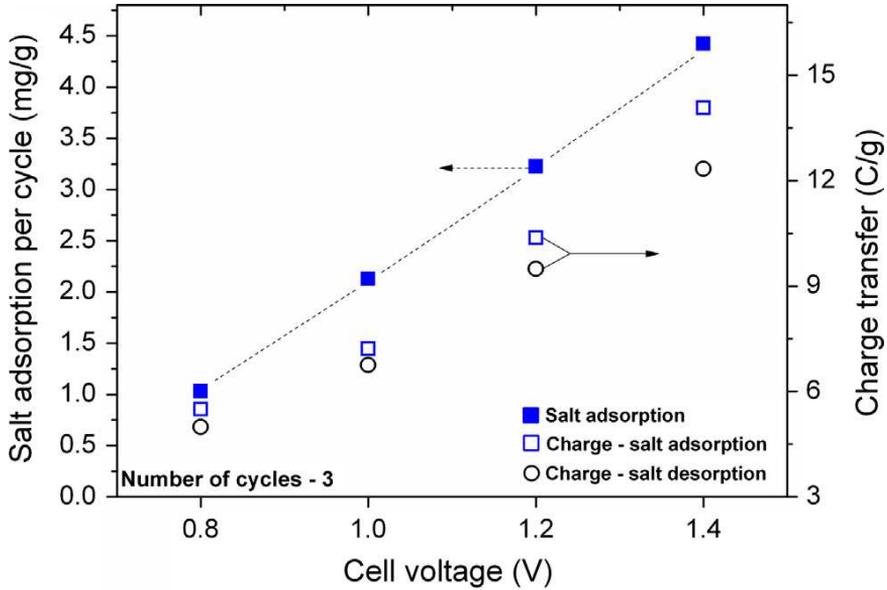
Figure 4.6: Experimental data of salt adsorption and charge transfer per cycle in wireless desalination, as function of maximum cell voltage difference, c_{salt}= 20 mM, data given per mass of both electrodes.

going to the rectifier and >95% of the power going to the electrodes.

   Furthermore the energy transfer efficiency of 18.5% was low compared to the optimal efficiency of 60% calculated with equation 3. The lower efficiency was due to the fact that the resistance of the load was not matched to the rest of the system. By matching the load to the system and increasing the number of receiving circuits to 25, an energy transfer efficiency of ¿90% can be achieved. The 25 receiving inductors will occupy 3.4% of the volume inside the transmitting inductor. Miniaturizing the receiving circuits will lead to a lower energy transfer efficiency but this can be overcome by increasing the number of receiving circuits. Keeping the volume percentage
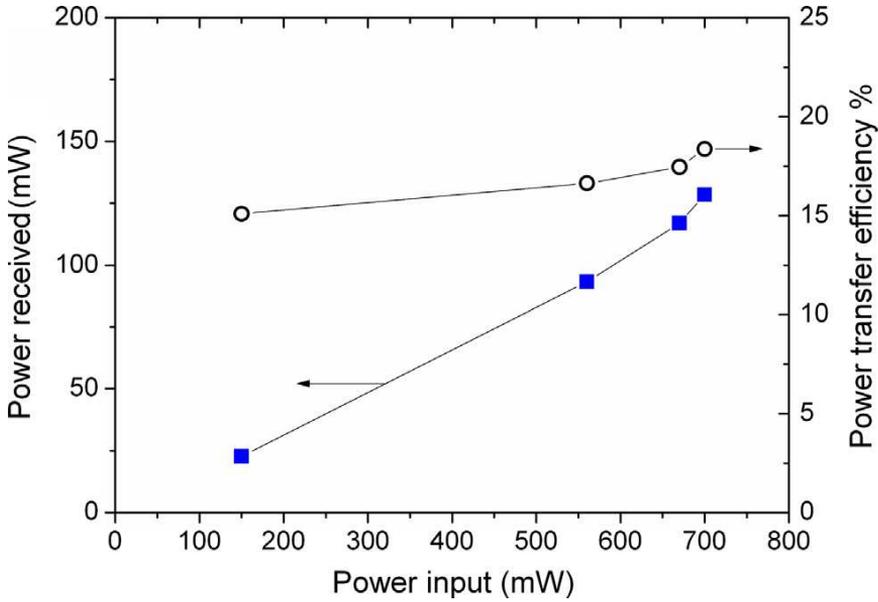
Figure 4.7: Power received at the load and the power transfer efficiency as function of the power input in the transmitting circuit.

of receiving inductor the same (3.4%) or higher will result in comparable, or higher energy transfer efficiency. The miniaturization will result in a higher surface per volume ratio, intensifying the removal of ions from saline water.

4.4 Conclusions

In conclusion, we have shown experimentally the possibility to wirelessly power porous carbon electrodes by application of resonant inductive coupling of an external electrical circuit to a miniature "energy receiving circuit" which charges one capacitive electrode relative to the other. This solu-

tion unlocks new cell design possibilities for water desalination technology using capacitive deionization (CDI) which utilize "desalination capsules" made of porous carbon electrodes, a receiving circuit, and ion-exchange membranes coated on the outside. Such capsules can freely flow or float inside either a packed bed or fluidized bed reactor without requiring the compartimentalization of standard CDI designs with fixed electrodes, or flowing carbon slurries. In sequence to desalination, regeneration (salt release) can be performed outside the freshwater compartment. The absence of thin channels and spacers, reduces fouling risk and pressure drop in the system. Various improvements of the presented concept are possible that can significantly increase power transfer efficiencies. The concept of wireless desalination can also be adapted to harvest energy from mixing river and sea water with the advantages of lower power losses due to pressure differences, and less stringent requirements of water pretreatment [162, 19, 20].

Acknowledgements

Chapter 5

Modeling of immersed UV-LEDs in a suspension of TiO$_2$ photocatalyst

Abstract

The purpose of this research was to investigate the optimal TiO_2 loading for UV-LEDs. A simple model is used that couples a radiation field model with a reaction kinetics model. The radiation field model is verified with experimental results and shows good fits. The reaction rate of a 10 mW radiant power UV-LED and 250 mW radiant power UV-LED are modeled as a function TiO_2 loading and show good fits to experimental results. The 250 mW radiant power UV-LED has a sharp optimum TiO_2 loading at 0.5 g/l and the 10 mW radiant power UV-LED showed a broader optimum TiO_2 at 1.44 g/l. The model predicts that the optimal TiO_2 loading increases for decreasing radiant power of UV-LEDs.

5.1 Introduction

Stress on existing water sources is high and will most likely increase further in the coming decades because of the simultaneous rise in population and water consumption of people [171]. A part of the solution can be in the reuse of treated wastewater [76]. Wastewater is often treated by aerobic or anaerobic biological treatment to remove macropollutants like organic pollutants, nitrogen and phosphorus. Micropollutants, however, are not well removed with biological treatment [49, 77]. Advanced oxidation processes are suitable to remove micropollutants and generally use strong oxidative species to oxidize the organic compounds. A promising AOP is heterogeneous photocatalysis which is based on catalyzed photolysis by a solid state semiconductor [127]. Heterogeneous photocatalysis is able to oxidize or transform organic pollutants, inorganic pollutants, pathogenic microorganisms and viruses at ambient temperature and without extra addition of oxidant chemicals [14, 82]. One of the challenges to develop heterogeneous photocatalysis further is the design and optimization of photocatalytic reactors for use on large scale [134]. Model based studies are a helpful tool to investigate the design, optimization and scale-up of photocatalytic reactors [30, 111]. Next to the usual parameters involved in designing, optimizing and scaling-up of chemical reactors, photocatalytic reactors have an additional parameter in the irradiation properties of a reactor [134]. A radiation field model is therefore a useful tool for the development of a photocatalytic reactor. A number of experimental studies have shown the importance of the intensity of the incident radiation on the reaction kinetics [145, 143, 129] and comprehensive models have been developed to combine the radiation field and reaction kinetics [111, 110, 45].

Most experimental and model based studies deal with the use of solar light or artificial light from mercury lamps as light source. Solar light has a broad emission spectrum but only a small percentage ($<5\%$) [197] of the solar energy is useful for the excitation of the photocatalyst, TiO_2. Mercury lamps are gas discharge lamps emitting UV light. A relative new light source for photocatalytic reactors are ultraviolet light emitting diodes (UV-LEDs). UV-LEDs are solid state light sources and compared to mercury

lamps, UV-LEDs are compact and robust, UV-LEDs are available with emission wavelengths between 210 and 400 nm with narrow bandwidth of the emitted wavelength ($\pm$ 5 nm) and power is low [174]. Recent studies have shown that UV-LEDs can compete with mercury discharge lamps as light source for photocatalytic oxidation [66]. Studies can be found on the modeling of UV-LEDs in reactors for odor abatement process [196] and for designing LED arrays [133], however, no studies can be found on the modeling of UV-LEDs in photocatalytic reactors for water treatment.

In this paper, a model is presented that couples a simple radiation field model with reaction kinetics. Methylene blue was used as a model compound to verify the model. The effect of the radiant power of the UV-LED on the optimal loading of TiO_2 was simulated and measured. The influence of the radiant power and the loading of TiO_2 on the illuminated surface area of a reactor is discussed. The model provides a useful tool for the design, optimization and scale-up of photocatalytic reactors.

5.2   Materials and methods

5.2.1   Radiation field model

A radiation field model was developed to determine the optimal loading of the catalyst for UV-LEDs. We considered an UV-LED as a point-source with a limited emission angle. Radiation from a point source is inversely proportional to the square of the distance from the source. Light traveling through an absorptive media is described by combining the inverse-square law with the Lambert-Beer law:

$$I_r = \frac{P10^{-Ar}}{r^2\Omega} \tag{5.1}$$

With r distance from UV-LED (cm), Ω the solid angle, I_r intensity (mW*cm^{-2}), P radiant power of the UV-LED (mW) and A the absorption coefficient (cm^{-1}) of the media. The solid angle was calculated from the emission angle ϕ of the UV-LED:

$$\Omega = 2\pi(1 - cos(\phi)) \tag{5.2}$$

5.2.2 Reaction kinetics model

In an illuminated photocatalyst particle, electron-hole recombination and interfacial electron-hole transfer are second and first order processes respectively. The density of electron-hole pairs increase with increasing absorbed light flux. The rate of electron-hole pair recombination is increased more relative to the electron-hole transfer and leads to a lower quantum efficiency at strong illumination [151]. This can be observed with the rate of photocatalytic oxidation following a linear increase as function of absorbed light flux below a certain threshold value of absorbed light flux. Above this value the rate increases with a square root function of absorbed light flux [118]. Many studies report 25 mW.cm^{-2} as the threshold value of absorbed light flux. The following equations were used in the model to represent the intensity dependency of the reaction rate:

$$I_a = -\frac{1}{r^2}\frac{d(I_r r^2)}{dr} \tag{5.3}$$

$$rate = fI_a \qquad\qquad (I_{min} < I_a < I_{trsh}) \tag{5.4}$$

$$rate = fI_a I_{trsh}^{0.5} \qquad\qquad (I_a > I_{trsh}) \tag{5.5}$$

$$rate = 0 \qquad\qquad (I_a < I_{min}) \tag{5.6}$$

With I_a the absorbed light flux (mW/cm^3), f, the quantum coefficient converting the amount of absorbed photons to oxidation rate (mg/mW), I_{trsh}, the treshold value of absorbed light flux above which the rate starts to increase with a square root function (mW/cm^3). I_{min}, the value absorbed light flux below which the oxidation rate is zero (mW/cm^3). The apparent reaction rate is calculated by averaging the local rates.

5.2.3   Chemicals and reagents

Methylene blue was obtained from Boom BV. Titanium dioxide (Aeroxide TiO_2 P25 Degussa) was obtained from Evonik Industries. All solutions were prepared with ultrapure water (MilliPore MilliQ). For the experiments determining the reaction rate, 500 ml of 15 mg/l methylene blue solutions were made to which TiO_2 was added. The suspension was sonificated for 30 minutes in an ultrasound bath to attain equal particle size distribution.

5.2.4   Photocatalysis experiment

The photocatalysis experiments were done in a reactor containing 500 ml of a TiO_2 suspension in a methylene blue solution. The UV-LEDs were submerged in the solution and turned on. During the experiments samples were taken every 5 minutes and the experiment was stopped after 60 minutes of irradiation.

5.2.5   Sample preparation and analysis

The samples were centrifuged for 3 hours at 14000 rpm with an eppendorf centrifuge. After centrifugation, the supernatant was diluted 10 times and analyzed for absorbance at 664 nm with a Shimadzu UV/VIS spectrophotometer.

5.2.6   UV-LEDs

UV-LEDs were obtained from Nichia. Two types of UV-LEDs NSPU 510 CS and NCSU 033B were used in the experiments. The radiant power of the NCSU033B was measured and increased linearly as a function of input power between 1 mW and 300 mW. The radiant power was measured with the radiometer from International Light. The UV-LEDs were powered by a Delta power supply. The voltage and current were measured with two FLUKE 8845A Precision Multimeters. The NSPU 510 CS was used in the experiments with a radiant power of 10 mW and the NCSU 033B was used

with a radiant power of 250 mW. Both UV-LEDs had an emission angle of 115 degrees.

5.2.7 Light intensity distribution measurements

The light distribution was measured with a photodiode, silicon photodetector OSD 5T from Centronic. The photodiode was mounted on a custom made robotic arm that was controlled with Matlab software. A scan was made of the light intensity in a horizontal plane perpendicular to the irradiation direction the UV-LEDs were irradiating towards.
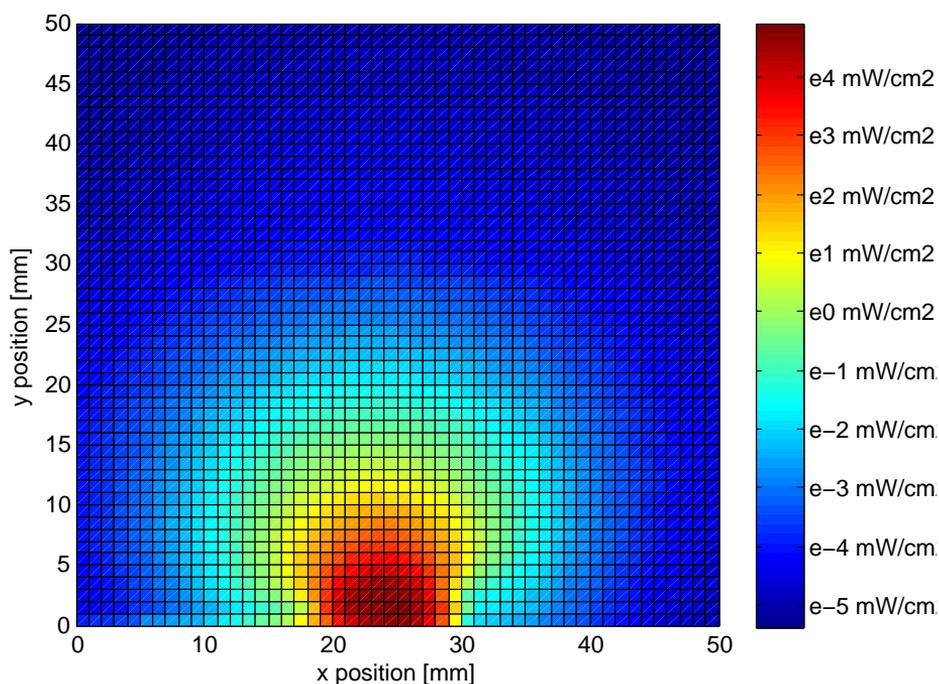
Figure 5.1: Light intensity measurement of 250 mW UV-LED in a TiO_2 suspension of 0.5 gl^{-1}

5.2.8 Calculation of reaction rate

The first order rate constant was calculated from experimental data with, $lnC_0/C = -k_{app}t$ and reaction rate follows from $r = k_{app}C$. With C_0, the start concentration, C, the concentration at time t, k_{app}, the first order rate constant and r, the reaction rate.

5.3 Results and discussion

5.3.1 Radiation field

Figure 5.1 shows the experimental light intensity as a function of the position for a 250 mW UV-LED in a TiO_2 suspension of 0.5 gl^{-1}. The light intensity was fitted with Equation 5.1 as can be seen in Figure 5.2 with an emission angle of 115 degrees and an absorption coefficient of 0.14 cm^{-1} for 0.1 g/l TiO_2 and 0.7 cm^{-1} for 0.5 g/l TiO_2. The specific absorption coefficient for TiO_2 is 1.4 l/g cm. The photodiode showed saturation above 100 mW*cm^{-2} and below 0.02 mW*cm^{-2}. The model shows a good fit with the results and gives confidence to model the light intensity with Equation 5.1.

5.3.2 Reaction rate as a function of TiO_2 loading with a 10 and 250 mW UV-LED

Figure 5.3 shows the relative reaction rate as a function of the TiO_2 loading with a radiant power of 10 mW and 250 mW. Both the 10 mW and 250 mW UV-LED show an optimum TiO_2 loading where the relative reaction rate is highest. The optimum is around 0.5 g/l TiO_2 for the 250 mW UV-LED and 1.5 g/l TiO_2 for the 10 mW UV-LED. The model fits measured results well. The 250 mW UV-LED has a sharp optimum and the relative reaction rate decreases significantly after 0.5 g/l. The 10 mW UV-LED has a broader optimum and the relative reaction rate does not decrease as steep as compared to the 250 mW UV-LED. These results show the strong dependency of the radiant power of the UV-LED on the reaction
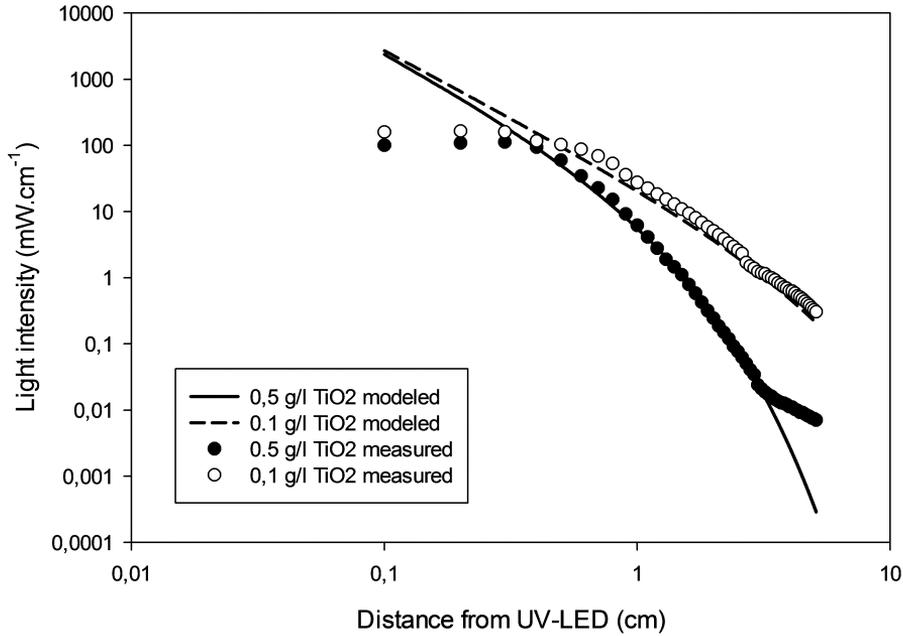
Figure 5.2: Light intensity measurement and modeled of 250 mW UV-LED in a TiO_2 suspension of 0.5 and 0.1 gl^{-1}

rate. The model can be used to predict the optimal TiO_2 loading for a UV-LED. Figure 5.4 shows the optimal TiO_2 loading as a funtion of the radiant power of the UV-LED calculated with the model. The results show a good fit with an inverse cube root $L_{TiO_2} = 3.1P^{-1/3}$, with L_{TiO_2}, the optimal loading of TiO_2 and P, the radiant power of the UV-LED.
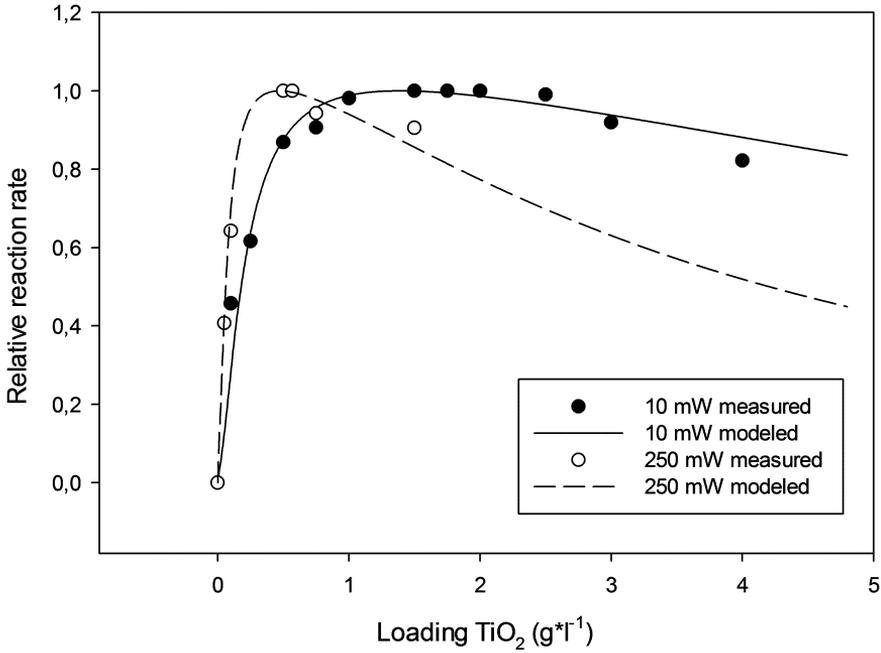
Figure 5.3: Relative reaction rate as function of TiO_2 loading measured and modeled with 10 and 250 mW radiant power UV-LEDs

5.3.3 Optimal TiO_2 loading as a function of emission angle

Figure 5.5 shows the hypothetical relation between the emission angle and optimal loading followed from the data of the model. The data from the model show that an increase in emission angle results in a higher optimal loading of the TiO_2.

An important parameter used to indicate the reactivity of a photo-catalytic reactor is the amount of illuminated surface area per reaction liquid volume (κ)[159, 185]. The loading of TiO_2 determines the maximum amount of surface area per reaction liquid volume. The developed model
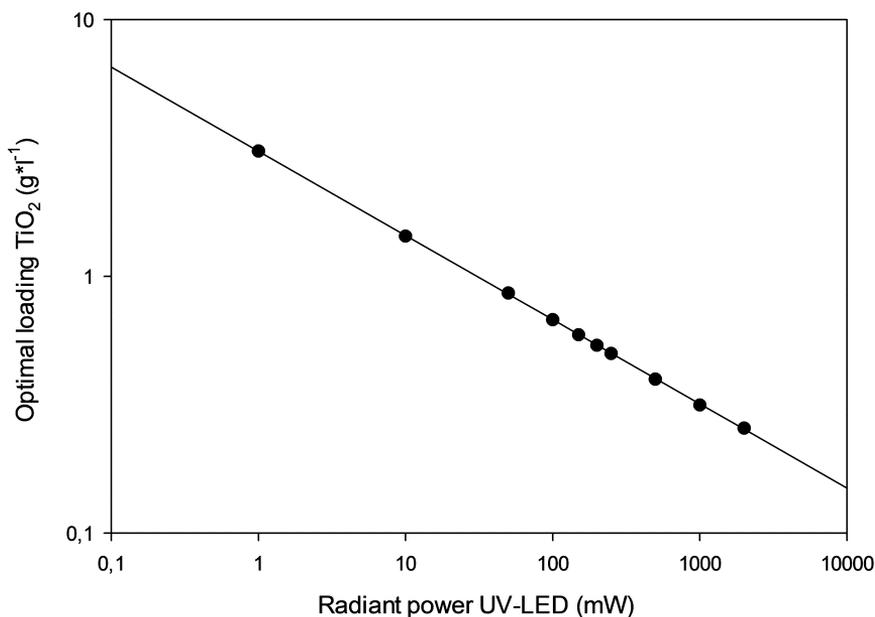
Figure 5.4: Optimal loading as function of the radiant power of the UV-LED

shows an inverse cube root relation between the radiant power of the UV-LED and optimum loading of TiO_2. The UV-LEDs with low radiant power result in high loading of TiO_2 and therefore high surface area per reaction liquid volume. One UV-LED with low radiant power illuminates however a small part of the total surface area due to the shallow penetration depth caused by the high loading. To attain a high illuminated surface per reaction liquid volume a high number of UV-LEDs need to be used. Currently LEDs of 200 μm by 200 μm by 100 μm are developed. In this size UV-LEDs can also be produced. With a high number of these micro-UV-LEDs a very high illuminated surface area per reaction liquid volume can be reached with an equal distribution of absorbed light flux over the photocatalyst

surface area resulting in high photocatalytic efficiency.

In this study we used the Lambert-Beer law to describe the absorption of light in the media. Other models include scattering from the photocatalyst particle [111]. Those models more closely represent nature but also increase the complexity of the models and increase the number of parameters which have to be measured or estimated.

Previous studies shown inverse relationship between absorbed light flux and quantum efficiency [151, 4, 3, 58, 131, 95, 145, 150]. High radiant power results in lower quantum efficiency but high irradiated surface. With micro-UV-LEDs, still a high overall degradation can be obtained by using a high number of micro-UV-LEDs. More research needs to be done on the increase of quantum yield with application of low radiant power micro-UV-LEDs. Peill and Hoffmann [150] showed that quantum efficiencies can be increased with smaller optical fibers distributing light with lower light intensity. Similar results can be reached with micro-UV-LEDs with low radiant power.

5.4   Conclusions

This study shows that the optimal loading of TiO_2 has a inverse cube root relation with the radiant power of a UV-LED. A model was developed and verified with experimental results. The model can be used as a tool to design and optimize photocatalytic reactors with suspended photocatalyst and immersed UV-LEDs as light source. A high number of micro-UV-LEDs can irradiate a large surface area with an efficient absorbed light flux resulting in an efficient photocatalytic process.

Acknowledgements
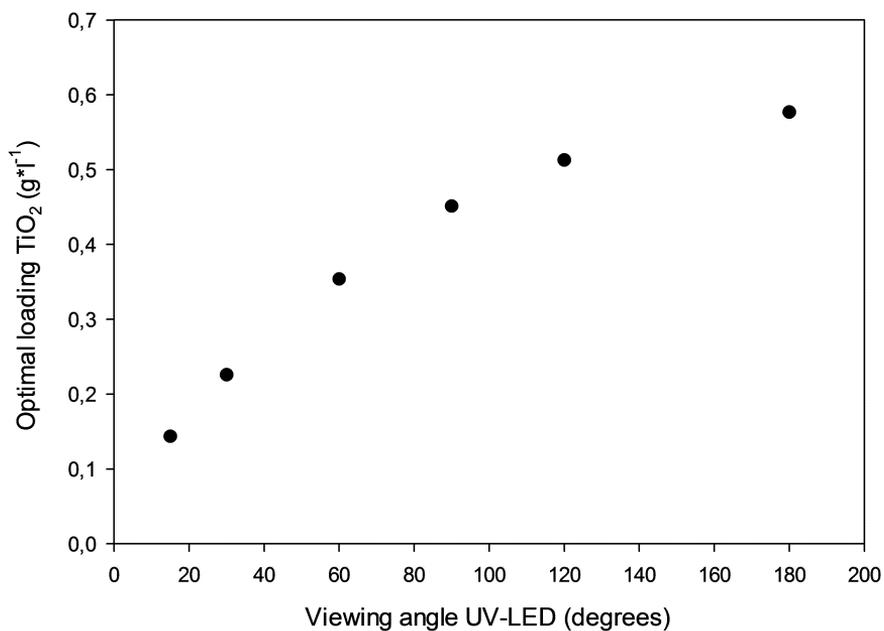
Figure 5.5: Optimal loading as function of emission angle of the 250 mW UV-LED

Chapter 6

Wirelessly powered ultraviolet light emitting diodes for photocatalytic oxidation

Abstract

A method is presented to distribute small scale light sources in a photocatalytic slurry reactor. The goal of distributing the light sources is to increase photon transfer efficiency, and thereby increasing the reaction rate, compared to using one single light source. The light sources used in this study were ultraviolet light emitting diodes with a wavelength of 375 nm. An up-flow of air into the photocatalytic reactor distributes the UV-LEDs throughout the reactor, mixes the reaction solution and saturates the solution with molecular oxygen. To make distribution of the UV-LEDs possible, the UV-LEDs were powered wirelessly by resonant inductive coupling. This article shows that UV-LEDs distributed throughout the reactor show a significant higher removal rate of methylene blue compared to the UV-LEDs concentrated on one plane in the reactor. The removal rate increased linearly with increasing numbers of UV-LEDs. The size of the UV-LEDs determined that up to 32 UV-LEDs could be wirelessly powered in a reactor volume of 500 ml. To increase the reactivity, a higher amount of UV-LEDs per reaction liquid volume and higher radiant power of the UV-LED can be used, bringing use of photocatalytic reactors closer to industrial applications.

6.1   Introduction

Reuse and safe disposal of treated wastewater is an important topic in a world of growing pressure on water resources [172]. Macropollutants, but also micropollutants, pathogenic bacteria and viruses have to be removed for safe reuse or disposal of wastewater [171]. Macropollutants are removed by conventional aerobic or anaerobic treatment but micropollutants, pathogenic bacteria and viruses need an additional treatment process [172]. A suitable processes are advanced oxidation processes (AOPs) for the removal of micropollutants, pathogenic bacteria and viruses. A promising AOP is heterogeneous photocatalysis.

Heterogeneous photocatalytic oxidation is a promising technology for advanced water treatment. Many studies have shown that photocatalytic oxidation can be used to oxidize, reduce or to transform a range of organic pollutants [34, 37], inorganic pollutants [34], pathogenic microorganisms and viruses [126]. Photocatalysis can be considered a sustainable treatment process as it uses a reusable solid state photocatalyst, produces no waste and uses photons as energy source. Photocatalysts are solid state semiconductors e.g. titanium dioxide (TiO_2), or zinc oxide (ZnO). The electrons in the valance band of a photocatalyst can be excited to the conduction band by a photon with an adequate energy level ($> 3{,}2$ eV for TiO_2), leaving an electron-hole pair. The electron-hole pair can act as a site for active oxidation and reduction of compounds or the electron-hole pair can react with water to produce hydroxyl radicals and other species that oxidize or transform dissolved compounds.

Much work on heterogeneous photocatalytic oxidation is done in the laboratory, but industrial implementation is still limited and on small scale [127]. The main issues preventing industrial application of heterogeneous photocatalytic oxidation are the development of photocatalytic reactors with good mass transfer, photon transfer and the ability for up-scaling [185, 134, 181]. Many different types of photocatalytic reactors were developed but the reactors demonstrate either good mass transfer or good photon transfer but not often both [134, 181]. Research to achieve higher mass transfer has resulted in significant advances with spinning disk reactors

[55], monolith reactors [113] and micro-reactors [6, 69].

Research to increase photon transfer is an important topic in photocatalytic oxidation. Photon transfer is the ability of a photocatalytic reactor to illuminate the surface of a photocatalyst. A photocatalytic reactor that illuminates a high surface area per reaction liquid volume with a homogeneous distribution of the light has good photon transfer. Ray and Beenackers [160] introduced a parameter (κ) to indicate the amount of illuminated surface per unit of reaction liquid volume inside the reactor ($m_{ill}^2/m_{reactor}^3$). Many different types of reactors have been proposed to increase the illuminated surface area per reaction liquid volume, e.g. slurry reactors (2631-170000 m^2/m^3), annular reactors (27-2700 m^2/m^3), optical fiber reactors (46-2000 m^2/m^3), monolith reactors (900-1300 m^2/m^3), spinning disk reactors (50-66000 m^2/m^3) and microreactors (7300-250000 m^2/m^3) [185]. There is a huge difference between the reported values of κ depending on the reactor type but also on the way the illuminated surface per volume is calculated. The value of κ can differ a lot by underestimating or neglecting the non-illuminated surface in the reactor. Van Gerven et al. [185] suggests a different parameter to compare photocatalytic reactors, illumination efficiency, η_{ill}, including the illuminated surface per volume (κ, m^{-1}), the average incident radiant power and the incident uniformity.

$$\eta_{ill} = \kappa \frac{P_{cat}}{P_{lamp}} \frac{A_{minE}}{A_{cat}} \tag{6.1}$$

With P_{cat} the power received at the catalyst surface, P_{lamp}, the power the lamp radiates, A_{minE}, the surface area receiving the mininal amount of energy and A_{cat}, the total amount of surface area.

In a slurry-type photocatalytic reactor the photocatalyst is suspended as a fine powder in the reaction liquid. The suspended fine powder gives a high surface area resulting in good mass transfer from the bulk of the liquid to the surface of the photocatalyst particle. The photon transfer, however, is poor due to the strong absorption and scattering of light by the suspension. The light penetration is very shallow and results in a small amount of illuminated photocatalyst particles by a single lamp. We attempt to increase the photon transfer by using a multitude of small-scale

light sources of micro-scale as suggested previously by Van Gerven et al. [185]. The small-scale light sources are distributed homogeneously in the suspension resulting in a high illuminated surface area.

Ultraviolet light emitting diodes (UV-LEDs) are used as small-scale light sources and have been investigated as light sources for photocatalytic oxidation in recent studies [66]. The most recent generation of UV-LEDs emit light with wavelength of 375 nm, have similar energetic efficiencies and similar lifetime as low pressure mercury discharge lamps and black light lamps. The UV-LEDs are expected still to be further developed while low pressure mercury lamps regarded as fully optimized. Advantages of UV-LEDs over low pressure mercury lamps are compact size, robustness against mechanical shocks and avalability of in different emitted wavelengths [174]. Simply replacing the low pressure mercury lamps by UV-LEDs and not changing the reactor design does not solve the fundamental problems of photocatalytic reactors. Because of the small size of the UV-LEDs the possibilities to design photocatalytic reactors enable otherwise impossible designs compared to conventional UV lamps.

This research focuses on developing a novel photocatalytic slurry-type reactor where a high number of UV-LEDs are distributed throughout a reactor volume. The wireless UV-LEDs are powered by resonant inductive coupling (RIC) with a small receiving inductor connected to the UV-LED (receiving circuit) which is inductively coupled to a transmitting inductor, placed around the reactor. A well-known application of RIC is charging of electrical toothbrushes [165], but RIC is thought to be advantageous for many other applications e.g., biomedical equipment [94], mechatronic systems [48], household electronics, charging batteries of portable devices [102], charging batteries of electrical powered automobiles and busses [189], and sensors.

One advantage of powering UV-LEDs with RIC is that the UV-LEDs, without any physical connections, will have freedom of movement. In previous studies we showed that a multitude of small receiving inductors submerged in water can be powered with one larger inductor with an energy transfer efficiency of >75% [98]. The conductivity and permittivity of water does not show a negative impact on the energy transfer efficiency [99].

In this article the characteristics of the novel photocatalytic slurry type reactor were studies. We investigated: i) the influence of distributing the UV-LEDs in the reactor compared to concentrating the UV-LEDs on one plane in the reactor, ii) the influence of aerating on the reaction rate, iii) the influence of the number of UV-LEDs on reaction rate, on κ and η_{ill}, and iv) the influence of the number of UV-LEDs on the energy efficiency.

6.2 Materials and methods

6.2.1 Inductive powering UV-LEDs

In Chapter 2, we discussed theoretical calculations supported with experimental results on how to optimize the energy transfer efficiency for linear resistive loads [98]. With Equation 2.1 the energy transfer efficiency can be calculated. The resistance of the load is not defined in case of nonlinear electronic components like LEDs. The equivalent load resistance of the LED can be calculated from the measured energy transfer efficiency.

6.2.2 Photocatalytic reactor

The photocatalytic reactor was a PVC tube with a diameter of 0.075 m and height of 0.2 m. The transmitting inductor was wound around the outside of the tube as a solenoid as can be seen in Figure 6.1. At the bottom of the reactor air was supplied through an air stone. All photocatalytic activity experiments were done with a solution of 500 ml in batch mode.

6.2.3 Resonant inductive powering

The operating frequency of the AC applied to the transmitting inductor was 45 kHz. The AC source was a TG2000 Function Generator from AIM & Thurlby Thandar Instruments, which signal was amplified by a type AB amplifier from Thell, type Accusound 101. The AC source was connected to a three loops inductor which was inductively coupled to the resonating transmitting inductor with a coupling factor of k_i= 0.75. A 0.1 Ω resistor
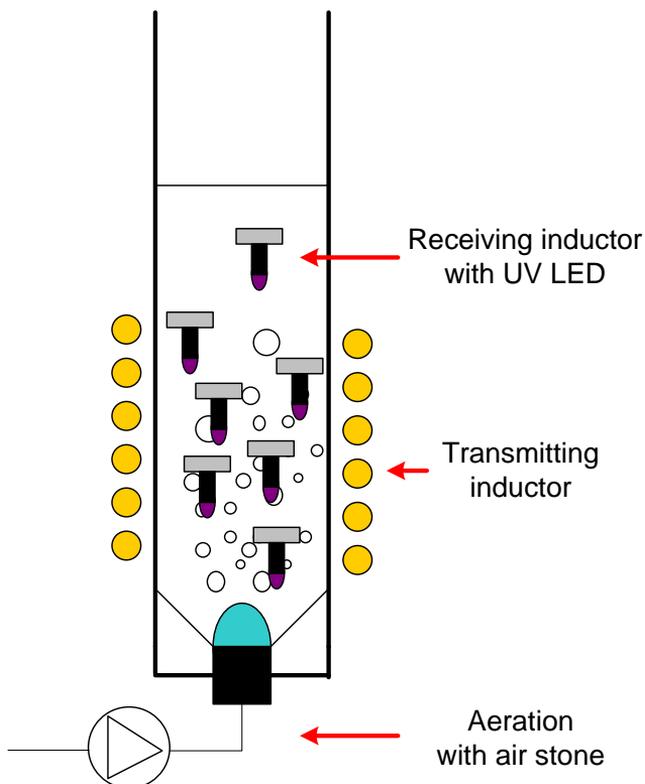
Figure 6.1: Schematic drawing of the photocatalytic reactor with aeration, transmitting inductor and the receiving inductor with UV-LED.

was connected in series with the three loops inductor. The voltage over the resistor, the voltage over both the resistor and three loops inductor and the difference in phase angle were measured with a digital oscilloscope from Pico Technology (Picoscoop 3404A). The resonating transmitting inductor was

wound as a solenoid with a copper enameled wire, 0.4 mm in diameter, with 180 turns around the photocatalytic reactor. The inductance, capacitance and resistance of components were measured with a HP 4194A impedance analyzer. The inductance of the transmitting inductor (L_t) was 1.40 mH with a quality factor (Q_t) of 150 at 45 kHz. Capacitors were connected in series with the transmitting inductor to obtain a resonance frequency of 45 kHz.

6.2.4 Receiving circuits

A schematic drawing of the receiving circuit can be seen in Figure 6.2. The receiving circuit consisted of a ferrite core inductor from Fastron, diameter of 7 mm and height of 10 mm, induction (L_r) of 10 mH with a quality factor (Q_r) of 90 at 45 kHz and series resistance (R_r) of 1.26 Ω, a 1 nF capacitor and a UV-LED connected in series. The coupling factor (k) between the transmitting and receiving inductor was 0.02. The UV-LEDs were from Nichia, type NSPU510CS, packaged in a 5 mm epoxy resin cylinder with a radiant flux of 10 mW, wavelength of 375 nm and energetic efficiency of 14%. Expanded polystyrene (EPS) was attached to the receiving circuits and tuned for the right density to be able to make the receiving inductor with UV-LED float in the reactor.

6.2.5 Chemicals and solutions

Titanium dioxide type P25 from Evonik Industries was used as the photocatalyst with methylene blue as a model compound to be photocatalytically oxidized. The reaction liquid was demineralized water. Experiments lasted for 1 hour and each 5 minutes a 2.5 ml sample was taken. The samples were centrifuged for 4 hours, diluted and the concentration of methylene blue was measured with an UV/VIS spectrophotometer of Shimadzu.

6.2.6 Aeration experiments

The influence of the aeration on the photocatalytic activity was measured in a 500 ml solution with 16 UV-LEDs, 10 mg/l methylene blue and 1.4
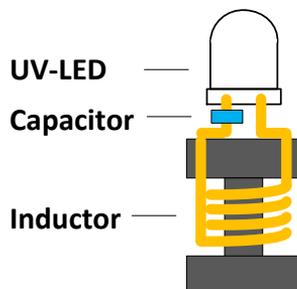
Figure 6.2: Schematic drawing of the receiving circuit with an inductor, capacitor and UV-LED.

g/l TiO$_2$. The airflow rate was varied between 0 to 4 l/min. Dissolved molecular oxygen was measured with WTW 3210 oxygen electrode.

6.2.7 Distributed and concentrated UV-LEDs

The difference between distributing or concentrating the UV-LEDs in the reactor was measured with two experiments, one with 16 UV-LEDs distributed inside the reactor and one with 16 UV-LEDs fixed in one plane on the level of the center of the transmitting inductor. TiO$_2$ loading of 1.4 g/l and airflow of 1 l/min ambient air was used for the experiments. The photocatalytic activity was measured in triplo at 6 different starting concentrations of 1, 5, 15, 25, 50 and 75 mg/l methylene blue and the kinetics of the two UV-LEDs configurations were compared by calculating Langmuir-Hinshelwood kinetic parameters:

$$r = -\frac{dC}{dt} = -k_r\Theta_x = -\frac{k_r K C}{1 + KC} \tag{6.2}$$

With reaction rate (r), reaction rate constant (k$_r$), fraction of the surface covered by substrate X (Θ_x), the substrate adsorption constant (K),

and concentration of substrate X (C). We assumed the value of K to be independent of the UV-LED configuration, which was confirmed by the experiments. The influence on the number of receiving UV-LEDs on the photocatalytic activity was measured with varying numbers of receiving circuits (4-32). The start concentration of methylene blue was 10 mg/l, TiO_2 loading of 1.4 g/l and airflow of 1 l/min ambient air.

6.2.8 Calculation of the illuminated catalyst surface per reaction liquid volume and illumination efficiency

The illuminated catalyst surface area per reaction liquid volume was calculated with 32 UV-LEDs in a reaction liquid volume of 500 ml with 1.4 g/l TiO_2. With a surface area of 50 m^2/g [78], the catalyst surface area (A_{cat}) is 50000 m^2/m^3. The spatial light distribution was measured with a photodiode, silicon photodetector OSD 5T from Centronic. The photodiode was mounted on a custom made robotic arm that was controlled with Matlab software. Scans were made of the light intensity in a 1.4 g/l TiO_2 suspension on the plane perpendicular to the direction of emitted light of the UV-LEDs.

The emission from a UV-LED was modeled with the following equation:

$$I_r = \frac{P10^{-Ar}}{r^2\Omega} \tag{6.3}$$

With r distance away from UV-LED (cm), Ω the solid angle, Ir intensity (mW/cm^2), P radiant power of the UV-LED (mW) and A the absorption coefficient (cm^{-1}). The solid angle was calculated from the emission angle ϕ of the UV-LED:

$$\Omega = 2\pi(1 - cos(\phi)) \tag{6.4}$$

The penetration depth (r_{min}) at which the radiation reaches the minimum amount of intensity ($I_{rmin} < 0.01$ mW/cm^2) was calculated from Equation 6.3 with radiant power (P) of the UV-LED, absorbance (A) of 1.96 cm^{-1} and emission angle (ϕ) of 115 degrees. The shape of the emitted

light is estimated by a half sphere as can be seen in Figure 6.6 and with the penetration depth (r_{min}) the irradiated volume was calculated:

$$V = \frac{4/3 \pi r_{min}^3}{2} \qquad (6.5)$$

From the above equation, A_{minE} was calculated and percentage irradiated surface area and η_{ill} was calculated with A_{cat} for the number of UV-LEDs as a function of the radiant power of the UV-LEDs.

6.3 Results and discussion

6.3.1 Influence distributed and concentrated UV-LEDs on reaction rate

Figure 6.3 shows the reaction rate as function of the initial concentration of methylene blue. The Langmuir Hinshelwood model was used for fitting the data of the experimental results. The apparent reaction rate constant k_a was respectively 0.12 and 0.079 mg/l*min for the distributed UV-LEDs and the concentrated UV-LEDs. The adsorption constant was 0.42 l/mg. The power input in both systems was equal resulting in an equal amount of radiant power. Assuming that the mass transfer is governed by mixing through aeration and the flow pattern around the UV-LEDs do not change with the difference in configuration, the mass transfer is equal with both distributed and concentrated UV-LEDs which was confirmed by the similar adsorption constant from the Langmuir Hinshelwood model.

The distributed UV-LEDs show a higher apparent reaction rate constant because they irradiate a larger surface area of catalyst over time compared to the concentrated UV-LEDs. The same amount of radiant power distributed over a larger surface area results in more electron-holes and in turn a higher apparent reaction rate constant.
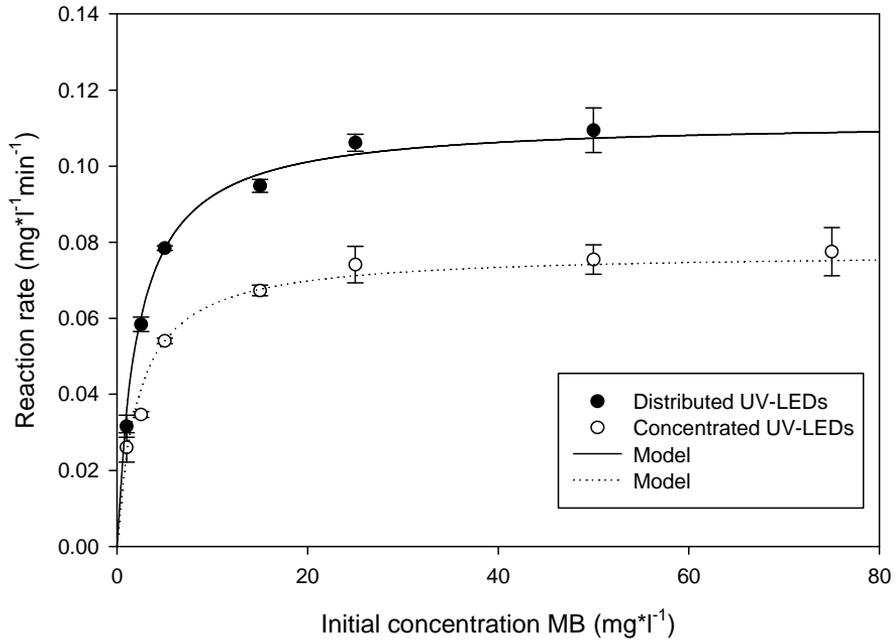
Figure 6.3: Reaction rate as a function of initial concentration methylene blue (MB). Model lines are Langmuir Hinshelwood fits.

6.3.2   Influence airflow rate on reaction rate

Figure 6.4 shows the reaction rate as a function of the airflow rate. The reaction rate increased significantly from 0 to 1 l/min and is constant from 1 to 4 l/min. The amount of dissolved molecular oxygen did not drop measurable when airflow of 0-1 l/min was used so the lower reaction can not be attributed to a lower amount of dissolved oxygen. The increase of airflow gave better distribution of the UV-LEDs. With 0 l/min the UV-LEDs are on the reactor bottom and partly distribution occured at 0.25 and 0.5 l/min. At 1 l/min, the UV-LEDs were completely distributed

throughout the reactor and with higher airflow the mixing became more turbulent but this did not result in a higher rate.
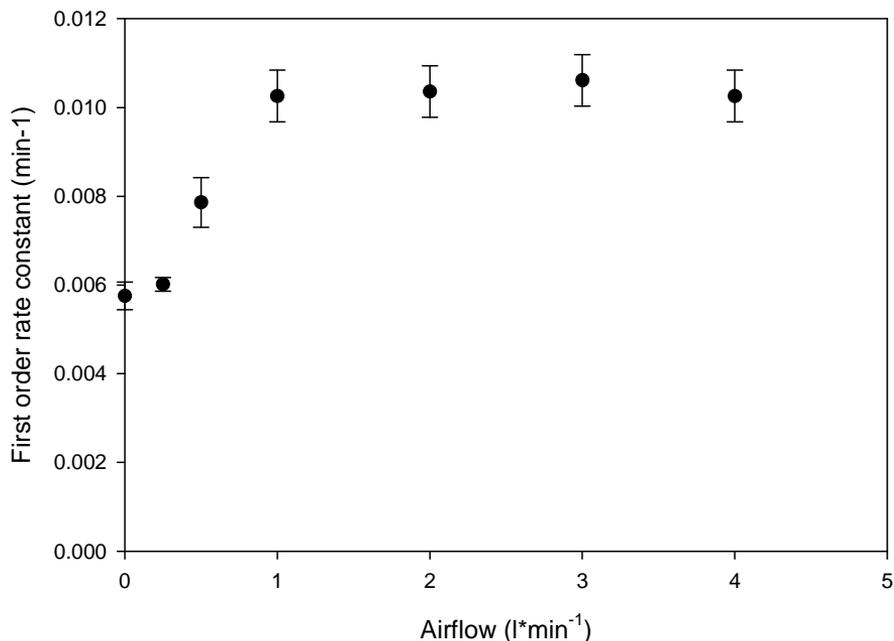
Figure 6.4: Reaction rate as function of airflow rate.

6.3.3 Influence of number of UV-LEDs and resulting illuminated catalyst per reaction liquid volume

Figure 6.5 shows the first order rate constant as a function of the number of UV-LEDs. The increase in reaction rate as function of the number of UV-LEDs is linear. The 64 UV-LEDs per liter did not negatively influence each other.

Figure 6.6 shows the result from the measurement of the light intensity
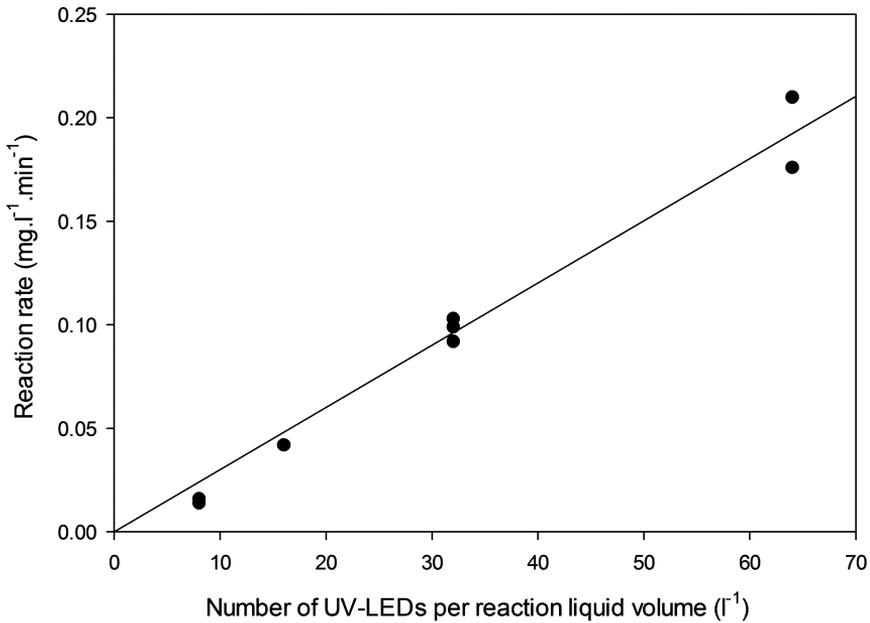
Figure 6.5: Reaction rate as function of number of UV-LEDs per reaction liquid volume.

in a TiO2 suspension of 1.4 g/l. The intensity of the light is lower than 0.01 mW/cm^2 after 13 mm and the measured results fit Equation 6.3 well.

In order to irradiate the total surface area of 72000 m^2/m^3 with an intensity of more than 0.01 mW/cm^2 a large number of low radiant power UV-LEDs can be used or a smaller amount of higher radiant power UV-LEDs as can be seen in Figure 6.7.

An amount of 64 UV-LEDs per liter and 10 mW radiant power as used in this research, results in a irradiation of 45% of the total surface area and resulting η_{ill} of 32000 m^2/m^3. To further increase the percentage of
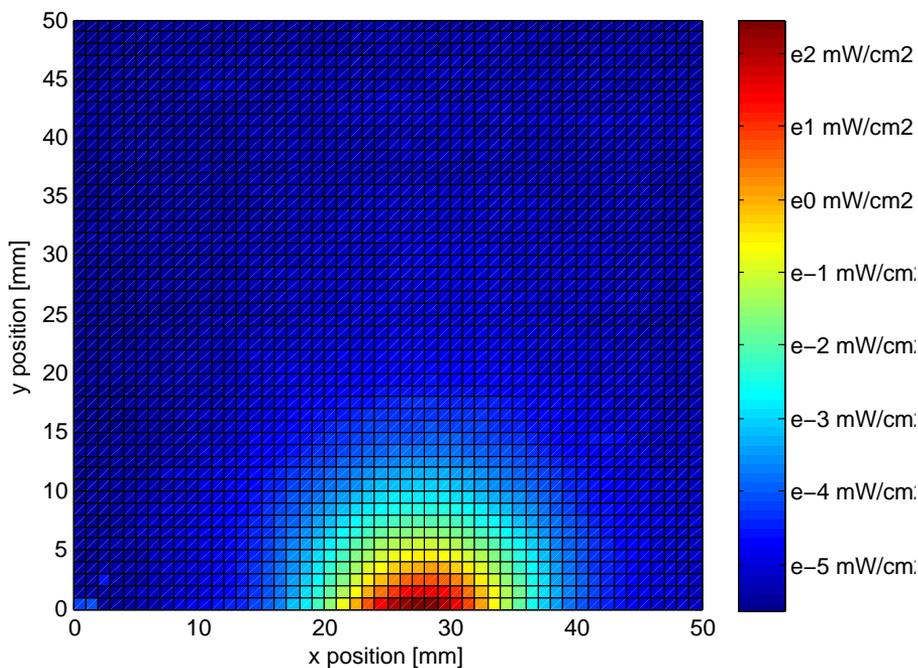
Figure 6.6: Measured light intensity of a 10 mW radiant power UV-LED irradiating into a TiO$_2$ suspension of 1 g/l.

irradiated surface area the number of UV-LEDs can be increased or the radiant power can be increased. With 10 mW radiant power UV-LEDs a total of 175 UV-LEDs per liter reaction liquid volume have to be used to irradiate the total surface area. With 64 UV-LEDs per liter reaction liquid a radiant power of 135 mW per UV-LED has to be used to irradiate the total surface area. A high number of low power UV-LEDs irradiate the surface area more efficiently than a low number of high power UV-LEDs. In order to increase the efficiency of irradiation and to increase the total radiation power of the reactor the number of UV-LEDs per liter have to be
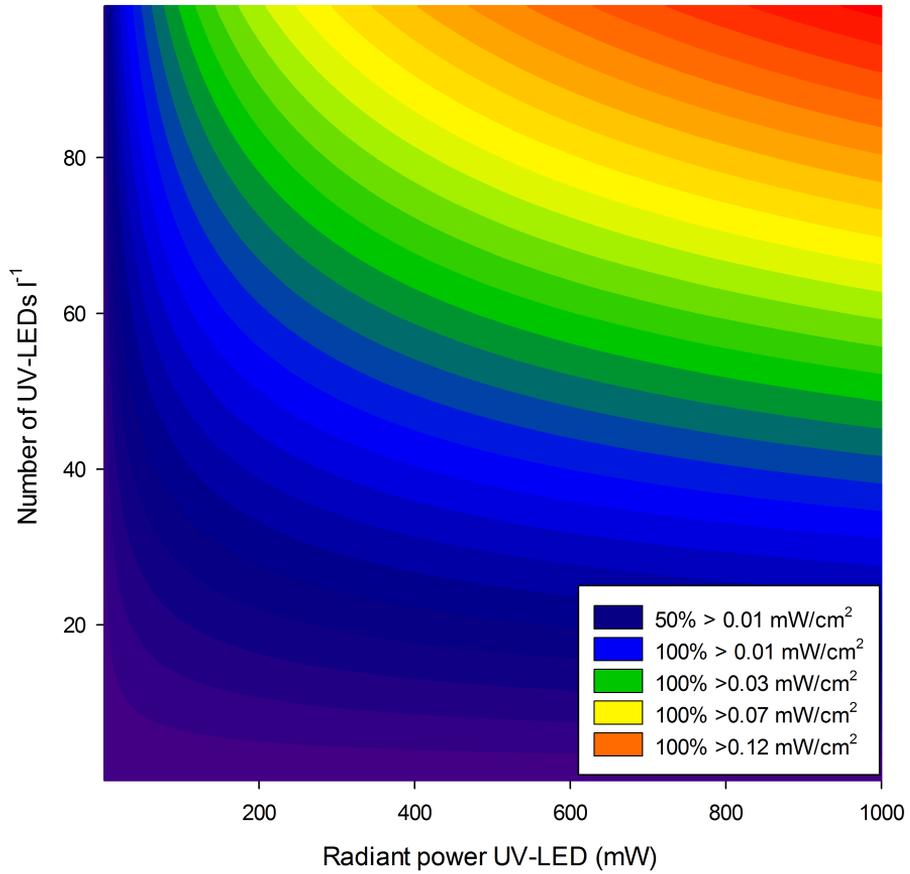
Figure 6.7: Contour plot showing the efficiency of illumination as a function of number of UV-LEDs per liter and the radiant power of the UV-LEDs.

increased but the radiant power of the UV-LED need to be decreased.

6.3.4   Energy transfer efficiency

Figure 6.8 shows the energy transfer efficiency as a function of number of receiving circuits. The efficiency increases with increasing number of UV-LEDs. The increase is due to the increased coupling between the transmitting and receiving inductors. Equation 2.1 fits the measured results well.
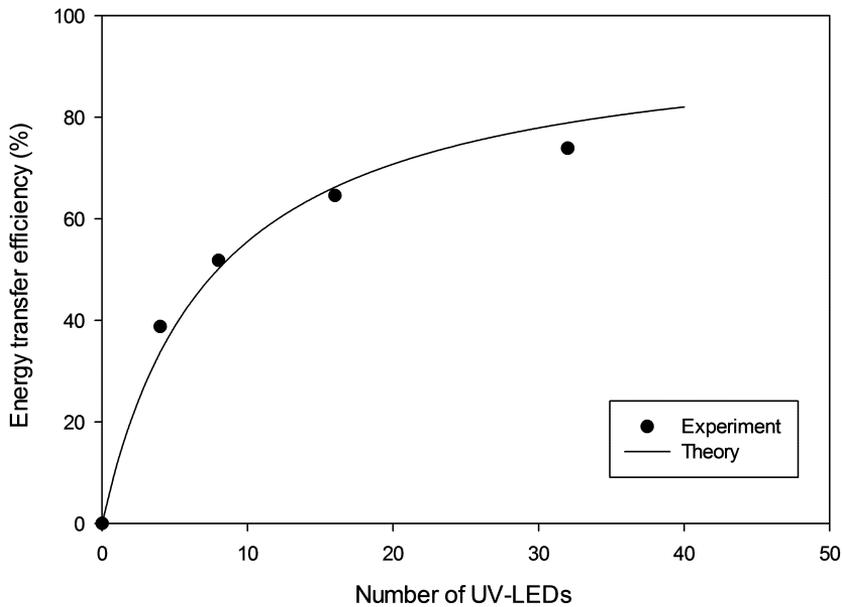
Figure 6.8: Energy transfer efficiency as a function of the number of UV-LEDs.

6.4 Conclusions

In this paper a new reactor design for photocatalytic oxidation has been presented that increases the photon transfer inside slurry reactors by distributing the light sources. Distribution of the UV-LEDs inside the reactor was achieved by up-flow of air. The UV-LEDs were powered by resonance inductive coupling. The reaction rate was increased by more than 30% through the distribution of the UV-LEDs compared to fixing the UV-LEDs on a plane inside the reactor. The increase of UV-LEDs resulted in a linear increase of the resulting reaction rate showing the UV-LEDs did not negatively influence each other. Up to 64 UV-LEDs per liter of reaction liquid were used in this research. A high illuminated surface area per reaction liquid volume (κ) and illumination efficiency (η_{ill}) can be achieved by using 64 UV-LEDs per liter reaction volume. Parameter η_{ill} can be further increased by using UV-LEDs with higher radiant power or to increase the number of UV-LEDs per volume of reactor by miniaturization of the components. The energy transfer efficiency of resonance inductive coupling increased with an increased number of UV-LEDs. This approach of small, distributed light sources shows a promising way to intensify photocatalytic reactors while maintaining a high efficiency of photon transfer.

Acknowledgements

Chapter 7

A novel distributed UV-LED photocatalysis process to remove pharmaceuticals from wastewater effluents

Abstract

A novel photocatalytic reactor, distributing wirelessly powered UV-LEDs in a suspension of TiO_2, was evaluated for its ability to remove seven pharmaceuticals from deionized water and membrane bioreactor (MBR) effluent. Two systems were tested: one with the UV-LEDs distributed throughout the reactor and another with the UV-LEDs concentrated on one plane inside the reactor. The distributed system showed a factor 2 higher reaction rate for all pharmaceuticals in both deionized water and MBR effluent. The removal rates of the pharmaceuticals correlate with their adsorption onto the TiO_2 surface. Five out of the seven pharmaceuticals showed lower amounts of adsorption onto TiO_2 in MBR effluent compared to the adsorption in deionized water. In MBR effluent, undefined organic compounds were 70 times higher in TOC concentrations compared to the pharmaceuticals. Applying MBR effluent results in a lowering of pharmaceutical removal rates by a factor 50 to values ranging between 0.012-0.001 min^{-1}. Two pharmaceuticals (ibuprofen and tetracycline) had similar or increased adsorption in MBR effluent resulting in similar and higher removal rates in MBR effluent (>0.25 min^{-1}). Based on electrical energy per order (EEO), the distributed UV-LEDs achieved the highest efficiency (0.03-0.18 kWh/m^3 in deionized water) and compare positively to photocatalytic reactors with conventional lamps. With the prospected increase in energetic efficiency of UV-LEDs and decrease in purchase costs, the novel distributed UV-LED photocatalytic reactor is a promising technology for removing micropollutants from wastewater effluent.

7.1   Introduction

Pharmaceuticals have played an important role in improving quality of life. As a result of the intensive use of pharmaceuticals, these compounds are commonly found in the environment [47]. The main route of (human) pharmaceuticals into the environment is through wastewater. Wastewater treatment plants are generally not designed to remove pharmaceuticals [49]. Most of these compounds are not biodegradable and they are discharged with the effluent into the environment [5]. The negative effects of pharmaceuticals in the environment are diverse [172]. For instance, the presence of antibiotics can trigger the development of antibiotic resistance in bacteria, and the presence of hormones can cause endocrine disruption in aquatic organisms. Removal of pharmaceuticals from effluent is therefore necessary to safeguard the quality of water bodies, particularly when they are used as drinking water sources [176, 171].

Promising technologies for the removal of pharmaceuticals from wastewater effluent are based on membrane filtration, adsorption onto activated carbon or advanced oxidation processes (AOP) [76]. Heterogeneous photocatalysis with TiO_2 is a type of AOP able to oxidize, reduce or to transform a range of organic pollutants, inorganic pollutants, pathogenic microorganisms and viruses [14, 82]. A broad range of pharmaceuticals can be oxidized with TiO_2 photocatalysis [89]. Research has been done to investigate the reaction kinetics and reaction pathways for complete mineralization of pharmaceuticals. The experiments are generally done in relatively high concentrations of one target compound in deionized water. The results cannot be used to predict the removal of low concentrations of a mixture of pharmaceuticals from wastewater effluents. Removal of mixed solutions of pharmaceuticals from deionized water has been investigated [40, 118]. The results of these publications show the influence of the affinity of the pharmaceutical to adsorb onto the surface of TiO_2 on the removal rate [103], the strong adsorbing compounds have higher removal rates. In order to predict the removal of low concentrations of a mixture of pharmaceuticals, the matrix effects have been investigated of wastewater effluent on photocatalytic oxidation. Experiments have been done at laboratory scale tests and pilot

Table 7.1: Published data on removal of pharmaceuticals from real wastewater with photocatalytic oxidation

Reactor type	Number pharm.	C_0	Wave-length	Lamp power	Amount of TiO2	Ref
		μg/l	nm	W	g/l	
Continuous 24 l/min	32	ng/l μg/l	254	Not reported	0.05	[13]
Pilot solar	22	ng/l	Solar		0.2	[175]
Batch 60 ml	5	300	254 360	4	0.5	[39]
Continuous 2.7 ml/min	4	50	365	75	Immob.	[26]
Batch 100 ml	3	20000	350	125	0.2 0.8	[9]
Batch 1 liter	1	10000	360	8	0.5	[104]

scale tests. In Table 7.1 an overview is given of experimental conditions of recent publications investigating the removal of pharmaceuticals from wastewater effluent. The differences in light sources applied, the amount of TiO$_2$, concentration and type of pharmaceuticals and different wastewater effluent matrices make it difficult to compare the published data, but generally the data show the matrix effects of the wastewater effluent decrease the oxidation rate of the pharmaceuticals. This decrease in oxidation rate is attributed to organic carbon and inorganic ions present as background compounds in wastewater effluent. Organic carbon and inorganic ions scavenge hydroxyl radicals [9], block active sites on the surface of TiO$_2$ [59], compete with adsorption and cause increase of the size of TiO$_2$ aggregates [63] reducing the effective surface area of TiO$_2$.

For efficient oxidation of pharmaceuticals in a photocatalytic reactor, photons, target compound and electron acceptor have to be transferred to the surface of the TiO$_2$ particle simultaneously [185, 134]. Without the photon, no reactive electron-hole pair will be produced to oxidize the target

compound. When the target compound is not close to the catalyst surface the non-selective electron-hole will oxidize other compounds or will form hydroxyl radicals. And without the electron acceptor the electron-hole pair will recombine. In an efficient and reactive photocatalytic slurry reactor, a large surface area of the photocatalyst has to be irradiated with a maximum intensity of incident light of 25 mW/cm^2 [40, 78]. The energy level of the incident photon needs to be higher than the band gap energy needed to excite an electron in the valence band to the conduction band in the photocatalyst. For TiO$_2$ the energy level of the incident photon has to be 3.2 eV or higher resulting in wavelength of 385 nm or lower. It is energetically favorable to use photons with energy levels just above the energy level of the band gap because one photon excites one electron and the excess energy of the photon is dissipated as heat [185]. In a photocatalytic slurry, the suspension of small catalyst particles results in a good mass transfer from the bulk of the liquid to the surface of the TiO$_2$ particle. The photon transfer, however, can be limiting due to shading caused by the catalyst particles. Light penetration into the suspension is very shallow at high TiO$_2$ loading and the light intensity for a point source drops exponentially with the distance due to adsorption and scattering. To increase photon transfer we use small scale ultraviolet light sources which are distributed throughout the suspension instead of large scale gas discharge lamps.

In Chapter 6, we showed the increase of oxidation rate of methylene blue in deionized water with ultraviolet light emitting diodes (UV-LEDs) distributed inside a reactor by fluidization compared to the same UV-LEDs concentrated on one plane inside the reactor. The distributed UV-LEDs had better distribution of light compared to the concentrated UV-LEDs resulting in higher oxidation rate. In this Chapter we want to investigate the photocatalytic oxidation of seven different pharmaceuticals with distributed UV-LEDs and concentrated UV-LEDs including the matrix effects of wastewater.

Opposed to the conventional gas discharge light sources, such as mercury lamps, UV-LEDs are solid state light sources. Compared to mercury lamps, UV-LEDs are compact and robust. UV-LEDs are available at wavelengths between 210 and 400 nm with a narrow bandwidth of the emitted

wavelength ($\pm$ 5 nm) and radiant power from 1 to 1200 mW [174]. UV-LEDs have been investigated for light sources in photocatalytic reactors [88, 141, 140, 180, 6, 31, 69, 173]. No publications could be found that used UV-LEDs as light sources for photocatalytic removal of pharmaceuticals from wastewater effluent. UV-LEDs are suitable light sources for photocatalysis because UV-LEDs emit light with a low intensity and with wavelength close to the band gap energy of the photocatalyst (3.2 eV for TiO_2 or 385 nm). To attain a reactor with high reactivity, a large surface area of photocatalyst has to be irradiated per volume reactor. This means a large number of UV-LEDs have to be present inside the reactor volume. Miniaturization of the UV-LEDs and increase of number per volume of reactor would increase the reactivity. As UV-LEDs will become more efficient and cheaper the possible application of UV-LEDs in photocatalytic reactors will be likely in near future.

This Chapter aims to demonstrate the potential application of a novel photocatalytic reactor with wirelessly powered distributed UV-LEDs for the removal of pharmaceuticals from wastewater effluent. This novel photocatalytic reactor uses small ultraviolet light emitting diodes (UV-LEDs) as light source which are powered wirelessly with resonant inductive coupling. The novel photocatalytic reactor was operated in two modes to compare the UV-LEDs distributed throughout a reactor or the UV-LEDs concentrated on one plane inside the reactor. The influence of the wastewater effluent characteristics on the novel photocatalytic reactor is investigated using effluent from a membrane bioreactor (MBR) ran on municipal wastewater and deionized water both spiked with low concentration of pharmaceuticals (<200 μg/l). Metoprolol, diclofenac, ibuprofen, cetirizine, carbamazepine, ciprofloxacin and tetracycline are chosen as model compounds. We evaluate the impact of the background organic compounds on the performance of distributed UV-LEDs and concentrated UV-LEDs for the removal of the different pharmaceuticals.

Table 7.2: Published data on removal of pharmaceuticals from real wastewater with photocatalytic oxidation

Compound	Therapeutic group	Biodegradable?
Tetracycline	Antibiotic	No [5]
Ciprofloxacin	Antibiotic	No literature
Diclofenac	Anti-inflammatory	Yes, but limited [25, 24, 101, 22]
Cetrizine	Antihistamine	No [96]
Carbamazepine	Antiepileptic	No [25, 24, 101, 43]
Metoprolol	Beta-blocker	No [101, 124]
Ibuprofen	Anti-inflammatory	Yes, but limited [25, 24, 101, 21]

7.2 Materials and methods

7.2.1 Chemicals and reagents

Metroprolol, diclofenac, ibuprofen, cetirizine, carbamazepine, ciprofloxacin and tetracycline were obtained from Sigma-Aldrich. Table 7.2 shows some selected properties of these compounds.

Titanium dioxed (Aeroxide TiO_2 P25 Degussa) was obtained from Evonik Industries. Deionized water was prepared by MilliQ-Millipore apparatus and MBR effluent was obtained from reactor described by Kappel et al. [90]. The MBR was fed with municipal waste water and effluent characteristic can be seen in Table 7.3.

A stock solution was prepared by directly dissolving 2 mg/l of each pharmaceutical into deionized water. Concentrations in the spiked solutions were measured prior to experimentation and are shown in Table 5.

7.2.2 Photocatalytic reactor

UV/TiO_2 experiments were done with the novel photocatalytic reactor described in Chapter 6 and shown in Figure 7.1. Two different setups of the photocatalytic reactor were investigated i) 16 UV-LEDs distributed throughout the reactor by fluidization and ii) 16 UV-LEDs concentrated

Table 7.3: Water characteristics of the effluent from an MBR fed with municipal wastewater.

Parameter	Concentration
Total carbon	19.4 mg/l
Total organic carbon	13.6 mg/l
Inorganic carbon	5.8 mg/l
Ca^{2+}	47 mg/l
Na^+	115 mg/l
Cl^-	178 mg/l
Conductivity	930 μS/cm
pH	7.1

on one plane inside the reactor. The UV-LEDs (NSPU510CS, Nichia Corporation) emitted UV light with a wavelength of 375±5 nm, typical applied power of 72 mW with a resulting radiant flux of 10 mW. The UV-LEDs were powered wirelessly with resonant inductive coupling, a detailed description is given in Chapter 6.

7.2.3   Irradiation procedure

A volume of 10 ml of stock solution containing the pharmaceuticals was added to a volume of 490 ml of deionized water and MBR effluent. TiO_2 loading of 1.4 g/l was used as this was the optimal loading for the distributed and concentrated UV-LEDs as described in previous Chapter 5. The TiO_2 was added to the solution and the suspension was sonificated for 30 minutes in an ultrasonic bath. After the ultrasonic bath the suspension was poured in the reactor and aerated for 60 min with airflow of 1 l/min. After 60 minutes of aeration the UV-LEDs were switched on by powering them with resonant inductive coupling. The suspension was irradiated for 120 minutes after which the experiment was stopped. Samples of 2 ml were taken from the batch reactor at the start of aeration, start of irradiation and after 10, 20, 30, 60 and 120 minutes of irradiation. The samples were centrifuged for 3 hours at 14000 rpm and the supernatant was analyzed
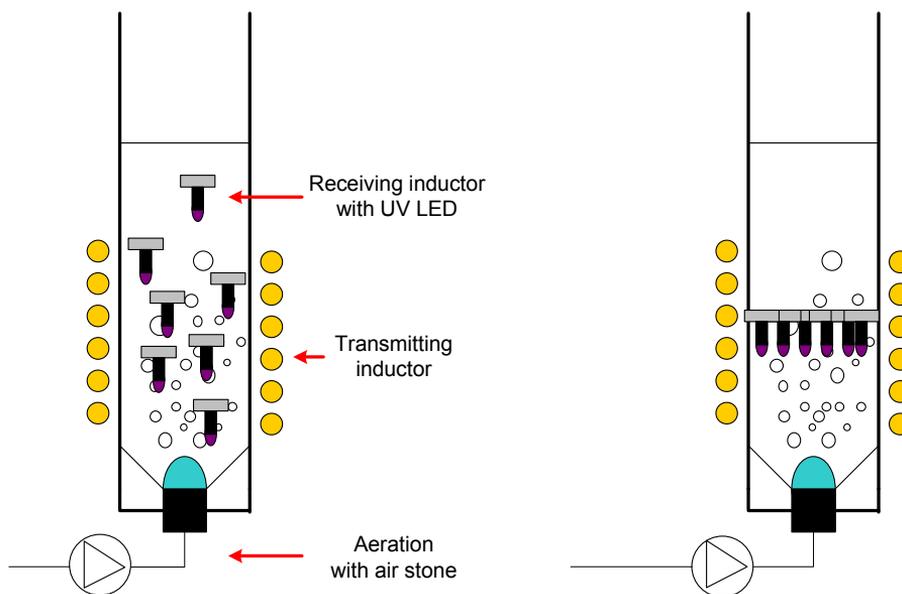
Figure 7.1: Distributed (left) and concentrated (right) light sources.

for the pharmaceuticals. The pH and temperature were measured with a WTW pH 3110 sensor. No decrease in dissolved oxygen was measured with WTW 3210 oxygen electrode during the experiment indicating sufficient aeration of the suspension. An oscilloscope (Picoscope 3404A, pico Technology) measured the rms voltage (V), rms current (I) and phase shift (Φ) applied to the transmitting inductor. The power (P) was calculated with the following equation:

The power emitted by the UV-LEDs was measured with an UV sensor

connected to a receiving inductor. The power applied to the transmitting inductor was tuned to the amount of emitted power measured by the UV sensor (10 mW).

7.2.4   Sample analysis

The sample analysis is described elsewhere [23, 49]. First order removal constants kapp were calculated for the pharmaceuticals with the following equation.

$$k_{app} = -\frac{dln(C)}{dt} \tag{7.1}$$

The 95% confidence interval of k_{app} was calculated with regression line statistics.

7.3   Results and discussion

7.3.1   Adsorption of pharmaceuticals onto TiO_2 in deionized water and MBR effluent

Weight percentage of pharmaceuticals that adsorbed to TiO_2 in the dark after 30 minutes ultrasound and 60 minutes of aeration can be seen in Table 7.4. The pharmaceuticals can be divided into four distinctive groups, in terms of sorption onto TiO_2 in different aqueous media, namely i) tetracycline, adsorbing strongly in deionized water and MBR effluent, ii) ciprofloxacin and diclofenac, adsorbing strongly in deionized water and less strong in MBR effluent, iii) cetirizine, carbamazepine and metoprolol adsorbing weakly in deionized water and negligible in MBR effluent and iv) ibuprofen, adsorbing weakly in deionized water but strongly in MBR effluent. The weaker adsorption of most pharmaceuticals onto TiO_2 in MBR effluent is attributed to adsorption of TOC and inorganic ions competing with adsorption of pharmaceuticals [103, 163]. Ibuprofen is an exception, comparable to findings of Laera et al. [103], who reported a stronger adsorption of congo red in wastewater effluent than in deionized water. The mechanism could be a bridging effect caused by divalent cations as suggested by Li et al. [109].

Table 7.4: Adsorption of pharmaceuticals onto TiO_2 in the dark after 30 minutes ultrasound and 60 minutes aeration.

Compound	Adsorption deionized water	Adsorption MBR effluent
Tetracycline	>95%	>95%
Ciprofloxacin	70%	20%
Diclofenac	65%	15%
Cetrizine	30%	Negligible
Carbamazepine	15%	Negligible
Metoprolol	15%	Negligible
Ibuprofen	30%	60%

Strong adsorption of diclofenac onto TiO_2 in deionized water was shown by Martínez et al. [120]. Previous publications report weak adsorption onto TiO_2 for carbamazepine and metoprolol [26, 103]. Tetracycline has a strong affinity for adsorption [49]. No previous results of adsorption or photocatalytic oxidation of cetrizine could be found in literature.

7.3.2 Oxidation of pharmaceuticals in deionized water with distributed and concentrated UV-LEDs

The concentration of ciprofloxacin, diclofenac, ibuprofen, carbamazepine, metoprolol and ibuprofen as a function of time in deionized water with distributed UV-LEDs and concentrated UV-LEDs can be seen in Figure 7.2a and 7.2b. Tetracycline is not shown in Figure 7.2 because it was removed from the solution by adsorption onto TiO_2 and could not be detected in the solution samples. Distributed UV-LEDs removed the pharmaceuticals in different times of irradiation: ciprofloxacin and diclofenac in 10 minutes, ibuprofen in 30 to 60 minutes, and cetrizine, carbamazepine and metoprolol in 60 to 120 minutes. For the concentrated UV-LEDs all pharmaceuticals took a longer time of irradiation for removal: ciprofloxacin in 10 minutes, diclofenac in 30 minutes, ibuprofen in 60 to 120 minutes and cetirizine, carbamazepine and metoprolol in 120 minutes.

The corresponding first order rate constants of the six pharmaceuticals
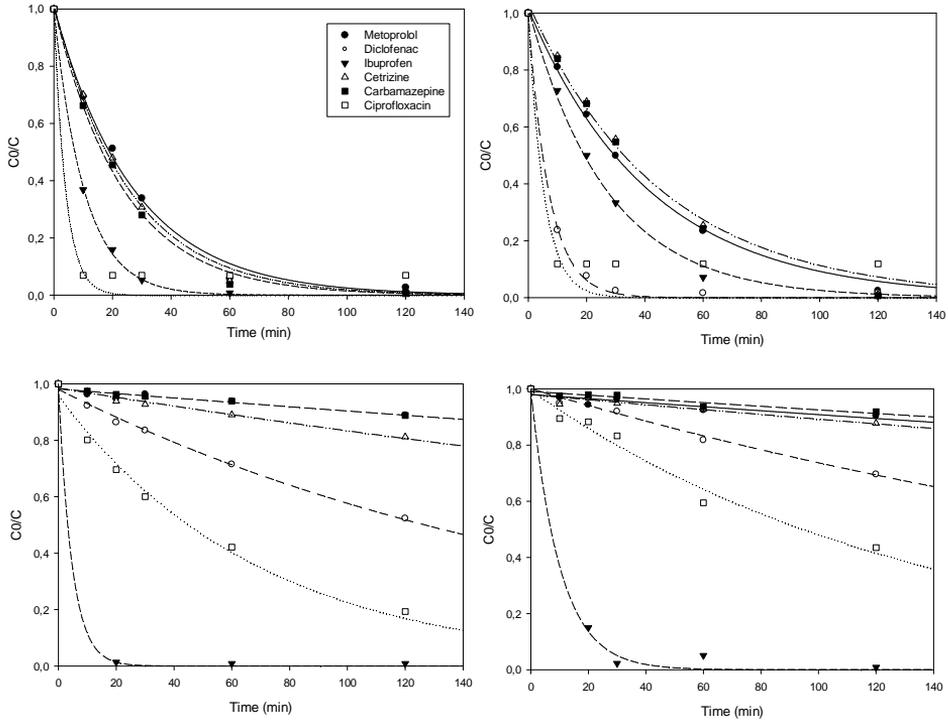
Figure 7.2: The start concentration (C_0) over the concentration in time (C) as a function of time of six pharmaceuticals with distributed (a) and concentrated (b) UV-LEDs in deionized water and with distributed (c) and concentrated (d) UV-LEDs in MBR effluent.

in deionized water can be seen in Figure 7.3. For the distributed UV-LEDs the rate constants are all around a factor 2 higher compared to the concentrated UV-LEDs, except for ciprofloxacin. These results are similar to those found in previous research with oxidation tests of methylene blue in deionized water. The higher reaction rate for distributed UV-LEDs is most likely due to the increase in photon transfer leading to an irradiation of a larger surface area by the distributed UV-LEDs compared to the distributed
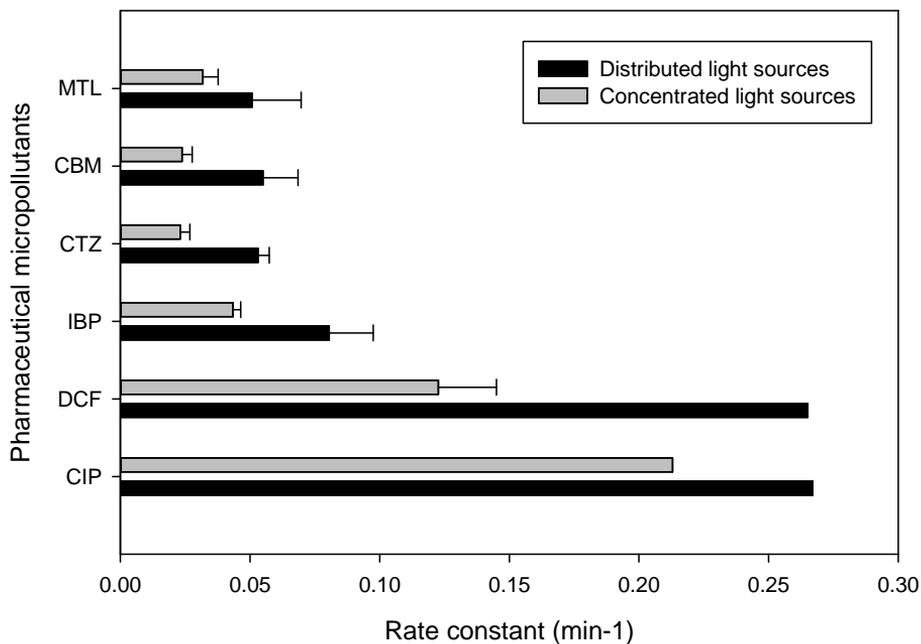
UV-LEDs.

Figure 7.3: Rate constants for removal of pharmaceutical micropollutants from deionized water with distributed and concentrated UV-LEDs, error bars indicate 95% confidence interval.

7.3.3 Oxidation of pharmaceuticals in MBR effluent with distributed and concentrated UV-LEDs

The concentrations of the pharmaceuticals as a function of time in MBR effluent with distributed UV-LEDs and concentrated UV-LEDs can be seen in Figure 7.2c and 7.2d. Concentrations of tetracycline at the start of irra-

diation were 10 μg/l and were removed from MBR effluent within 10 minutes irradiation both with distributed and concentrated UV-LEDs. The distributed UV-LEDs removed ibuprofen after 20 minutes of irradiation. Ciprofloxacin showed 80% removal after 120 minutes of irradiation, diclofenac showed 45% removal, cetirizine showed 20% removal and metoprolol and carbamazepine showed 10% removal. The concentrated UV-LEDs removed ibuprofen after 30 minutes of irradiation from MBR effluent. Ciprofloxacin showed 60% removal after 120 minutes of irradiation, diclofenac showed 25% removal, cetirizine showed 10% removal and metoprolol and carbamazepine showed 10% removal.

The corresponding first order rate constants for distributed and concentrated UV-LEDs can be seen in Figure 7.4. The rate constants are a factor 1.3 to 1.9 higher for the distributed UV-LEDs compared to the concentrated UV-LEDs with the exclusion of metoprolol and carbamazepine; comparable values were found for first order rate constants but with a relatively large 95% confidence interval.

7.3.4 Influence adsorption on photocatalytic oxidation

In both deionized water and MBR effluent there seems to be a relation between rate constant and adsorption, as can be seen in Figure 7.5. The reduction in the rate constant is around a factor 50 for the pharmaceuticals in MBR effluent compared to deionized water indicating a similar impact of the background organic compounds on rate constants in the MBR effluent for the different pharmaceuticals, as can be seen in Figure 7.6.

Tetracycline and ibuprofen were removed from MBR effluent after 10 minutes of irradiation and ibuprofen showed higher first order rate constant in MBR effluent compared to deionized water. The exception is ibuprofen because it showed a faster removal in MBR effluent probably due to stronger adsorption caused by bridging effects [109]. No definite proof can be given and other possible explanations such as stripping of ibuprofen due to aeration is not likely because of the low Henry coefficient [183]. More research has to be done on why ibuprofen was removed faster from the MBR effluent. The five other pharmaceuticals had first order rate constants around
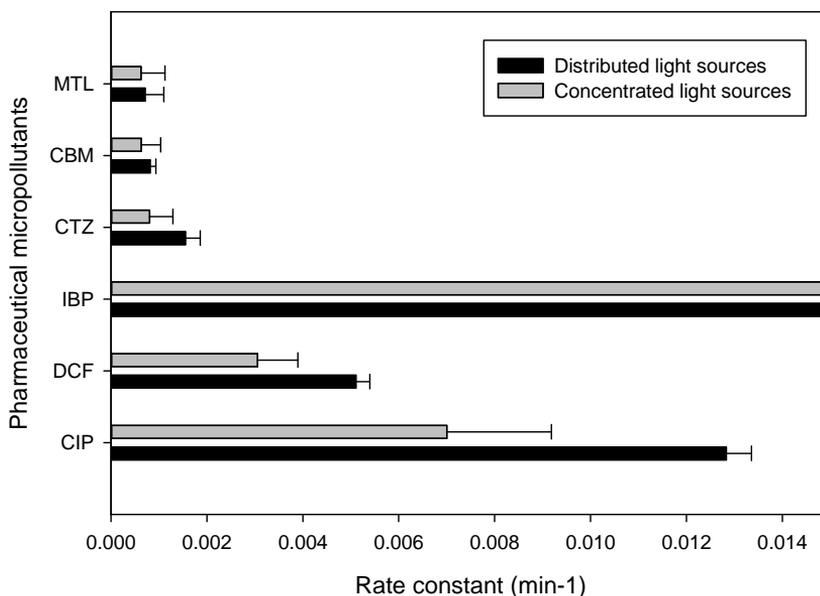
Figure 7.4: Rate constants for removal of pharmaceutical micropollutants from MBR effluent with distributed and concentrated UV-LEDs, error bars indicate 95% confidence interval.

a factor 50 smaller for MBR effluent compared to deionized water. This decrease is in line with the concentration of total organic carbon (TOC) of 14 mg/l, which is a factor 70 higher than the concentration of pharmaceuticals in the range of <200 μg/l. Previous researchers reported that competing adsorption, scavenging of hydroxyl radicals and blocking active site on TiO_2 surface by TOC and inorganic ions retarded the oxidation rate [9, 59]. The good adsorption and removal of diclofenac from wastewater in a photocatalytic reactor has been reported by other researchers [175, 120] as well as removal of ciprofloxacin from hospital wastewater [187].
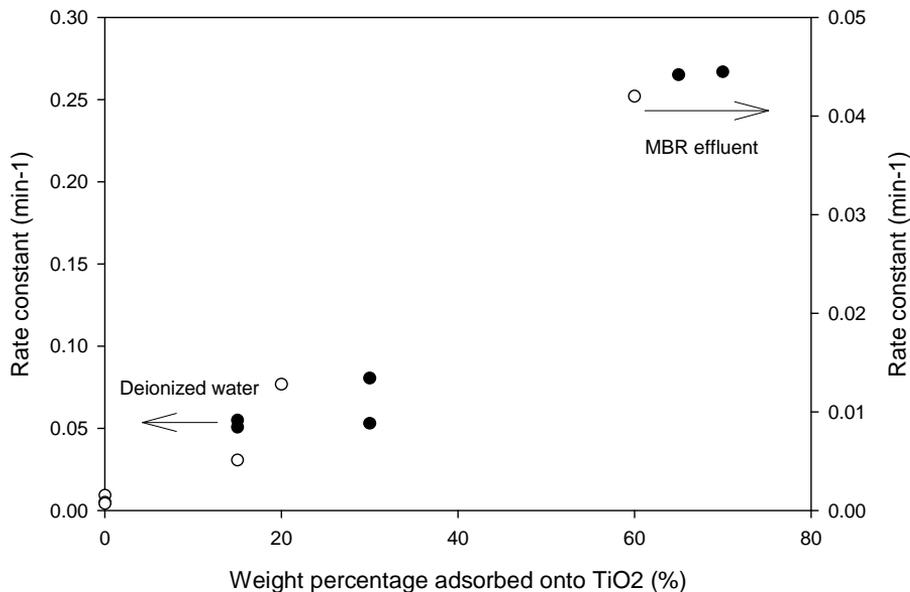
Figure 7.5: Rate constant as a function of weight percentage adsorbed onto TiO2, solid symbols are deionized water and open symbols MBR effluent .

7.3.5   Energy consumption

To compare different AOP technologies a figure of merit is used as described by Bolton et al. [16]. The electrical energy requirement for the removal of a compound by one order of magnitude EEO (kWh/m^3) was calculated as described in [13] as:

$$EEO = \frac{ln(10)}{k} \qquad (7.2)$$

With removal constant k (m^3/kWh) calculated with:

$$k = \frac{k_{app}}{OP} \qquad (7.3)$$
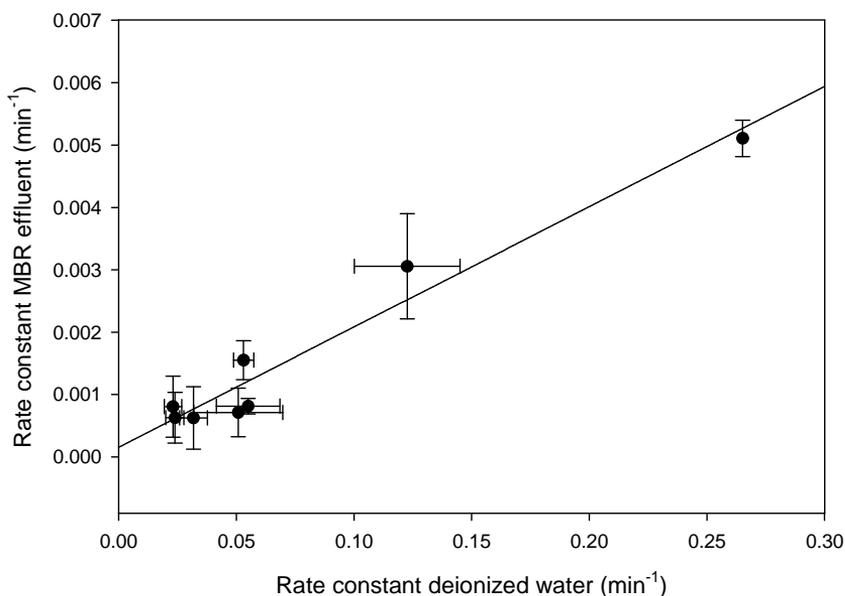
Figure 7.6: Rate constant for distributed UV-LEDs in MBR effluent as a function of the rate constant for distributed UV-LEDs in deionized water, error bars indicate 95% confidence interval.

With kapp calculated with Equation 1 and OP with output power of the UV-LEDs (kWh/min/m^3) of 4E-3 kWh/min/m^3. EEOs were calculated for each compound and the results can be seen in Table 5.

Distributed UV-LEDs showed lower EEOs for the removal of the selected pharmaceuticals from deionized water and from MBR effluent. The matrix effects of MBR effluent caused a significant increase in EEOs for all pharmaceuticals except for tetracycline and ibuprofen. Benotti reported EEOs for the removal of pharmaceuticals from river water with a significantly lower TOC (2.6 mg/l) of 2.1 kWh/m^3 for carbamazepine, 0.21 kWh/m^3 for diclofenac, and 2.9 kWh/m^3 for ibuprofen [13]. Those EEOs

Table 7.5: Start concentration and EEOs of the selected pharmaceuticals in deionized water and MBR effluent with distributed and concentrated UV-LEDs

Compound	C_0	Distr. Deionized	Conc. Deionized	Distr. MBR	Conc. MBR
	μg/l	kWh/m^3	kWh/m^3	kWh/m^3	kWh/m^3
Tetracycline	190	<0.03	<0.03	<0.03	<0.03
Ciprofloxacin	200	<0.03	<0.03	0.72	1.32
Diclofenac	170	<0.03	0.08	1.80	3.01
Cetirizine	110	0.17	0.40	5.94	11.5
Carbamazepine	140	0.17	0.39	11.3	14.7
Metoprolol	150	0.18	0.29	12.9	14.8
Ibuprofen	170	0.11	0.21	<0.03	<0.03

are in between the EEOs calculated for deionized water and MBR effluent for distributed UV-LEDs, which is in line with our results since these TOC values are in between TOC values for pharmaceutical solutions using deionized and MBR effluent. Ibuprofen has much lower EEO in MBR effluent because of the adsorption in MBR effluent. Autin et al. [8] reports an EEO of 41.1 kWh/m^3 for removal of metaldehyde from matrix with 120 mg/l alkalinity and 18.94 μM of natural organic matter.

7.4   Conclusions

This paper shows the first time wirelessly powered UV-LEDs being used as light sources in a photocatalytic reactor for the removal of pharmaceuticals. The results are promising for new reactor design with distributed UV-LEDs in a high loaded photocatalyst suspension. The reaction rate of the distributed UV-LEDs are a factor 1.3 to 1.9 higher in both deionized water and in MBR effluent compared to the concentrated UV-LEDs. Matrix effects of the MBR effluent have a negative effect on the reaction rate of 5 of the 7 investigated pharmaceuticals, ibuprofen and tetracycline being the exceptions. The affinity of the pharmaceuticals and competing

organic effluent compounds to adsorb onto the surface of the photocatalyst plays an important role on the reaction rate. The matrix effects reduced adsorption of 5 of the 7 pharmaceuticals tested, whereas the adsorption and degradation of ibuprofen and tetracycline was enhanced. The results show promising electrical energy requirements for the removal of the pharmaceuticals by one order of magnitude compared to the energy requirements of photocatalytic reactors with conventional lamps. UV-LEDs have already doubled in energetic efficiency from 15% to 30%, in the last 2 years. We therefore expect further favorable developments in energy efficiency of UV-LEDs and wirelessly powered UV-LED based photocatalytic reactors. Another important innovation to proceed, is to increase the reactivity of these reactors by miniaturizing the receiving inductor and UV-LED in order to get more UV-LEDs per volume of reactor. Photocatalytic oxidation with wirelessly powered UV-LEDs is a promising development for micropollutant removal from wastewater effluents.

Acknowledgements

Chapter 8

General discussion

8.1   Introduction

Distributed light sources for photocatalytic water treatment is presented in this thesis. The main conclusions and outcomes of the previous Chapters are given in this Chapter, followed by an outlook of different possibilities offered by wirelessly powered UV-LEDs to further improve photocatalytic reactors. A cost comparison is made between photocatalytic reactors with low, and medium pressure mercury lamps and UV-LEDs. The energy transfer efficiency with RIC is discussed and a method to design the RIC system is suggested. The photon transfer of the developed distributed UV-LED reactor is discussed and compared to other photocatalytic reactors. Some possibilities are suggested to further increase photon transfer. This thesis shows that mass transfer is an important parameter for removal of micropollutants. Different possibilities are introduced how to increase the mass transfer and how these technologies can be integrated with the distributed UV-LED reactor. Finally, possible applications are given for the distributed UV-LED reactor together with the possible improvements needed to make a distributed UV-LED reactor a competitive technology.

8.2   General conclusions

This thesis aims to increase the distribution of light in a photocatalytic reactor by using distributed UV-LEDs freely moving in a TiO_2 suspension. The UV-LEDs are powered wirelessly with RIC and the first part of the thesis deals with the influence of the number of receiving inductors and water salinity on the RIC energy transfer efficiency. In the second part of the thesis, the development and application of a novel RIC based photocatalytic reactor with UV-LEDs is described. The application of RIC for capacitive deionization shows that also other water treatment technologies can be powered with RIC.

   The feasibility to power multiple small scale electronic devices with RIC while dispersed in water is investigated in Chapter 2. A theoretical model is verified with experimental results and shows that multiple small scale elec-

tronic devices can successfully be powered even when the coupling between the transmitting and receiving inductor is low. We found that the energy transfer efficiency strongly increases with the number of receiving inductors and can be higher than 75%. The energy transfer efficiency depends on the coupling factor between the transmitting and receiving inductors, the quality factors of the inductors and number of receiving inductors. Applying small receiving inductors powered by a larger transmitting inductor with given coupling and quality factors, the efficiency can be increased further by increasing the number of receiving inductors. The cumulative coupling factor of the ensemble of secondary inductors increases with the square root of the number of receiving inductors and at high numbers it approaches asymptotically 100%. Important in optimizing energy transfer efficiency is the matching of the load to the impedance of the system. With an increasing number of receiving inductors the range of resistance of the load that can be powered with high energy transfer efficiency becomes broader as does the width of the resonance peak. The results indicate that RIC can successfully be used to power multiple small scale electronic devices submerged in water.

Chapter 3 describes the influence of water salinity on the energy transfer efficiency. Water has influence on the transmitting inductor as the transmitting inductor encloses the water making it the core material of the inductor. Water does not have any influence on the receiving inductor as it has a ferrite core. The influence of the relative permittivity and the resistivity of the core material are modeled with a lumped parameter circuit and the results of the model are verified with experimental results. Water has two effects on the transmitting inductor, i) the relative permittivity of water has an influence on the turn-to-core capacitance of the transmitting inductor, and ii) the resistivity of the water has influence on the series resistance of the turn-to-turn capacitance of the inductor. With the model, the quality factor of a electrolyte filled inductor with a given capacitance and resistance in air can successfully be calculated, making it a helpful tool to find the optimal frequency for RIC. The effect of the salinity is strongest in the concentration range of 6 to 50 μS/cm where it reduces the quality factor of the transmitting inductor.

Chapter 4 concerns the application of RIC to power porous carbon electrodes used for water desalination with capacitive deionization. A capacitor and a rectifier were connected in series to the receiving inductor. The rectifier converts the AC signal from the inductor into DC for the electrodes. The electrodes were charged with constant current from the rectifier. The experiments showed that desalination occurred but the energy transfer efficiency was very low. The efficiency can be increased by matching the load the rectifier and the rest of the RIC system. The ability to wirelessly power porous carbon electrodes unlocks new cell design and applications.

In Chapters 5 through 7, ultraviolet light emitting diodes powered with RIC for application in a novel photocatalytic reactor design with suspended TiO_2 are studied. In Chapter 5, a model is presented that describes the effects of TiO_2 loading and the emitted radiant power of submerged UV-LEDs on the rector performance. The model is verified with experimental results and show that the optimal loading of TiO2 is inversely proportional to the radiant power of the immersed UV-LED and that the optimal TiO_2 loading increases with the viewing angle of the UV-LED.

In Chapter 6 a photocatalytic reactor with distributed UV-LEDs freely moving in the TiO_2 suspension is characterized and compared to the same UV-LEDs concentrated in one plane inside the reactor, mimicking a single UV light source. In the photocatalytic oxidation of methylene blue the distributed UV-LEDs showed a factor 1.5 higher reaction rate as compared to the concentrated UV-LEDs leading to energy savings of 35%. This result is attributed to an increased photon transfer. The reaction rate increases linearly with the number of distributed UV-LEDs. Up to 64 UV-LEDs per liter reaction liquid volume could be placed in the photocatalytic reactor and were powered with an energy transfer efficiency of 75 %. A high surface area per reaction liquid volume of 72000 m^2/m^3 and illumination efficiency of 32000 m^{-1} is reached and can be increased further when the number of UV-LEDs per liter reaction liquid are increased and when the output power of the UV-LEDs are decreased. The surface area per reaction liquid volume is comparable to values reported for slurry reactors, however, the illuminated surface per reaction liquid volume and illumination efficiency is much larger for the distributed UV-LED reactor. Compared to

the immobilized systems, annular, optical fiber, monolith and spinning disk reactors, the distributed UV-LED reactor shows a factor 10-20 higher illuminated surface per reaction liquid volume. Microreactors show similar and higher surface per reaction liquid volume but unlike the distributed UV-LED reactor, cannot be up-scaled. The distributed UV-LED reactor shows promising results with high surface area per reaction liquid volume resulting in good mass transfer and high illumination efficiency resulting in good photon transfer. The reactor can be scaled up and intensified while retaining the good mass and photon transfer, by increasing the number of UV-LEDs per reaction liquid volume and decreasing the radiant power of the UV-LED. The main disadvantage compared to immobilized reactors is the need for post treatment to removed the suspended photocatalyst.

In Chapter 7, photocatalytic oxidation of pharmaceuticals representing the micro pollutants that enter the environment in effluent discharges, using the novel reactor is described. Freely moving distributed LEDs are compared with fixed LEDs. The influence of the effluent matrix is quantified by comparing results of oxidation in deionized water with results of oxidation in membrane bioreactor effluent. The reaction rate of the distributed UV-LEDs were a factor 1.3 to 2 higher compared to the reaction rate of the concentrated UV-LEDs. This increase in rate implies 25% - 50% energy savings. The reaction rates were considerable lower in MBR effluent compared to deionized water.

8.3   Cost estimation for a photocatalytic reactor

In order to make a comparison between a distributed UV-LED reactor and reactors with conventional lamps, cost estimations are made for both systems. The costs are divided in capital- and operating cost for the light sources.

The capital costs and energy costs for different light sources are calculated in euro per kilowatt-hour output power (€/kWh). Other costs, e.g. electronic components, reactor materials, maintenance, cost for pumping and others, are excluded because they are assumed to be significantly lower

than capital and energy costs for the light sources and might be of the same order of magnitude for both systems.

Table 8.1 shows the capital costs, energy costs and total costs in euro per kilowatt-hour output energy (€/kWh) for low pressure Hg, medium pressure Hg, UV-LEDs used in this research and the expected price for miniaturized UV-LEDs that still have to be developed. The price for miniaturized UV-LEDs is assumed to be that of the current price of blue LEDs, 0.05 €/piece. This is based on the fact that the materials and manufacturing are very similar for both LEDs. Table 1 shows that the capital costs of a reactor with UV-LEDs currently available are high compared to the medium pressure and low pressure lamps. Operational costs of the UV-LEDs are similar to the low pressure mercury lamps. Based on the results in Chapter 7 we assume that the distributed UV-LEDs have a factor two or higher reaction rate, so more than twice the amount of water can be treated by the distributed UV-LEDs compared to a reactor with low or medium pressure lamps with the same power. The energy used by UV-LEDs can be lowered further by applying a multitude of low power UV-LEDs (Chapter 5 and 6). When power efficiency and capital costs of the UV-LEDs approaches the values of the blue LEDs, total costs of 0.09 /kWh can be reached. Treatment costs are estimated based on electrical energy per order (EEO) to remove ciprofloxacin from MBR effluent (Chapter 7). For low and medium pressure mercury lamps the value is used for concentrated light sources (1.32 kWh/m^3) and for the UV-LEDs the value is used for distributed light sources (0.72 kWh/m^3). The table shows that the costs of UV-LEDs have to be decreased by a factor 2-3 in order to compete with low pressure mercury lamps. In water with a lower concentration of background organic compounds the treatment costs will be lower. The treatment costs can be decreased further by e.g., increasing the energy efficiency of the light sources, decreasing the costs of the light sources, increasing the efficiency of photon transfer, increasing mass transfer and increasing the quantum yield of the photocatalyst.

8.4 Energy transfer efficiency RIC

This thesis shows that high energy transfer efficiencies can be reached when powering a multitude of small scale light sources with the use of low cost, mass produced electronic components. In Chapter 2 and 3, the parameters are shown that determine the energy transfer efficiency: coupling factor, quality factors and number of receiving inductors. Reducing the size of the receiving inductor compared to the transmitting inductor will lead to a lower coupling factor. The lower coupling factor can be overcome by a higher number of receiving inductors. With the proposed miniaturization of the receiving inductor this will be possible within the volume of the reactor.

Conductivity and electromagnetic permittivity of water has an influence on the quality factor of the transmitting inductor as can be seen in Chapter 3. One inductor wound around a glass beaker was used in the experiments and showed the influence of water and permittivity. Large negative influence of conductivity can be seen from 6 to 50 μS/cm. Drinking water typically has a conductivity higher than 500 μS/cm and the resulting wastewater typically has a higher conductivity as drinking water. These values of conductivity will not give a negative influence on the quality factor of transmitting inductors and will result in high energy transfer efficiencies of RIC in these types of water.

Other geometries of inductors can be investigated to decrease parasitic capacitance in trying to achieve higher quality factors for the transmitting inductor than reported in this thesis. Different types of inductors, like honeycomb, and Helmholtz inductors can be applied. The influence of the magnetic permeability of the water in the core of the transmitting inductor is not investigated. No obvious water pollutants with high magnetic permeability could be identified, and therefore the permeability does not seem to be a relevant factor. An exception would be scaling of iron oxides, like magnetite and deposits of iron on the reactor wall.

8.5   Photon transfer and intensification

The number of UV-LEDs per reaction liquid volume can be increased by
miniaturization of the receiving inductor, capacitor and UV-LED. A higher
number of UV-LEDs per reaction liquid volume increases the efficiency
of the photon transfer further as can be seen in Chapter 5. With the
smallest commercial available size of LEDs, inductors and capacitors, a
RIC powered UV-LED can be made with size of 250 by 200 by 300 μm.
Compared to the receiving inductor, capacitor and UV-LED of 2.0 cm in
height and 0.7 cm in diameter, used in this thesis, the miniaturized UV-
LED is 50000 times smaller. With a 4.5 volume percent of UV-LEDs (64
UV-LEDs per liter) as applied in Chapter 5, the amount of miniaturized
UV-LEDs would be higher than 3 million UV-LEDs per liter with the same
volume percentage. Assuming 10 mW radiant power UV-LEDs this would
results a total radiant flux of 30 kW per liter. With an optimal loading of
TiO_2 of 1.4 g/l, a surface area of 50 m^2/l for TiO_2 and assuming the TiO_2
would absorb all of the radiation, the average absorbed light flux would be
43 mW/cm^2, higher than the threshold absorbed light flux value I$_{trsh}$ of 25
mW/cm^2 and leading to inefficient irradiation of the TiO_2.

Table 8.2 shows the reactor power and the illuminated surface area per
reaction liquid volume of UV-LEDs with different radiant power. For the
optimal TiO_2 loading of the UV-LEDs the penetration depth was calculated
after which the light intensity was lower than 25 mW/cm^2 with Equation
6.3 and the resulting irradiated volume of one UV-LED is calculated with
Equation 6.5. The number of UV-LEDs per liter is than calculated by
dividing the irradiated volume of one UV-LED by the total reaction liquid
volume. The results can be seen in Table 8.2.

Table 8.2 shows that higher number of UV-LEDs with lower radiant
power will increase the power of the reactor while maintaining a high quan-
tum efficiency. For a 1 mW radiant power UV-LED, the optimal loading is
3.1 g/l TiO_2, and the resulting penetration depth is 0.5 mm after which the
light intensity is lower than 25 mW/cm^2. It is unknown when the overlap of
neighboring radiation fields of UV-LEDs negatively start to influence each
other. A 1 liter reactor with total radiant power of 3.5 kW/l could then

theoretically treat 4.9 m^3 MBR effluent per hour using 0.72 kWh/m^3 to remove the pharmaceutical ciprofloxacin 1 order of magnitude. Next step for future research is to model the radiation field of multiple UV-LEDs and optimize for the radiant power of UV-LED and number of UV-LEDs per liter reactor.

The UV-LED consisting of a receiving inductor, capacitor and UV-LED, used in this research are distributed throughout the reactor by an up-flow of water and air. In order to make the UV-LEDs float around in the reactor the drag forces acting on the UV-LED by the up-flow of the water and air have to be equal to the gravitational forces acting on the UV-LED. The up-flow velocity of water and air is used to equalize these forces. The up-flow velocity for the UV-LEDs used in this research needed to be 1.7 m/s. This is a relatively high up-flow velocity and was overcome by adding expanded polystyrene (EPS) to lower the density of the UV-LED. A miniaturized receiving inductor, UV-LED and capacitor with the same density will result in a decreased up-flow velocity of 0.19 m/s. The miniaturized UV-LEDs will therefore be easier to distributed throughout the reactor and will also need relatively less EPS to reduce the density. This will reduce the total size of the miniaturized UV-LED further compared to the UV-LED used in this research. The amount of energy needed to distribute a UV-LED reduces with the size of UV-LED because surface area per density increases with a decrease in size.

Photon transfer efficiency can be increased further by adding a sensor to the UV-LEDs for measuring light intensity in the reactor. To avoid high or low irradiation values inside the reactor, the radiant power can be controlled by the sensor.

In experiments described in this thesis, the photocatalyst was present as a suspension. The suspension needs a post treatment step to remove the photocatalyst particles from the solution such as ultrafiltration, centrifugation or settling. Alternatively, the photocatalyst can be immobilized inside the photocatalytic reactor. The coated material can be attached to the UV-LED, the UV-LED itself could be coated or the coated material and UV-LEDs could be present separately in the reactor. Because of the flexibility of a wirelessly powered UV-LED many possibilities are available

for material and type of reactor that can be applied. A challenge will be Some examples are

8.6   Mass transfer

Adsorption of chemical compounds is an important and rate determining step as can be seen from the results in Chapter 7. Increasing adsorption capacity on TiO_2 particles is an important challenge in order to increase reaction rates and decrease treatment costs. Adsorption can possibly be increased by using a porous photocatalyst [146], coating of adsorbents, such as graphene [87], activated carbon, silica and zeolites [184], changing pH and applying an electrostatic force. A combination can be made of these technologies when the porous carbon electrodes, described in Chapter 4, are coated with photocatalyst and irradiated with an UV-LED. This system can be miniaturized into a microreactor with an active in and outflow of water [100]. In such a system, the adsorption can be increased by the porous material, the possibility of locally changing the pH, or by applying an electrostatic force. Not all compounds will react similar to porous surfaces, differences in pH, or electrostatic forces. Perhaps micro-reactors can be specialized in removal of a specific group of compounds. With a number of these specialized micro-reactors in a larger reaction volume, the treatment efficiency of such a group of heterogeneous micro-reactors can be higher in such a system.

8.7   Application of distributed UV-LEDs

This thesis shows that a distributed UV-LED reactor is a promising reactor design for photocatalytic oxidation. The wireless powering with RIC is done with 75% efficiency with relatively few optimization steps. The efficiency can be increased further to values >90%. Energetic efficiency of UV-LEDs are increasing rapidly, currently the energetic efficiency is 30%, the costs are high compared to low pressure mercury lamps but the costs are expected to go down. Photocatalytic quantum efficiency is relatively low

<5% compared to the energy transfer efficiency and energetic efficiency of the UV-LEDs. Increasing the quantum efficiency can theoretically reduce the treatment costs by a factor 20. With the current photocatalyst and further increase in photon transfer and mass transfer with high numbers of low radiant power UV-LEDs distributed throughout the reactor, very high surface area and illuminated surface area per reaction liquid volume can be reached >150000 m^2/m^3. These developments ensure an efficient irradiation of the photocatalyst and an intensified reactor able of treating large volumes of water. These advantages make the distributed UV-LED reactor a promising technology for the removal of micropollutants from wastewater effluent streams.

Table 8.1: Capital, energy and treatment costs of photocatalytic reactors with different light sources.

Type	Input power	Radiant power	Lifetime	Price	Capital costs	Energy costs	Total costs	Treatment costs
	W	W	hr	€	€/kWh	€/kWh	€/kWh	€/m^3
Low pressure Hg	140	45	9000	45.2 [156]	0.11	0.19	0.30	0.39
Medium pressure Hg	6000	750	9000	136 [156]	0.02	0.48	0.50	0.66
UV-LED	0.072	0.022	60000	1.35 [12]	1.02	0.2	1.22	0.88
LED	0.064	0.05	100000	0.05 [62]	0.01	0.08	0.09	0.06

Table 8.2: Reactor intensification with increase in number of UV-LEDs

Radiant power UV-LED mW	Number per reactor 10^6/l	Power reactor kW/l	Illuminated surface area per reaction liquid volume $10^3\mathrm{m}^{-1}$
1000	0.00029	0.29	15.5
100	0.0063	0.63	33.4
10	0.14	1.4	72
1	3.5	3.5	155
0.1	89	8.9	334

Summary

A novel photocatalytic reactor with distributed light sources for photocatalytic water treatment is presented in this thesis. Photocatalytic oxidation is a promising technology to remove micropollutants from wastewater effluents but an efficient reactor design is needed that ensures efficient irradiation of the photocatalyst and good mass transfer of the pollutants from the bulk of the solution to the surface of the photocatalyst. The novel photocatalytic reactor wirelessly powers ultraviolet light emitting diodes that are distributed throughout the reactor with energy transfer efficiency >75%. The UV-LEDs are powered with resonant inductive coupling and distributed with an up-flow of air and water mixture. The distributed UV-LEDs irradiate a large photocatalytic surface area (>32000 m^2/m^3) in an efficient way and the suspended photocatalyst shows good mass transfer (total photocatalyst surface 72000 m^2/m^3). The novel reactor is expected to be scaled-up without sacrificing irradiation efficiency and is therfore considered a promising development for future photocatalytic reactors.

Chapter 1 introduces a driving force behind the development of new water treatment technologies: forthcoming freshwater shortage. In order to protect our existing freshwater sources, wastewater has to be treated appropriately. A problem that receives more attention is pollution of freshwater sources with micropollutants. A source of micropollutants is wastewater effluent because of low removal by existing wastewater treatment. Removal of micropollutants from wastewater is possible but energy costs are generally high. One of the existing water treatment technologies for micropollutant removal is advanced oxidation with photocatalytic oxidation. The princi-

ple of photocatalytic oxidation is introduced in Chapter 1 together with already existing reactors. Light sources are an important part of the reactors dictating the possibilities for reactor design. Ultraviolet light emitting diodes (UV-LEDs) are rather new light sources for photocatalytic reactors and unlock new possibilities for reactor design. A new possibility is to distribute the UV-LEDs in a reactor and power them wirelessly with resonant inductive coupling. The expected advantage will be a more efficient irradiation of the photocatalyst. The principle of resonant inductive coupling is introduced together with existing applications for this technology.

In Chapter 2, the energy transfer efficiency is investigated to power a multitude of electronic devices dispersed in water. A theoretical model describes the energy transfer between one transmitting inductor and multiple receiving inductors that resonate with the same frequency. Data from the model are in accordance with experimental results. The parameters determining the energy transfer efficiency are: i) The coupling factor between transmitting and receiving inductors, ii) the quality factors of the transmitting and receiving inductors, iii) the number of receiving inductors and iv) the impedance matching of the receiving inductor to the load. The experimental results show that one transmitting inductor can successfully power more than 18 receiving inductors dispersed in water with efficiency higher than 75%. Compared to vacuum or air, water as core material of the transmitting inductor reduces the quality factor at high frequencies. This would have a negative effect on energy transfer efficiency but can be avoided by using the frequency range that shows no negative effect. The transmitting inductor used in Chapter 2 showed no negative influence of water until 50 kHz with maximum quality factor of 150. The results show a promising way to wirelessly power ultraviolet light emitting diodes and other electronic devices dispersed in water.

In Chapter 3 we more closely investigate the possible effects of water and salinity on resonant inductive coupling. Water has effects on the electric properties (impedance) of the transmitting inductor. The transmitting inductor encircles the water and can be interpreted as the core material of the inductor. Compared to vacuum or air, water has a higher relative electromagnetic permittivity, variable resistivity and equal electromagnetic

permeability. The influence of permittivity and resistivity is modeled with a lumped parameter circuit model of a transmitting inductor. The model is verified with experimental results and shows that the permittivity has influence on the turn-to-core capacitance and the resistivity has influence on the turn-to-turn capacitance of the transmitting inductor. The higher permittivity of water increased the self-capacitance, reduced the self-resonance frequency and thereby reduces the useful frequency range of the transmitting inductor. The resistivity adds more self-capacitance to the transmitting inductor and shows a linear relation with the series resistance of the added self-capacitance. With the model the influence of resistivity and permittivity of the core material can be predicted and this is a useful tool to predict the quality factor as a function of frequency in order to find the frequency at which the quality factor is maximum. The tranmitting inductor used in Chapter 3 showed a maximum quality factor of 160 at 150 kHz.

Chapter 4 shows wireless desalination with inductively powered porous carbon electrodes. In this chapter two porous carbon electrodes are powered with resonant inductive coupling and are used to desalinate water with capacitive deionization. A voltage is created between the two electrodes by the induced voltage in the receiving inductor. The voltage forces the positive charged ions to flow to the negative charged electrode and the negative ions to flow to the positive charged electrode. The ions are adsorbed in the porous carbon and this reduces the amount of ions in the water between the electrodes. The data shows successful desalination and that the powering with resonant inductive coupling results in a constant current in the salt adsorption step. This chapter shows that resonant inductive coupling can be used for capacitive deionization and other possible applications and opens possibilities for new reactor designs such as an application of this technology to desalination capsules in a fluidized or packed bed.

In Chapter 5, a model is described that is used to investigate the optimal photocatalyst loading for UV-LEDs. Titanium dioxed (TiO_2) is used as te photocatalyst. The model is based on a simple radiant field model that describes the light intensity of a UV-LED in a TiO_2 suspension coupled with a reaction kinetic model. The radiant field model is verified with experimental results and shows good fits with the experimental results.

The coupled model predicts the reaction rate as function of TiO_2 loading for UV-LEDs with different radiant power. The results from the coupled model are in accordance with the experimental results from a 10 mW and 250 mW radiant power UV-LEDs. The model predicts an increase in optimal loading of TiO_2 for a decrease in radiant power.

In Chapter 6, a characterization is made of the new photocatalytic reactor with distributed light sources. Ultraviolet light emitting diodes with 10 mW radiant power are used as light sources. The UV-LEDs are wirelessly powered with resonant inductive coupling and distributed throughout the reactor with an up-flow of air and water. Distributed UV-LEDs are compared to concentrated UV-LEDs mimicking a single light source. The distributed UV-LEDs show a factor 1.5 higher reaction rate compared to the concentrated UV-LEDs leading to energy savings of 35%.

Removal of seven pharmaceuticals, tetracycline, ciprofloxacin, diclofenac, cetrizine, carbamazepine, metoprolol and ibuprofen from membrane bioreactor effluent are shown in Chapter 7. A comparison was made between distributed and localized UV-LEDs and with water matrix (MBR effluent) and without water matrix (deionized water). Distributed UV-LEDs show a factor 1.3 to 1.9 higher reaction rates in both deionized water and MBR effluent. The affinity of the pharmaceuticals and competing organic effluent compounds to adsorb onto the surface of the photocatalyst plays an important role on the reaction rate. The matrix effects reduced adsorption of 5 of the 7 pharmaceuticals tested, whereas the adsorption and degradation of ibuprofen and tetracycline was enhanced or equal to the adsorption in deionized water. The results show promising electrical energy requirements for the removal of the pharmaceuticals by one order of magnitude compared to the energy requirements of photocatalytic reactors with conventional lamps. UV-LEDs have already doubled in energetic efficiency from 15% to 30% in the last 2 years. We therefore expect further developments in energy efficiency of UV-LEDs and wirelessly powered UV-LED based photocatalytic reactors. Another important innovation to proceed, is to increase the reactivity of these reactors by miniaturizing the receiving inductor and UV-LED in order to get more UV-LEDs per volume of reactor. Photocatalytic oxidation with wirelessly powered UV-LEDs is a promising

development for micropollutant removal from wastewater effluents.

In Chapter 8, the general conclusions of this thesis are given and in the general discuscussion the costs of a distributed UV-LED reactor is compared to reactors with low pressure and medium pressure lamps. Currently, the costs of UV-LEDs need to be decrease by a factor 2-3 to be competitive with low pressure mercury discharge lamps. Further improvements in energy transfer efficiency for resonant inductive coupling is discussed as well as the further increase in photon and mass transfer. The distributed UV-LED reactor shows to be a promising technology for the removal of micropollutants from wastewater effleunt and this will further increase with the future miniaturization, reduction in costs and increase in energetic efficiency.

Samenvatting

In dit proefschrift wordt een nieuwe fotokatalytische reactor met gedistribueerde lichtbronnen gepresenteerd. Fotokatalytische oxidatie is een veelbelovende technologie voor het verwijderen van microverontreinigingen uit afvalwater maar een ontwerp van een efficiënte reactor is nodig om voor een goede belichting van een groot fotokatalytisch oppervlakte en voor een goede massatransport van de bulk van het afvalwater naar de oppervlakte van de fotokatalyst te zorgen. De nieuwe fotokatalytische reactor maakt gebruik van draadloze energie overdracht om ultraviolet-licht-emitterende diodes (UV-LEDs) van energie te voorzien. De draadloze UV-LEDs worden gedistribueerd door de reactor en verdelen hun licht over het oppervlakte van de fotokatalyst. De draadloze energie overdracht komt tot stand door resonerende inductieve koppeling en de distributie door een opwaartse stroom van water en lucht. De gedistribueerde UV-LEDs kunnen een groot fotokatalytisch oppervlakte beschijnen (> 32000 m^2/m^3) op een efficiënte manier en dit resulteert in een goede massatransport (totaal oppervlakte fotokatalyst is 72000 m^2/m^3). De nieuwe reactor kan na verwachting goed kunnen worden opgeschaald zonder dat de goede belichting moeten worden opgeofferd en is daarom een veelbelovende ontwikkeling voor toekomstige fotokatalytische reactoren.

In hoofdstuk 1 wordt de drijvende kracht achter de voortdurende ontwikkeling van nieuwe waterbehandelingstechnologieën besproken, namelijk de al bestaande en toenemende waterschaarste. Om in staat te zijn om de bestaande zoetwaterbronnen te beschermen moet afvalwater voldoende worden behandeld. Een probleem dat steeds meer aandacht krijgt zijn

de zogenaamde microverontreinigingen. Een deel van deze microveron-
treinigingen komen in het milieu terecht via lozing van behandeld of onbe-
handeld afvalwater. De bestaande afvalwaterzuiveringen verwijderen slechts
een klein deel of verwijderen microverontreinigingen helemaal niet. Verwi-
jdering van microverontreinigingen met nieuwe technologieën is mogelijk
maar erg kostbaar. Een bestaande technologie voor het verwijderen van
microverontreinigingen is geavanceerde oxidatie met heterogene fotokatal-
yse. De beginselen van fotokatalyse worden in hoofdstuk 1 geïntroduceerd
samen met bestaande fotokatalytische reactoren. Een belangrijk onderdeel
van een fotokatalytische reactor is de lichtbron en deze bepaald in grote
mate de mogelijkheden van het ontwerp van de reactor. UV-LEDs zijn
relatief nieuwe lichtbronnen en openen mogelijkheden voor ontwerpen van
nieuwe reactoren. Het distribueren van de UV-LEDs in de reactor in combi-
natie met draadloze energie overdracht is een voorbeeld van de mogelijkhe-
den. De verwachte voordelen van gedistribueerde UV-LEDs is een betere
belichting van de fotokatalyst. De beginselen van resonerende inductieve
koppeling worden geïntroduceerd met al bestaande technologieën die hier
gebruik van maken.

In hoofdstuk 2 wordt de efficiëntie van draadloze energieoverdracht on-
derzocht om meerdere kleine elektronische apparaten in water van energie te
voorzien. Een theoretisch model beschrijft de energieoverdracht tussen één
zendende spoel en meerdere ontvangende spoelen die op dezelfde frequentie
resoneren. De gegevens van het theoretische model is in overeenstemming
met de experimentele gegevens en hieruit kunnen verschillende parameters
worden geïdentificeerd die de energie-efficiëntie van de overdracht bepalen:
i) koppelingsfactor tussen zendende en ontvangende spoel, ii) kwaliteitsfac-
tor van de zendende en ontvangende spoel, iii) aantal ontvangende spoelen,
en iv) de impedantie van het systeem aanpassen aan de belasting van de ont-
vangende spoel. De experimentele resultaten laten zien dat één zendende
spoel meer dan 18 ontvangende spoelen ondergedompeld in water van en-
ergie kan voorzien met een energie-efficiëntie hoger dan 75%. Vergeleken
met een vacuüm of lucht verlaagd water de kwaliteitsfactor aanzienlijk bij
hogere frequenties. Dit heeft een negatief effect op de energie-efficiëntie en
daarom moet deze hoge frequenties worden vermeden. De zendende spoel

gebruikt in dit hoofdstuk, laat geen negatieve invloeden van water zien tot 50 kilohertz met een redelijk hoge kwaliteitsfactor van 150. De resultaten laten een veelbelovende manier zien om UV-LEDs en andere elektronische apparaten ondergedompeld in water, draadloos van energie te voorzien.

In hoofdstuk 3 onderzoeken we nader de mogelijke effecten van water en het zoutgehalte van het water op resonerende inductieve koppeling. Water heeft invloed op de elektrische eigenschappen (impedantie) van de zendende spoel. De zendende spoel omcirkeld het water en het water kan worden gezien als het kernmateriaal van de zendende spoel. Vergeleken met vacuüm of lucht heeft water een hogere elektromagnetische permittiviteit, variabele elektrische weerstand en vergelijkbare elektromagnetische permeabiliteit. De invloed van de permittiviteit en weerstand van het water is gemodelleerd met een elektrisch circuit van een zendende spoel. Het model is geverifieerd met experimentele resultaten en toont dat de permittiviteit invloed heeft op de winding-kern capaciteit en de weerstand invloed heeft op de winding-winding capaciteit van de zendende spoel. Een hogere permittiviteit van water verhoogd de zelf-capaciteit, verlaagd de zelf-resonantie en verlaagd hiermee het bruikbare frequentiegebied van de spoel. De weerstand voegt zelf-capaciteit toe aan de spoel, de vervangingsweerstand in serie met deze toegevoegde zelf-capaciteit, laat een lineair verband zien met de weerstand van het water. Met het model kan de invloed van de weerstand en de permittiviteit van het kernmateriaal op de spoel worden voorspeld en het model is bruikbaar voor het voorspellen van de kwaliteitsfactor als functie van de frequentie. De zendende spoel zoals gebruikt in hoofdstuk 3 heeft een maximale kwaliteitsfactor van 160 met een frequentie van 150 kilohertz.

Hoofdstuk 4 toont poreuze koolstof elektrodes welke met inductie worden aangedreven om water draadloos mee te ontzouten. In dit hoofdstuk worden twee elektrodes aangedreven met resonerende inductieve koppeling en gebruikt om water mee te ontzouten met behulp van capacitieve deionizatie. Een spanningsverschil is gecreëerd door middel van een geïnduceerde spanning in de ontvangende spoel. De spanning dwingt de positieve ionen naar de negatief geladen elektrode en de negatieve ionen naar de positief geladen elektrode. De ionen worden geadsorbeerd in het poreuze koolstof en verlaagd de concentratie ionen in het water tussen de elektrodes. De ex-

perimentele gegevens laten succesvolle ontzouting zien. De aandrijving met resonerende inductieve koppeling resulteert in een constante stroom tijdens de zoutadsorptiestap. Dit hoofdstuk laat zien dat resonerende inductieve koppeling kan worden gebruikt voor capacitieve deionizatie en andere mogelijke toepassingen en opent nieuwe mogelijkheden voor reactorontwerpen zoals een toepassing van deze technologie in ontzoutingscapsules in een gefluidizeerd of een gepakt bed.

In hoofdstuk 5 wordt een model beschreven dat kan worden gebruikt voor het onderzoeken van de optimale lading van een fotokatalyst (TiO_2) voor een UV-LED. Het model is gebaseerd op een simpel radiatiemodel dat de lichtintensiteit van een UV-LED beschrijft welke in een TiO_2 suspensie schijnt gekoppeld aan een reactiekinetiekmodel. Het radiatiemodel is geverifieerd met experimentele resultaten en is in overeenstemming met elkaar. Het gekoppelde model voorspeld de reactiesnelheid als functie TiO_2 lading voor UV-LEDs met een verschillend stralingsvermogen. De resultaten van het gekoppelde model is in overeenstemming met de experimentele resultaten van een UV-LED met een stralingsvermogen van 10 mW en een UV-LED met een stralingsvermogen van 250 mW. Het model voorspelt een toenemende optimale lading van TiO_2 bij een afnemende stralingsvermogen.

In hoofdstuk 6 wordt de nieuwe fotokatalytische reactor, met gedistribueerde lichtbronnen, gekarakteriseerd. UV-LEDs met 10 mW stralingsvermogen worden gebruikt als lichtbronnen. De UV-LEDs worden draadloos van energie voorzien door resonerende inductieve koppeling en worden gedistribueerd in de reactor door een opstroom van lucht en water. De gedistribueerde UV-LEDs worden vergeleken met geconcentreerde UV-LEDs. De gedistribueerde UV-LEDs tonen een 1.5 maal hogere reactiesnelheid vergeleken met de geconcentreerde UV-LEDs en dit leid tot een energiebesparing van 35%.

Verwijdering van 7 medicijnen, tetracycline, ciprofloxacin, diclofenac, cetrizine, carbamazepine, metoprolol en ibuprofen uit het effluent van membraanbioreactor wordt bestudeerd in hoofdstuk 7. Een vergelijking wordt gemaakt met gedistribueerde en gelokaliseerde UV-LEDs in MBR effluent en in gedemineraliseerd water. De gedistribueerde UV-LEDs tonen een

factor 1.3 tot 1.9 hogere reactiesnelheid aan in MBR effluent en in gedemineraliseerd water. De affiniteit van de medicijnen om te adsorberen op het TiO_2 oppervlakte speelt een belangrijke rol in de verwijderingseffectiviteit. De aanwezige achtergrondorganische vervuiling in het MBR effluent heeft een negatieve invloed op de adsorptie van 5 van de 7 medicijnen en een positieve of geen effect op 2 van de 7 medicijnen. De resultaten laten goede elektrische energie behoefte zien ten opzichte van fotokatalytische reactoren met conventionele lampen. De efficiëntie van UV-LEDs is de laatste 2 jaar verdubbeld en verdere verbetering is gaande en aanstaande. Daarom verwachten we dat veelbelovende ontwikkelingen van fotokatalytische reactoren met UV-LEDs en draadloos aangedreven met RIC. Met de miniaturisatie van de UV-LEDs kan een zeer hoog fotokatalytisch oppervlakte efficiënt en gelijkmatig worden belicht waardoor de reactiviteit van fotokatalytische reactoren enorm kunnen toenemen. Hierdoor kan fotokatalytische oxidatie van medicijnresten een veelbelovende technologie voor de toekomst worden.

In hoofdstuk 8 worden de algemene conclusies van dit proefschrift besproken. De kosten van een reactor met gedistribueerde UV-LEDs wordt vergeleken met een reactor met conventionele lage- en middendrukkwiklampen. Momenteel zijn de UV-LEDs nog een factor 2-3 duurden dan de lagedrukkwiklamp. De mogelijke manieren om de energie-efficintie van RIC te verhogen, massatransport te verbeteren en fotontransport te optimaliseren worden besproken. De verdere miniaturisatie van de UV-LEDs, verlaging van de kosten van de UV-LEDs en hogere energie-efficiëntie van de UV-LEDs is nodig om de technologie concurrerend te maken met bestaande technologieën.

References

[1] Ahn, D., Hong, S., 2013. Effect of coupling between multiple transmitters or multiple receivers on wireless power transfer. IEEE Transactions on Industrial Electronics 60 (7), 2602–2613.

[2] Ahn, D., Hong, S., 2013. A study on magnetic field repeater in wireless power transfer. IEEE Transactions on Industrial Electronics 60 (1), 360–371.

[3] Al-Sayyed, G., D'Oliveira, J. C., Pichat, P., 1991. Semiconductor-sensitized photodegradation of 4-chlorophenol in water. Journal of Photochemistry and Photobiology, A: Chemistry 58 (1), 99–114.

[4] Albery, W. J., Brown, G. T., Darwent, J. R., Saievar-Iranizad, E., 1985. Time-resolved photoredox reactions of colloidal CdS. Journal of the Chemical Society, Faraday Transactions 1: Physical Chemistry in Condensed Phases 81 (8), 1999–2007.

[5] Alexy, R., Kümpel, T., Kümmerer, K., 2004. Assessment of degradation of 18 antibiotics in the closed bottle test. Chemosphere 57 (6), 505–512.

[6] Aran, H. C., Salamon, D., Rijnaarts, T., Mul, G., Wessling, M., Lammertink, R. G. H., 2011. Porous photocatalytic membrane microreactor (P2M2): A new reactor concept for photochemistry. Journal of Photochemistry and Photobiology A: Chemistry 225 (1), 36–41.

[7] Augugliaro, V., Loddo, V., Marcì, G., Palmisano, L., López-Muñoz, M. J., 1997. Photocatalytic oxidation of cyanides in aqueous titanium dioxide suspensions. Journal of Catalysis 166 (2), 272–283.

[8] Autin, O., Hart, J., Jarvis, P., MacAdam, J., Parsons, S. A., Jefferson, B., 2013. Comparison of UV/TiO_2 and UV/H_2O_2 processes in an annular photoreactor for removal of micropollutants: Influence of water parameters on metaldehyde removal, quantum yields and energy consumption. Applied Catalysis B: Environmental 138-139, 268–275.

[9] Autin, O., Hart, J., Jarvis, P., MacAdam, J., Parsons, S. A., Jefferson, B., 2013. The impact of background organic matter and alkalinity on the degradation of the pesticide metaldehyde by two advanced oxidation processes: UV/H_2O_2 and UV/TiO_2. Water Research 47 (6), 2041–2049.

[10] Barthe, P., Letourneur, D., Themont, J., Woehl, P., Jul. 23 2002. Method and microfluidic reactor for photocatalysis. EP Patent 1,415,707.

[11] Beh, T. C., Kato, M., Imura, T., Oh, S., Hori, Y., 2013. Automated impedance matching system for robust wireless power transfer via magnetic resonance coupling. IEEE Transactions on Industrial Electronics 60 (9), 3689–3698.

[12] Benkritly, M., January 2012. Personal communication about costs UVA-LED Nichia.

[13] Benotti, M. J., Stanford, B. D., Wert, E. C., Snyder, S. A., 2009. Evaluation of a photocatalytic reactor membrane pilot system for the removal of pharmaceuticals and endocrine disrupting compounds from water. Water Research 43 (6), 1513–1522.

[14] Blake, D. M., 1994. Bibliography of work on the heterogeneous photocatalytic removal of hazardous compounds from water and air. Vol. 1617. National Renewable Energy Laboratory.

[15] Bodzek, M., Rajca, M., 2012. Photocatalysis in the treatment and disinfection of water. Part I. Theoretical backgrounds. Ecological Chemistry and Engineering S 19 (4), 489–512.

[16] Bolton, J. R., Bircher, K. G., Tumas, W., Tolman, C. A., 2001. Figures-of-merit for the technical development and application of advanced oxidation technologies for both electric- and solar-driven systems. Pure and Applied Chemistry 73 (4), 627–637.

[17] Bouhadana, Y., Avraham, E., Noked, M., Ben-Tzion, M., Soffer, A., Aurbach, D., 2011. Capacitive deionization of NaCl solutions at non-steady-state conditions: Inversion functionality of the carbon electrodes. Journal of Physical Chemistry C 115 (33), 16567–16573.

[18] Bowker, C., Sain, A., Shatalov, M., Ducoste, J., 2011. Microbial UV fluence-response assessment using a novel UV-LED collimated beam system. Water Research 45 (5), 2011–2019.

[19] Brogioli, D., 2009. Extracting renewable energy from a salinity difference using a capacitor. Physical Review Letters 103 (5).

[20] Burheim, O. S., Liu, F., Sales, B. B., Schaetzle, O., Buisman, C. J. N., Hamelers, H. V. M., 2012. Faster time response by the use of wire electrodes in capacitive salinity gradient energy systems. Journal of Physical Chemistry C 116 (36), 19203–19210.

[21] Buser, H. R., Poiger, T., Mäller, M. D., 1999. Occurrence and environmental behavior of the chiral pharmaceutical drug ibuprofen in surface waters and in wastewater. Environmental Science and Technology 33 (15), 2529–2535.

[22] Buser, H. R., Poiger, T., Müller, M. D., 1998. Occurrence and fate of the pharmaceutical drug diclofenac in surface waters: Rapid photodegradation in a lake. Environmental Science and Technology 32 (22), 3449–3456.

[23] Butkovskyi, A., Jeremiasse, A. W., Hernandez Leal, L., Van Der Zande, T., Rijnaarts, H., Zeeman, G., 2014. Electrochemical conversion of micropollutants in gray water. Environmental Science and Technology 48 (3), 1893–1901.

[24] Carballa, M., Fink, G., Omil, F., Lema, J. M., Ternes, T., 2008. Determination of the solid-water distribution coefficient (Kd) for pharmaceuticals, estrogens and musk fragrances in digested sludge. Water Research 42 (1-2), 287–295.

[25] Carballa, M., Omil, F., Ternes, T., Lema, J. M., 2007. Fate of pharmaceutical and personal care products (PPCPs) during anaerobic digestion of sewage sludge. Water Research 41 (10), 2139–2150.

[26] Carbonaro, S., Sugihara, M. N., Strathmann, T. J., 2013. Continuous-flow photocatalytic treatment of pharmaceutical micropollutants: Activity, inhibition, and deactivation of TiO_2 photocatalysts in wastewater effluent. Applied Catalysis B: Environmental 129, 1–12.

[27] Carta, R., Sfakiotakis, M., Pateromichelakis, N., Thone, J., Tsakiris, D. P., Puers, R., 2011. A multi-coil inductive powering system for an endoscopic capsule with vibratory actuation. Sensors and Actuators a-Physical 172 (1), 253–258.

[28] Carta, R., Tortora, G., Thoné, J., Lenaerts, B., Valdastri, P., Menciassi, A., Dario, P., Puers, R., 2009. Wireless powering for a self-propelled and steerable endoscopic capsule for stomach inspection. Biosensors and Bioelectronics 25 (4), 845–851.

[29] Casanova, J. J., Low, Z. N., Lin, J., 2009. A loosely coupled planar wireless power system for multiple receivers. IEEE Transactions on Industrial Electronics 56 (8), 3060–3068.

[30] Cassano, A. E., Alfano, O. M., 2000. Reaction engineering of suspended solid heterogeneous photocatalytic reactors. Catalysis Today 58 (2), 167–197.

[31] Chen, D. H., Ye, X., Li, K., 2005. Oxidation of PCE with a UV LED photocatalytic reactor. Chemical Engineering and Technology 28 (1), 95–97.

[32] Chen, J., 1997. Advanced oxidation technologies: Photocatalytic treatment of wastewater. Landbouwuniversiteit Wageningen.

[33] Chen, J., Ollis, D. F., Rulkens, W. H., Bruning, H., 1999. Kinetic processes of photocatalytic mineralization of alcohols on metallized titanium dioxide. Water Research 33 (5), 1173–1180.

[34] Chen, J., Ollis, D. F., Rulkens, W. H., Bruning, H., 1999. Photo-catalyzed deposition and concentration of soluble uranium(VI) from TiO_2 suspensions. Colloids and Surfaces A: Physicochemical and Engineering Aspects 151 (1-2), 339–349.

[35] Chen, J., Ollis, D. F., Rulkens, W. H., Bruning, H., 1999. Photo-catalyzed oxidation of alcohols and organochlorides in the presence of native TiO_2 and metallized TiO_2 suspensions. Part (I): Photocatalytic activity and pH influence. Water Research 33 (3), 661–668.

[36] Chen, J., Ollis, D. F., Rulkens, W. H., Bruning, H., 1999. Photocat-alyzed oxidation of alcohols and organochlorides in the presence of native TiO_2 and metallized TiO_2 suspensions. Part (II): Photocatalytic mechanisms. Water Research 33 (3), 669–676.

[37] Chen, J., Rulkens, W. H., Bruning, H., 1997. Photochemical elimination of phenols and COD in industrial wastewaters. Water Science and Technology 35 (4), 231–238.

[38] Chen, L., Liu, S., Zhou, Y. C., Cui, T. J., 2013. An optimizable circuit structure for high-efficiency wireless power transfer. IEEE Transactions on Industrial Electronics 60 (1), 339–349.

[39] Choi, J., Lee, H., Choi, Y., Kim, S., Lee, S., Choi, W., Lee, J., 2014. Heterogeneous photocatalytic treatment of pharmaceutical micropol-

lutants: Effects of wastewater effluent matrix and catalyst modifications. Applied Catalysis B: Environmental 147, 8–16.

[40] Chong, M. N., Jin, B., Chow, C. W. K., Saint, C., 2010. Recent developments in photocatalytic water treatment technology: A review. Water Research 44 (10), 2997–3027.

[41] Chua, C. L., Fork, D. K., Van Schuylenbergh, K., Lu, J. P., 2003. Out-of-plane high-Q inductors on low-resistance silicon. Journal of Microelectromechanical Systems 12 (6), 989–995.

[42] Cipollina, A., Micale, G., Rizzuti, L., 2009. Seawater Desalination Conventional and Renewable Energy Processes.

[43] Clara, M., Strenn, B., Kreuzinger, N., 2004. Carbamazepine as a possible anthropogenic marker in the aquatic environment: Investigations on the behaviour of carbamazepine in wastewater treatment and during groundwater infiltration. Water Research 38 (4), 947–954.

[44] Cohen-Tanugi, D., Grossman, J. C., 2012. Water desalination across nanoporous graphene. Nano Letters 12 (7), 3602–3608.

[45] Colina-Márquez, J., MacHuca-Martínez, F., Puma, G. L., 2010. Radiation absorption and optimization of solar photocatalytic reactors for environmental applications. Environmental Science and Technology 44 (13), 5112–5120.

[46] Danion, A., Disdier, J., Guillard, C., Abdelmalek, F., Jaffrezic-Renault, N., 2006. Characterization and study of a single TiO_2-coated optical fiber reactor. International Journal of Applied Electromagnetics and Mechanics 23 (3-4), 187–201.

[47] Daughton, C. G., Ternes, T. A., 1999. Pharmaceuticals and personal care products in the environment: Agents of subtle change? Environmental Health Perspectives 107, 907–938.

[48] De Boeij, J., Lomonova, E., Duarte, J. L., Vandenput, A. J. A., 2008. Contactless power supply for moving sensors and actuators in high-precision mechatronic systems with long-stroke power transfer capability in x-y plane. Sensors and Actuators, A: Physical 148 (1), 319–328.

[49] de Graaff, M. S., Vieno, N. M., Kujawa-Roeleveld, K., Zeeman, G., Temmink, H., Buisman, C. J. N., 2011. Fate of hormones and pharmaceuticals during combined anaerobic treatment and nitrogen removal by partial nitritation-anammox in vacuum collected black water. Water Research 45 (1), 375–383.

[50] Demirer, O. N., Naylor, R. M., Rios Perez, C. A., Wilkes, E., Hidrovo, C., 2013. Energetic performance optimization of a capacitive deionization system operating with transient cycles and brackish water. Desalination 314, 130–138.

[51] Dijkstra, M. F. J., Buwalda, H., De Jong, A. W. F., Michorius, A., Winkelman, J. G. M., Beenackers, A. A. C. M., 2001. Experimental comparison of three reactor designs for photocatalytic water purification. Chemical Engineering Science 56 (2), 547–555.

[52] Dijkstra, M. F. J., Koerts, E. C. B., Beenackers, A. A. C. M., Wesselingh, J. A., 2003. Performance of immobilized photocatalytic reactors in continuous mode. AIChE Journal 49 (3), 734–744.

[53] Dijkstra, M. F. J., Michorius, A., Buwalda, H., Panneman, H. J., Winkelman, J. G. M., Beenackers, A. A. C. M., 2001. Comparison of the efficiency of immobilized and suspended systems in photocatalytic degradation. Catalysis Today 66 (2-4), 487–494.

[54] Dijkstra, M. F. J., Panneman, H. J., Winkelman, J. G. M., Kelly, J. J., Beenackers, A. A. C. M., 2002. Modeling the photocatalytic degradation of formic acid in a reactor with immobilized catalyst. Chemical Engineering Science 57 (22-23), 4895–4907.

[55] Dionysiou, D. D., Balasubramanian, G., Suidan, M. T., Khodadoust, A. P., Baudin, I., Lan, J. M., 2000. Rotating disk photocatalytic reactor: Development, characterization, and evaluation for the destruction of organic pollutants in water. Water Research 34 (11), 2927–2940.

[56] Długołęcki, P., Van Der Wal, A., 2013. Energy recovery in membrane capacitive deionization. Environmental Science and Technology 47 (9), 4904–4910.

[57] Dodd, C. V., Deeds, W. E., 1968. Analytical solutions to eddy-current probe-coil problems. Journal of Applied Physics 39 (6), 2829.

[58] D'Oliveira, J. C., Al-Sayyed, G., Pichat, P., 1990. Photodegradation of 2- and 3-chlorophenol in TiO_2 aqueous suspensions. Environmental Science and Technology 24 (7), 990–996.

[59] Doll, T. E., Frimmel, F. H., 2005. Photocatalytic degradation of carbamazepine, clofibric acid and iomeprol with P25 and Hombikat UV100 in the presence of natural organic matter (NOM) and other organic water constituents. Water Research 39 (2-3), 403–411.

[60] Elimelech, M., Phillip, W. A., 2011. The future of seawater desalination: Energy, technology, and the environment. Science 333 (6043), 712–717.

[61] Faraday, M., 1836. Experimental researches in electricity. Eighth series. Journal of the Franklin Institute 21 (4), 282–286.

[62] Farnell, June 2014. Costs SMD LEDs.
URL `http://nl.farnell.com`

[63] French, R. A., Jacobson, A. R., Kim, B., Isley, S. L., Penn, L., Baveye, P. C., 2009. Influence of ionic strength, pH, and cation valence on aggregation kinetics of titanium dioxide nanoparticles. Environmental Science and Technology 43 (5), 1354–1359.

[64] Fritzmann, C., Löwenberg, J., Wintgens, T., Melin, T., 2007. State-of-the-art of reverse osmosis desalination. Desalination 216 (1-3), 1–76.

[65] Fujishima, A., Honda, K., 1972. Electrochemical photolysis of water at a semiconductor electrode. Nature 238 (5358), 37–38.

[66] Ghosh, J. P., Sui, R., Langford, C. H., Achari, G., Berlinguette, C. P., 2009. A comparison of several nanoscale photocatalysts in the degradation of a common pollutant using LEDs and conventional UV light. Water Research 43 (18), 4499–4506.

[67] Gogate, P. R., Kabadi, A. M., 2009. A review of applications of cavitation in biochemical engineering/biotechnology. Biochemical Engineering Journal 44 (1), 60–72.

[68] Goodeve, C. F., Kitchener, J. A., 1938. Photosensitisation by titanium dioxide. Transactions of the Faraday Society 34 (0), 570–579.

[69] Gorges, R., Meyer, S., Kreisel, G., 2004. Photocatalysis in microreactors. Journal of Photochemistry and Photobiology A: Chemistry 167 (2-3), 95–99.

[70] Grandi, G., Kazimierczuk, M. K., Massarini, A., Reggiani, U., 1999. Stray capacitances of single-layer solenoid air-core inductors. IEEE Transactions on Industry Applications 35 (5), 1162–1168.

[71] Greenlee, L. F., Lawler, D. F., Freeman, B. D., Marrot, B., Moulin, P., 2009. Reverse osmosis desalination: Water sources, technology, and today's challenges. Water Research 43 (9), 2317–2348.

[72] Hall, R., Fenner, G., Kingsley, J., Soltys, T., Carlson, R., 1962. Coherent light emission from Ga-As junctions. Phys. Rev. Lett 9, 366.

[73] Hamam, R. E., Karalis, A., Joannopoulos, J. D., Soljačić, M., 2009. Efficient weakly-radiative wireless energy transfer: An EIT-like approach. Annals of Physics 324 (8), 1783–1795.

[74] Han, L., Karthikeyan, K. G., Anderson, M. A., Wouters, J. J., Gregory, K. B., 2013. Mechanistic insights into the use of oxide nanoparticles coated asymmetric electrodes for capacitive deionization. Electrochimica Acta 90, 573–581.

[75] Hayashi, N., Yasutomi, R., Kasai, E., 2010. Development of dispersed-type sonophotocatalytic process using piezoelectric effect caused by ultrasonic resonance. Ultrasonics Sonochemistry 17 (5), 884–891.

[76] Hernandez-Leal, L., Temmink, H., Zeeman, G., Buisman, C. J. N., 2011. Removal of micropollutants from aerobically treated grey water via ozone and activated carbon. Water Research 45 (9), 2887–2896.

[77] Hernandez Leal, L., Vieno, N., Temmink, H., Zeeman, G., Buisman, C. J. N., 2011. Occurrence of xenobiotics in gray water and removal in three biological treatment systems. Environmental Science and Technology 45 (1), 351.

[78] Herrmann, J. M., 1999. Heterogeneous photocatalysis: Fundamentals and applications to the removal of various types of aqueous pollutants. Catalysis Today 53 (1), 115–129.

[79] Hofstadler, K., Bauer, R., 1994. New reactor design for photocatalytic wastewater treatment with TiO_2 immobilized on fused-silica glass fibers: Photomineralization of 4- chlorophenol. Environmental Science and Technology 28 (4), 670–674.

[80] Holonyak Jr, N., Bevacqua, S., 1962. Coherent (visible) light emission from Ga (As1-XPx) junctions. Applied Physics Letters 1, 82–83.

[81] Hu, A., Zhang, X., Luong, D., Oakes, K. D., Servos, M. R., Liang, R., Kurdi, S., Peng, P., Zhou, Y., 2012. Adsorption and photocatalytic degradation kinetics of pharmaceuticals by TiO_2 nanowires during water treatment. Waste and Biomass Valorization 3 (4), 443–449.

[82] Huang, A., Wang, N., Lei, M., Zhu, L., Zhang, Y., Lin, Z., Yin, D., Tang, H., 2013. Efficient oxidative debromination of decabromodiphenyl ether by TiO_2-mediated photocatalysis in aqueous environment. Environmental Science and Technology 47 (1), 518–525.

[83] Huntington, T. G., 2006. Evidence for intensification of the global water cycle: Review and synthesis. Journal of Hydrology 319 (1-4), 83–95.

[84] Hwang, S., Morgan, D., Kesler, A., Lachab, M., Zhang, B., Heidari, A., Nazir, H., Ahmad, I., Dion, J., Fareed, Q., Adivarahan, V., Islam, M., Khan, A., 2011. 276nm substrate-free flip-chip AlGaN light-emitting diodes. Applied Physics Express 4 (3).

[85] Imoberdorf, G. E., Cassano, A. E., Alfano, O. M., Irazoqui, H. A., 2006. Modeling of a multiannular photocatalytic reactor for perchloroethylene degradation in air. AIChE Journal 52 (5), 1814–1823.

[86] Jeon, S. I., Park, H. R., Yeo, J. G., Yang, S., Cho, C. H., Han, M. H., Kim, D. K., 2013. Desalination via a new membrane capacitive deionization process utilizing flow-electrodes. Energy and Environmental Science 6 (6), 1471–1475.

[87] Jiang, G., Lin, Z., Chen, C., Zhu, L., Chang, Q., Wang, N., Wei, W., Tang, H., 2011. TiO_2 nanoparticles assembled on graphene oxide nanosheets with high photocatalytic activity for removal of pollutants. Carbon 49 (8), 2693–2701.

[88] Jo, W. K., Eun, S. S., Shin, S. H., 2011. Feasibility of light-emitting diode uses for annular reactor inner-coated with TiO_2 or nitrogen-doped TiO_2 for control of dimethyl sulfide. Photochemistry and Photobiology 87 (5), 1016–1023.

[89] Kanakaraju, D., Glass, B. D., Oelgemöller, M., 2013. Titanium dioxide photocatalysis for pharmaceutical wastewater treatment. Environmental Chemistry Letters, 1–21.

[90] Kappel, C., Kemperman, A. J. B., Temmink, H., Zwijnenburg, A., Rijnaarts, H. H. M., Nijmeijer, K., 2014. Impacts of NF concentrate recirculation on membrane performance in an integrated MBR and NF membrane process for wastewater treatment. Journal of Membrane Science 453, 359–368.

[91] Karalis, A., Joannopoulos, J. D., Soljačić, M., 2008. Efficient wireless non-radiative mid-range energy transfer. Annals of Physics 323 (1), 34–48.

[92] Kazimierczuk, M. K., Wojda, R. P., 2010. Foil winding resistance and power loss in individual layers of inductors. International Journal of Electronics and Telecommunications 56 (3), 237–246.

[93] Khawaji, A. D., Kutubkhanah, I. K., Wie, J. M., 2008. Advances in seawater desalination technologies. Desalination 221 (1-3), 47–69.

[94] Ko, W. H., Liang, S. P., Fung, C. D. F., 1977. Design of radio-frequency powered coils for implant instruments. Medical and Biological Engineering and Computing 15 (6), 634–640.

[95] Kormann, C., Bahnemann, D. W., Hoffmann, M. R., 1991. Photolysis of chloroform and other organic molecules in aqueous TiO_2 suspensions. Environmental Science and Technology 25 (3), 494–500.

[96] Kosonen, J., Kronberg, L., 2009. The occurrence of antihistamines in sewage waters and in recipient rivers. Environmental Science and Pollution Research 16 (5), 555–564.

[97] Kuipers, J., Bruning, H., Bakker, S., Rijnaarts, H., 2012. Near field resonant inductive coupling to power electronic devices dispersed in water. Sensors and Actuators, A: Physical 178, 217–222.

[98] Kuipers, J., Bruning, H., Bakker, S., Rijnaarts, H., 2012. Near field resonant inductive coupling to power electronic devices dispersed in water. Sensors and Actuators, A: Physical 178, 217–222.

[99] Kuipers, J., Bruning, H., Yntema, D., Bakker, S., Rijnaarts, H., 2014. Self-capacitance and resistive losses of saline-water-filled inductors. IEEE Transactions on Industrial Electronics 61 (5), 2356–2361.

[100] Kuipers, J., Yntema, D. R., Bakker, S. M., Jul. 23 2012. Hydrophone pump, container and method therefor. WO/2012/047,106.

[101] Kujawa-Roeleveld, K., Schuman, E., Grotenhuis, T., Kragic, D., Mels, A., Zeeman, G., 2008. Biodegradability of human pharmaceutically active compounds (PhAC) in biological systems treating source separated wastewater streams. In: Proceeding of the IWA international conference Sanitation Challenge. pp. 19–21.

[102] Kurs, A., Karalis, A., Moffatt, R., Joannopoulos, J. D., Fisher, P., Soljačić, M., 2007. Wireless power transfer via strongly coupled magnetic resonances. Science 317 (5834), 83–86.

[103] Laera, G., Chong, M. N., Jin, B., Lopez, A., 2011. An integrated MBR-TiO$_2$ photocatalysis process for the removal of carbamazepine from simulated pharmaceutical industrial effluent. Bioresource Technology 102 (13), 7012–7015.

[104] Laera, G., Jin, B., Zhu, H., Lopez, A., 2011. Photocatalytic activity of TiO$_2$ nanofibers in simulated and real municipal effluents. Catalysis Today 161 (1), 147–152.

[105] Lee, J. B., Park, K. K., Eum, H. M., Lee, C. W., 2006. Desalination of a thermal power plant wastewater by membrane capacitive deionization. Desalination 196 (1-3), 125–134.

[106] Lee, J. H., Bae, W. S., Choi, J. H., 2010. Electrode reactions and adsorption/desorption performance related to the applied potential in a capacitive deionization process. Desalination 258 (1-3), 159–163.

[107] Lenaerts, B., Puers, R., 2007. An inductive power link for a wireless endoscope. Biosensors and Bioelectronics 22 (7), 1390–1395.

[108] Li, X., Fitzgerald, P., Bowen, L., 1992. Sensitized photo-degradation of chlorophenols in a continuous flow reactor system. Water Science and Technology 26 (1-2), 367–376.

[109] Li, X. Z., Fan, C. M., Sun, Y. P., 2002. Enhancement of photocatalytic oxidation of humic acid in TiO_2 suspensions by increasing cation strength. Chemosphere 48 (4), 453–460.

[110] Li Puma, G., Brucato, A., 2007. Dimensionless analysis of slurry photocatalytic reactors using two-flux and six-flux radiation absorption-scattering models. Catalysis Today 122 (1-2), 78–90.

[111] Li Puma, G., Khor, J. N., Brucato, A., 2004. Modeling of an annular photocatalytic reactor for water purification: Oxidation of pesticides. Environmental Science and Technology 38 (13), 3737–3745.

[112] Lim, T. H., Kim, S. D., 2004. Trichloroethylene degradation by photocatalysis in annular flow and annulus fluidized bed photoreactors. Chemosphere 54 (3), 305–312.

[113] Lin, H., Valsaraj, K. T., 2005. Development of an optical fiber monolith reactor for photocatalytic wastewater treatment. Journal of Applied Electrochemistry 35 (7-8), 699–708.

[114] Liu, X., Ng, W. M., Lee, C. K., Hui, S. Y., 2008. Optimal operation of contactless transformers with resonance in secondary circuits. In: Conference Proceedings - IEEE Applied Power Electronics Conference and Exposition - APEC. pp. 645–650.

[115] Low, Z. N., Chinga, R. A., Tseng, R., Lin, J., 2009. Design and test of a high-power high-efficiency loosely coupled planar wireless power transfer system. IEEE Transactions on Industrial Electronics 56 (5), 1801–1812.

[116] Lucklum, F., Jakoby, B., 2008. Novel magnetic-acoustic resonator sensors for remote liquid phase measurement and mass detection. Sensors and Actuators, A: Physical 145, 44–51.

[117] Madawala, U. K., Thrimawithana, D. J., 2011. A bidirectional inductive power interface for electric vehicles in V2G systems. IEEE Transactions on Industrial Electronics 58 (10), 4789–4796.

[118] Malato, S., Fernndez-Ibez, P., Maldonado, M. I., Blanco, J., Gernjak, W., 2009. Decontamination and disinfection of water by solar photocatalysis: Recent overview and trends. Catalysis Today 147 (1), 1–59.

[119] Mani, A., Bazant, M. Z., 2011. Deionization shocks in microstructures. Physical Review E - Statistical, Nonlinear, and Soft Matter Physics 84 (6).

[120] Martínez, F., López-Muñoz, M. J., Aguado, J., Melero, J. A., Arsuaga, J., Sotto, A., Molina, R., Segura, Y., Pariente, M. I., Revilla, A., Cerro, L., Carenas, G., 2013. Coupling membrane separation and photocatalytic oxidation processes for the degradation of pharmaceutical pollutants. Water Research 47 (15), 5647–5658.

[121] Massarini, A., Kazimierczuk, M. K., 1997. Self-capacitance of inductors. IEEE Transactions on Power Electronics 12 (4), 671–676.

[122] Massarini, A., Kazimierczuk, M. K., Grandi, G., 1996. Lumped parameter models for single- and multiple-layer inductors. In: 27th Annual IEEE Power Electronics Specialists Conference, Volumes I and II. IEEE Power Electronics Specialists Conference Records. pp. 295–301.

[123] Matsushita, Y., Kumada, S., Wakabayashi, K., Sakeda, K., Ichimura, T., 2006. Photocatalytic reduction in microreactors. Chemistry Letters 35 (4), 410–411.

[124] Maurer, M., Escher, B. I., Richle, P., Schaffner, C., Alder, A. C., 2007. Elimination of beta-blockers in sewage treatment plants. Water Research 41 (7), 1614–1622.

[125] Mazzeo, B. A., 2010. Analytic solutions for capacitance of cylinders near a dielectric interface. IEEE Transactions on Dielectrics and Electrical Insulation 17 (6), 1877–1883.

[126] McCullagh, C., Robertson, J. M., Bahnemann, D. W., Robertson, P. K., 2007. The application of TiO_2 photocatalysis for disinfection of water contaminated with pathogenic micro-organisms: A review. Research on Chemical Intermediates 33 (3-5), 359–375.

[127] McCullagh, C., Skillen, N., Adams, M., Robertson, P. K., 2011. Photocatalytic reactors for environmental remediation: A review. Journal of Chemical Technology and Biotechnology 86 (8), 1002–1017.

[128] Medhurst, R., 1947. High frequency resistance and self-capacitance of single-layer solenoids. Wireless Engineer, 35–43.

[129] Mehos, M. S., Turchi, C. S., 1993. Field testing solar photocatalytic detoxification on TCE contaminated groundwater. Environmental progress 12 (3), 194–199.

[130] Mills, A., Davies, R. H., Worsley, D., 1993. Water purification by semiconductor photocatalysis. Chem. Soc. Rev. 22 (6), 417–425.

[131] Mills, G., Hoffmann, M. R., 1993. Photocatalytic degradation of pentachlorophenol on TiO_2 particles: Identification of intermediates and mechanism of reaction. Environmental Science and Technology 27 (8), 1681–1689.

[132] Montgomery, M. A., Elimelech, M., 2007. Water and sanitation in developing countries: Including health in the equation - Millions suffer from preventable illnesses and die every year. Environmental Science and Technology 41 (1), 17–24.

[133] Moreno, I., Avendao-Alejo, M., Tzonchev, R. I., 2006. Designing light-emitting diode arrays for uniform near-field irradiance. Applied Optics 45 (10), 2265–2272.

[134] Mukherjee, P. S., Ray, A. K., 1999. Major challenges in the design of a large-scale photocatalytic reactor for water treatment. Chemical Engineering and Technology 22 (3), 253–260.

[135] Murthy-Bellur, D., Bauer, A., Kerin, W., Kazimierczuk, M. K., 2012. Inverter using loosely coupled inductors for wireless power transfer. In: Proceedings of the 55th IEEE Midwest Symposium on Circuits and Systems. pp. 1164–1167.

[136] Mylonas, A., Papaconstantinou, E., 1994. Photocatalytic degradation of chlorophenols to CO_2 and HCl with polyoxotungstates in aqueous solution. Journal of Molecular Catalysis 92 (3), 261–267.

[137] Nakamura, S., Harada, Y., Seno, M., 1991. Novel metalorganic chemical vapor deposition system for GaN growth. Applied Physics Letters 58 (18), 2021–2023.

[138] Nakamura, S., Mukai, T., Senoh, M., 1991. High-power GaN pn junction blue-light-emitting diodes. Japanese Journal of Applied Physics 30 (12A), L1998–L2001.

[139] Narukawa, Y., Ichikawa, M., Sanga, D., Sano, M., Mukai, T., 2010. White light emitting diodes with super-high luminous efficacy. Journal of Physics D: Applied Physics 43 (35).

[140] Natarajan, K., Natarajan, T. S., Bajaj, H. C., Tayade, R. J., 2011. Photocatalytic reactor based on $UV-LED/TiO_2$ coated quartz tube for degradation of dyes. Chemical Engineering Journal 178, 40–49.

[141] Natarajan, T. S., Natarajan, K., Bajaj, H. C., Tayade, R. J., 2011. Energy efficient UV-LED source and TiO_2 nanotube array-based reactor for photocatalytic application. Industrial and Engineering Chemistry Research 50 (13), 7753–7762.

[142] Oh, H. J., Lee, J. H., Ahn, H. J., Jeong, Y., Kim, Y. J., Chi, C. S., 2006. Nanoporous activated carbon cloth for capacitive deionization of aqueous solution. Thin Solid Films 515 (1), 220–225.

[143] Okamoto, K.-i., Yamamoto, Y., Tanaka, H., Itaya, A., 1985. Kinetics of heterogeneous photocatalytic decomposition of phenol over anatase TiO_2 powder. Bulletin of the Chemical Society of Japan 58 (7), 2023–2028.

[144] Oki, T., Kanae, S., 2006. Global hydrological cycles and world water resources. Science 313 (5790), 1068–1072.

[145] Ollis, D. F., Pelizzetti, E., Serpone, N., 1991. Destruction of water contaminants. Environmental Science and Technology 25 (9), 1523–1529.

[146] Pan, J. H., Dou, H., Xiong, Z., Xu, C., Ma, J., Zhao, X. S., 2010. Porous photocatalysts for advanced water purifications. Journal of Materials Chemistry 20 (22), 4512–4528.

[147] Pankove, J., Miller, E., Berkeyheiser, J., 1972. GaN blue light-emitting diodes. Journal of Luminescence 5 (1), 84–86.

[148] Pasta, M., Battistel, A., La Mantia, F., 2012. Batteries for lithium recovery from brines. Energy and Environmental Science 5 (11), 9487–9491.

[149] Pasta, M., Wessells, C. D., Cui, Y., La Mantia, F., 2012. A desalination battery. Nano Letters 12 (2), 839–843.

[150] Peill, N. J., Hoffmann, M. R., 1995. Development and optimization of a TiO_2-coated fiber-optic cable reactor: Photocatalytic degradation of 4-chlorophenol. Environmental Science and Technology 29 (12), 2974–2981.

[151] Peill, N. J., Hoffmann, M. R., 1996. Chemical and physical characterization of a TiO_2-coated fiber optic cable reactor. Environmental Science and Technology 30 (9), 2806–2812.

[152] Philips, N.V., K. P. E., 2011. Knowing you're safe; Philips UV purification lamp systems.

[153] Porada, S., Sales, B. B., Hamelers, H. V. M., Biesheuvel, P. M., 2012. Water desalination with wires. Journal of Physical Chemistry Letters 3 (12), 1613–1618.

[154] Porada, S., Zhao, R., Van Der Wal, A., Presser, V., Biesheuvel, P. M., 2013. Review on the science and technology of water desalination by capacitive deionization. Progress in Materials Science 58 (8), 1388–1442.

[155] Presser, V., Dennison, C. R., Campos, J., Knehr, K. W., Kumbur, E. C., Gogotsi, Y., 2012. The electrochemical flow capacitor: A new concept for rapid energy storage and recovery. Advanced Energy Materials 2 (7), 895–902.

[156] Prolight, June 2014. Costs of Philips UV lamps.
URL http://prolight.info/philips.html

[157] Puers, R., Carta, R., Thoné, J., 2011. Wireless power and data transmission strategies for next-generation capsule endoscopes. Journal of Micromechanics and Microengineering 21 (5), 15pp.

[158] R. P. Wojda and M. K. Kazimierczuk, 2012. Proximity-effect winding loss in different conductors using magnetic field averaging. Compel The International Journal for Computation and Mathematics in Electrical and Electronic Engineering 31 (6), 1793–1814.

[159] Ray, A. K., 1999. Design, modelling and experimentation of a new large-scale photocatalytic reactor for water treatment. Chemical Engineering Science 54 (15-16), 3113–3125.

[160] Ray, A. K., Beenackers, A. A. C. M., 1998. Novel photocatalytic reactor for water purification. AIChE Journal 44 (2), 477–483.

[161] Reatti, A., Kazimierczuk, M. K., 2002. Comparison of various methods for calculating the AC resistance of inductors. IEEE Transactions on Magnetics 38 (3), 1512–1518.

[162] Rica, R. A., Ziano, R., Salerno, D., Mantegazza, F., Brogioli, D., 2012. Thermodynamic relation between voltage-concentration dependence and salt adsorption in electrochemical cells. Physical Review Letters 109 (15).

[163] Rizzo, L., Meric, S., Guida, M., Kassinos, D., Belgiorno, V., 2009. Heterogenous photocatalytic degradation kinetics and detoxification of an urban wastewater treatment plant effluent contaminated with pharmaceuticals. Water Research 43 (16), 4070–4078.

[164] Sample, A. P., Meyer, D. A., Smith, J. R., 2011. Analysis, experimental results, and range adaptation of magnetically coupled resonators for wireless power transfer. IEEE Transactions on Industrial Electronics 58 (2), 544–554.

[165] Satkunas, B., Jul. 23 1968. Driving unit for electric toothbrush. US Patent 3,394,277.

[166] Sauer, M. L., Ollis, D. F., 1994. Acetone oxidation in a photocatalytic monolith reactor. Journal of Catalysis 149 (1), 81–91.

[167] Schubert, E. F., Kim, J. K., 2005. Solid-state light sources getting smart. Science 308 (5726), 1274–1278.

[168] Schuder, J., Stephenson, H., 1963. Energy transport into the closed chest from a set of very-large mutually orthogonal coils. American Institute of Electrical Engineers, Part I: Communication and Electronics, Transactions of the 81 (6), 527–534.

[169] Schuder, J. C., Stephenson Jr, H. E., 1963. Energy transport and conversion for a permanently implanted artificial heart. ASAIO Journal 9 (1), 286–291.

[170] Schuder, J. C., Stephenson Jr, H. E., Townsend, J. F., 1961. Energy transfer into a closed chest by means of stationary coupling coils and a portable high-power oscillator. ASAIO Journal 7 (1), 327–331.

[171] Schwarzenbach, R. P., Egli, T., Hofstetter, T. B., Von Gunten, U., Wehrli, B., 2010. Global water pollution and human health. Annual Review of Environment and Resources 35, 109–136.

[172] Schwarzenbach, R. P., Escher, B. I., Fenner, K., Hofstetter, T. B., Johnson, C. A., Von Gunten, U., Wehrli, B., 2006. The challenge of micropollutants in aquatic systems. Science 313 (5790), 1072–1077.

[173] Shie, J. L., Lee, C. H., Chiou, C. S., Chang, C. T., Chang, C. C., Chang, C. Y., 2008. Photodegradation kinetics of formaldehyde using light sources of UVA, UVC and UVLED in the presence of composed silver titanium oxide photocatalyst. Journal of Hazardous Materials 155 (1-2), 164–172.

[174] Shur, M. S., Gaska, R., 2010. Deep-ultraviolet light-emitting diodes. IEEE Transactions on Electron Devices 57 (1), 12–25.

[175] Sousa, M. A., Gonalves, C., Vilar, V. J. P., Boaventura, R. A. R., Alpendurada, M. F., 2012. Suspended TiO_2-assisted photocatalytic degradation of emerging contaminants in a municipal WWTP effluent using a solar pilot plant with CPCs. Chemical Engineering Journal 198-199, 301–309.

[176] Stackelberg, P. E., Furlong, E. T., Meyer, M. T., Zaugg, S. D., Henderson, A. K., Reissman, D. B., 2004. Persistence of pharmaceutical compounds and other organic wastewater contaminants in a conventional drinking-water-treatment plant. Science of the Total Environment 329 (1-3), 99–113.

[177] Suss, M. E., Baumann, T. F., Bourcier, W. L., Spadaccini, C. M., Rose, K. A., Santiago, J. G., Stadermann, M., 2012. Capacitive desalination with flow-through electrodes. Energy and Environmental Science 5 (11), 9511–9519.

[178] Tadatomo, K., Okagawa, H., Ohuchi, Y., Tsunekawa, T., Imada, Y., Kato, M., Taguchi, T., 2001. High output power InGaN ultraviolet

light-emitting diodes fabricated on patterned substrates using met-alorganic vapor phase epitaxy. Japanese Journal of Applied Physics, Part 2: Letters 40 (6 B), 583–585.

[179] Takei, G., Kitamori, T., Kim, H. B., 2005. Photocatalytic redox-combined synthesis of l-pipecolinic acid with a titania-modified mi-crochannel chip. Catalysis Communications 6 (5), 357–360.

[180] Tayade, R. J., Natarajan, T. S., Bajaj, H. C., 2009. Photocat-alytic degradation of methylene blue dye using ultraviolet light emit-ting diodes. Industrial and Engineering Chemistry Research 48 (23), 10262–10267.

[181] Teoh, W. Y., Scott, J. A., Amal, R., 2012. Progress in heterogeneous photocatalysis: From classical radical chemistry to engineering nano-materials and solar reactors. Journal of Physical Chemistry Letters 3 (5), 629–639.

[182] Terman, F. E., 1943. Radio Engineers' Handbook, 1st Edition. McGraw-Hill Book Company, Inc., New York and London.

[183] Tixier, C., Singer, H. P., Oellers, S., Müller, S. R., 2003. Occurrence and fate of carbamazepine, clofibric acid, diclofenac, ibuprofen, keto-profen, and naproxen in surface waters. Environmental Science and Technology 37 (6), 1061–1068.

[184] Torimoto, T., Ito, S., Kuwabata, S., Yoneyama, H., 1996. Effects of adsorbents used as supports for titanium dioxide loading on pho-tocatalytic degradation of propyzamide. Environmental Science and Technology 30 (4), 1275–1281.

[185] Van Gerven, T., Mul, G., Moulijn, J., Stankiewicz, A., 2007. A review of intensification of photocatalytic processes. Chemical Engineering and Processing: Process Intensification 46 (9 SPEC. ISS.), 781–789.

[186] Vandevoorde, G., Puers, R., 2001. Wireless energy transfer for stand-alone systems: A comparison between low and high power applicability. Sensors and Actuators, A: Physical 92 (1-3), 305–311.

[187] Vasconcelos, T. G., Kümmerer, K., Henriques, D. M., Martins, A. F., 2009. Ciprofloxacin in hospital effluent: Degradation by ozone and photoprocesses. Journal of Hazardous Materials 169 (1-3), 1154–1158.

[188] Vilhunen, S., Sillanpaa, M., 2010. Recent developments in photochemical and chemical AOPs in water treatment: A mini-review. Reviews in Environmental Science and Bio-Technology 9 (4), 323–330.

[189] Villa, J. L., Sallán, J., Llombart, A., Sanz, J. F., 2009. Design of a high frequency inductively coupled power transfer system for electric vehicle battery charge. Applied Energy 86 (3), 355–363.

[190] Walsh, F. C., 2001. Electrochemical technology for environmental treatment and clean energy conversion. Pure and Applied Chemistry 73 (12), 1819–1837.

[191] Wang, C. S., Stielau, O. H., Covic, G. A., 2005. Design considerations for a contactless electric vehicle battery charger. IEEE Transactions on Industrial Electronics 52 (5), 1308–1314.

[192] Wang, E. N., 2012. Water desalination: Graphene cleans up water. Nature Nanotechnology 7 (9), 552–554.

[193] Wang, G., Dong, Q., Ling, Z., Pan, C., Yu, C., Qiu, J., 2012. Hierarchical activated carbon nanofiber webs with tuned structure fabricated by electrospinning for capacitive deionization. Journal of Materials Chemistry 22 (41), 21819–21823.

[194] Wang, G., Qian, B., Dong, Q., Yang, J., Zhao, Z., Qiu, J., 2013. Highly mesoporous activated carbon electrode for capacitive deionization. Separation and Purification Technology 103, 216–221.

[195] Wang, W., Ku, Y., 2003. Photocatalytic degradation of gaseous benzene in air streams by using an optical fiber photoreactor. Journal of Photochemistry and Photobiology A: Chemistry 159 (1), 47–59.

[196] Wang, Z., Liu, J., Dai, Y., Dong, W., Zhang, S., Chen, J., 2012. CFD modeling of a UV-LED photocatalytic odor abatement process in a continuous reactor. Journal of Hazardous Materials 215-216, 25–31.

[197] Wilke, K., Breuer, H., 1999. The influence of transition metal doping on the physical and photocatalytic properties of titania. Journal of Photochemistry and Photobiology A: Chemistry 121 (1), 49–53.

[198] Wojda, R. P., Kazimierczuk, M. K., 2012. Optimum foil thickness of inductors conducting DC and non-sinusoidal periodic currents. IET Power Electronics 5 (6), 801–812.

[199] Wojda, R. P., Kazimierczuk, M. K., 2012. Winding resistance of litzwire and multi-strand inductors. IET Power Electronics 5 (2), 257–268.

[200] Wojda, R. P., Kazimierczuk, M. K., 2013. Analytical optimization of solid-round-wire windings. IEEE Transactions on Industrial Electronics 60 (3), 1033–1041.

[201] World Water Assessment, P., 2009. The united nations world water development report 3: Water in a changing world. The United Nations World Water Development Report 3: Water in a Changing World.

[202] Wu, J. C. S., Lin, H. M., Lai, C. L., 2005. Photo reduction of CO_2 to methanol using optical-fiber photoreactor. Applied Catalysis A: General 296 (2), 194–200.

[203] Würtele, M. A., Kolbe, T., Lipsz, M., Külberg, A., Weyers, M., Kneissl, M., Jekel, M., 2011. Application of GaN-based ultraviolet-C light emitting diodes - UV LEDs - for water disinfection. Water Research 45 (3), 1481–1489.

[204] Yang, J., Zou, L., Choudhury, N. R., 2013. Ion-selective carbon nanotube electrodes in capacitive deionisation. Electrochimica Acta 91, 11–19.

[205] Yu, L., Weon, D. H., Kim, J. I., Mohammadi, S., 2010. Integrated high-inductance three-dimensional toroidal inductors. Journal of Vacuum Science and Technology B: Microelectronics and Nanometer Structures 28 (5), 903–907.

[206] Yu, Q., Holmes, T. W., 2001. A study on stray capacitance modeling of inductors by using the finite element method. IEEE Transactions on Electromagnetic Compatibility 43 (1), 88–93.

[207] Yu, Q., Holmes, T. W., Naishadham, K., 2002. RF equivalent circuit modeling of ferrite-core inductors and characterization of core materials. IEEE Transactions on Electromagnetic Compatibility 44 (1), 258–262.

[208] Zhao, R., Biesheuvel, P. M., Van Der Wal, A., 2012. Energy consumption and constant current operation in membrane capacitive deionization. Energy and Environmental Science 5 (11), 9520–9527.

[209] Zhao, R., Satpradit, O., Rijnaarts, H. H. M., Biesheuvel, P. M., van der Wal, A., 2013. Optimization of salt adsorption rate in membrane capacitive deionization. Water Research 47 (5), 1941–1952.

[210] Zou, L., Li, L., Song, H., Morris, G., 2008. Using mesoporous carbon electrodes for brackish water desalination. Water Research 42 (8-9), 2340–2348.

Publications

Kuipers, J., Bruning, H., Bakker, S., Rijnaarts, H., 2012. Near field resonant inductive coupling to power electronic devices dispersed in water. Sensors and Actuators, A: Physical. 178, 217-222.

Kuipers, J., Porada, S., 2013. Wireless desalination using inductively powered porous carbon electrodes. Separation and Purification Technology. 120, 6-11.

Kuipers, J., Bruning, H., Yntema, D., Bakker, S., Rijnaarts, H., 2014. Self-capacitance and resistive losses of saline-water-filled inductors. IEEE Transactions on Industrial Electronics. 61(5), 2356-2361.

Kuipers, J., Bruning, H., Yntema, D., Rijnaarts, H., 2014. Wirelessly powered ultraviolet light emitting diodes for photocatalytic oxidation. Submitted to Journal of Photochemistry and Photobiology A: Chemistry.

Kuipers, J., Bruning, H., Yntema, D., Rijnaarts, H., 2014. Modeling of immersed UV-LEDs in a suspension of TiO_2 photocatalyst. Submitted to Journal of Hazardous Materials.

Kuipers, J., Hernandez Leal, L., Bruning, H., Yntema, D., Rijnaarts, H., 2014. A novel distributed UV-LED photocatalysis process to remove pharmaceuticals from wastewater effluent. Submitted to Environmental Science and Technology.

Conference proceedings

Kuipers, J., Bruning, H., Yntema, D., Rijnaarts, H., 2013. Increasing photon transfer with distributed UV-LEDs. ICCE, 15-19 June 2013, Barcelona, Spain.

Patents

Mayer, M.J.J., Kuipers, J., 2010. Apparatus and method for treating a liquid. WO 2010033020.

Kuipers, J., Yntema, D.R., Bakker, S.M., 2012. Hydrophone pump, container and method therefor. WO 2012047106.

Bakker, S., Bruning, H., Kuipers, J., Rijnaarts, H., Yntema, D.R., 2012. Wireless sound source, device and method for disinfecting a fluid. WO 2012060692.

Bakker, S., Kuipers, J., Metz, S.J., 2012. Device and method for photocatalytic treatment of a fluid. WO 2012115509.

Acknowledgements

After 5 years of doing this nice job I can hardly imagine I will reach this milestone where I receive a PhD degree for the fun work I did in the lab. Not all fun work of course, the last year was very difficult for me, where I had to write my thesis and wrap things up, but thanks to a lot of people who supported me and helped in very different ways I was able to do it. Hereby I want to thank all the people for their help.

First, I would like to thank Cees, Johannes and all the other people for creating Wetsus. They had this crazy idea to start a knowledge institute in Leeuwarden. Thanks to you guys I had the great opportunity to come into contact with academic research and this formed my further studies and career. Where I didn't know what I wanted to do with my life before I got into contact with Wetsus, after that contact I knew, became very motivated and had a goal in my life. I find it amazing what you guys do for Friesland and Leeuwarden and I am very proud that I was able to be a small part of that success.

I would like to thank all my supervisors. Huub, my promoter, thanks for all the meetings and input. In September 2009 you started as the new professor at ETE and I started at the same time as a PhD student. Thanks for making me realize I needed some intensive sessions in Wageningen to finish my thesis in time. Harry, thanks for all your help, time and patience. I always find it amazing how fast you replied to my emails with corrections and comments. Thanks to your input and help I was able to make the deadline for the thesis submission. Simon Bakker, thanks for the daily supervision at Wetsus at the start of my PhD. Unfortunately you fell ill

and had to take it easy so you couldn't continue as a supervisor for me. Doekle, you are so good at so many things in the lab. I remember a Friday afternoon experiment with the "hydrophonic pump" where we made and tested the device in one afternoon! This was amazing for me. Thanks for very often helping me out and saving a lot of time. Thanks for all you help Doekle!

I would like to thank the technical staff at Wetsus who helped me building my setup, Wim, Jan, Ernst, Harry and Harm. Although I liked to try and build my own setups, sometimes I had to ask the help of the experts. You guys where always open to help.

Thanks to the analytical staff, Bob, Janneke, Jelmer, Mieke, Ton, and Marianne. Thanks for answering questions, doing the analyses, keeping analytic machines running and calibrated and always wanting to explain me things. Thanks Ton for measuring my pharmaceutical samples on such a short notice!

I would like to thank the secretariat, PR department and financial department for making sure that Wetsus runs so smoothly. Also a big thanks goes out to the talent development team at Wetsus doing the most important work of inspiring the children for a career in science.

To my colleagues at Wetsus, Ana, Lena, Daniel, Natalia, Taina, Heleen, Hester, Ingo, Martina, Kamuran, Martijn W. Arie, Henk, Jordy, Jan M., Joao, Jan Jurjen, Marco, Jan P., Jos, Petra, Agnieszka, Claudia, Enver, Gert Jan, Ime, Monir, Oliver, Vytautas, Dries, Lina, Adam, Ricardo, Bob, Bert, Elsemiek, Rik, Jouke, David, Elmar, Astrid, Fei, Ran, Hardy, Leon, Roel, Urania, Michel, Pedro, Paula, Philipp, Pau, Pawel, Tom, Sanne, thanks for the scientific input and talks at breaks. The coffee breaks were a great time and most of the time I didn't mind making new coffee even though I didn't even finish it.

I would like to thank Slawomir for being my neighbor for so many years, it was a pleasure working together with you.

Thanks Hellen for visiting us every now and then. I really like your visits and we will soon visit you on your farm again.

Cycling is a great way for me to relax. I used to do that alone but I recently discovered the joy of cycling behind somebody, thanks Martijn B.,

Lieven, Sam, Joeri, and Zlatica for keeping me out of the wind!

Maarten, thanks for arranging all the stuff going on in the theme advanced waste water. I would also like to thank you for your help on Chapter 4 of this thesis; I hope it passes your very high standards.

Thanks to my old office mates, Christina, Florian, Slawomir, Mariapia and my new office mates Tim, Judita, Sofia and Jorrit. Thanks to you guys the working atmosphere was always very rowdy and I could hardly concentrate.

Sybrand, I started at Wetsus under your supervision. The project became a great success and that was because you are so open to innovation and new solutions. Thanks to you I realized I was creative and innovative and I am trying to develop these trades further. I am very happy that after my PhD I am able to continue working with you in your company, Metalmembranes.com (check out the website people!).

Mateo Mayer, thanks for the confidence and help you gave me when I started my work at Wetsus.

Grietje en Paul, thanks for letting me stay in your beautiful house in Wageningen, our family will come soon to stay over at your place for a weekend.

Colleagues at Wageningen ETE, thanks for always being so hospitable when I came to the department. It was always very enjoyable. The Leeuwarden/Wageningen PhD day was a very nice event, thanks Nora for co-organizing this day with me.

Thanks to the people in the Water Group and later the Micropollutant and Pathogen group.

Thanks to the members of the theme Advanced Waste Water Treatment for their input and interest in my topic. The theme meetings always were very instructive for me.

I would like to thank my students, Sonia, Douwe, Natasha, Boris, and Tianye for all their work and I want to thank them for all they have taught me.

Oane, neist in hurde wurker bringst sto in hiel protte plezier mei dy mei nei it wurk. Bedankt ast myn paranimf wêze wolst en ik hoopje dat wy noch in protte tegearre wurkjen gjin yn e takomst.

About the author

Johannes Kuipers was born on the 15th of February 1984 in Dokkum, the Netherlands. He studied Chemical Technology at the Noordelijke Hogeschool Leeuwarden where he obtained a BSc degree in 2007. His thesis subject at Wetsus was on the removal of antiscalants from Reverse Osmosis concentrate streams. In September 2007 he started his MSc studies at Wageningen University, Environmental Sciences. He did his MSc thesis on resonant inductive coupling of electronic devices submerged in water and after successfully earning an MSc degree he continued the research as a PhD student on this topic. Since September 2014 he works as Scientific Researcher at Metalmembranes.

SENSE

**Netherlands Research School for the
Socio-Economic and Natural Sciences of the Environment**

D I P L O M A

For specialised PhD training

The Netherlands Research School for the
Socio-Economic and Natural Sciences of the Environment
(SENSE) declares that

Johannes Kuipers

born on 15 February 1984 in Dokkum, The Netherlands

has successfully fulfilled all requirements of the
Educational Programme of SENSE.

Leeuwarden, 10 October 2014

the Chairman of the SENSE board

Prof. dr. Huub Rijnaarts

the SENSE Director of Education

Dr. Ad van Dommelen

The SENSE Research School declares that **Mr Johannes Kuipers** has successfully fulfilled all requirements of the Educational PhD Programme of SENSE with a work load of 39.3 ECTS, including the following activities:

SENSE PhD Courses

o Environmental Research in Context (2010)
o Research Context Activity: Co-organising Wetsus Science and Technology Challenge (2010) and PhD day Environmental Technology (2013)

Other PhD and Advanced MSc Courses

o High Voltage Course (2009)
o Working Safely in the Lab (2010)
o Entrepreneurial Bootcamp Madison & Wageningen University (2010)
o Introduction to Matlab (2011)
o Scientific Writing (2013)

Management and Didactic Skills Training

o Supervision of BSc thesis 'Investigation of UV-light disinfection for advanced wastewater treatment'(2012)
o Supervision of MSc student internship 'Novel photocatalytic reactor with a multitude of wirelessly powered ultraviolet light emitting diodes with an attached surface of titanium dioxide' (2013)
o Supervision of MSc thesis 'Development of an innovative photocatalytic reactor using a fluidized bed of wirelessly powered ultraviolet light emitting diodes'(2013)

Oral Presentations

o *Increasing photon transfer with distributed UV-LEDs.* ICCE, 15-19 June 2013, Barcelona, Spain
o *Micropollutants and microelectronics.* Wetsus Congress, 28 November 2013, Leeuwarden, The Netherlands
o *Distributed UV-LEDs.* Wetsus Congress, 17 April 2014, Leeuwarden, The Netherlands

SENSE Coordinator PhD Education

Dr. ing. Monique Gulickx

Pictures on the cover by Marcelo Hernández Leal.